

University of Windsor

## Scholarship at UWindor

---

Electronic Theses and Dissertations

Theses, Dissertations, and Major Papers

---

1-1-2006

### An investigation of a micro-scale Ranque-Hilsch vortex tube.

Amar F. Hamoudi  
*University of Windsor*

Follow this and additional works at: <https://scholar.uwindsor.ca/etd>

---

#### Recommended Citation

Hamoudi, Amar F., "An investigation of a micro-scale Ranque-Hilsch vortex tube." (2006). *Electronic Theses and Dissertations*. 7053.  
<https://scholar.uwindsor.ca/etd/7053>

This online database contains the full-text of PhD dissertations and Masters' theses of University of Windsor students from 1954 forward. These documents are made available for personal study and research purposes only, in accordance with the Canadian Copyright Act and the Creative Commons license—CC BY-NC-ND (Attribution, Non-Commercial, No Derivative Works). Under this license, works must always be attributed to the copyright holder (original author), cannot be used for any commercial purposes, and may not be altered. Any other use would require the permission of the copyright holder. Students may inquire about withdrawing their dissertation and/or thesis from this database. For additional inquiries, please contact the repository administrator via email ([scholarship@uwindsor.ca](mailto:scholarship@uwindsor.ca)) or by telephone at 519-253-3000ext. 3208.

**AN INVESTIGATION OF A MICRO-SCALE RANQUE-HILSCH VORTEX  
TUBE**

by

Amar F. Hamoudi

A Thesis

Submitted to the Faculty of Graduate Studies and Research  
through Mechanical, Automotive and Materials Engineering  
in Partial Fulfillment of the Requirements for  
the Degree of Master of Applied Science at the  
University of Windsor

Windsor, Ontario, Canada

2006

© Amar F. Hamoudi



Library and  
Archives Canada

Bibliothèque et  
Archives Canada

Published Heritage  
Branch

Direction du  
Patrimoine de l'édition

395 Wellington Street  
Ottawa ON K1A 0N4  
Canada

395, rue Wellington  
Ottawa ON K1A 0N4  
Canada

*Your file* *Votre référence*  
*ISBN: 978-0-494-35914-3*  
*Our file* *Notre référence*  
*ISBN: 978-0-494-35914-3*

**NOTICE:**

The author has granted a non-exclusive license allowing Library and Archives Canada to reproduce, publish, archive, preserve, conserve, communicate to the public by telecommunication or on the Internet, loan, distribute and sell theses worldwide, for commercial or non-commercial purposes, in microform, paper, electronic and/or any other formats.

The author retains copyright ownership and moral rights in this thesis. Neither the thesis nor substantial extracts from it may be printed or otherwise reproduced without the author's permission.

**AVIS:**

L'auteur a accordé une licence non exclusive permettant à la Bibliothèque et Archives Canada de reproduire, publier, archiver, sauvegarder, conserver, transmettre au public par télécommunication ou par l'Internet, prêter, distribuer et vendre des thèses partout dans le monde, à des fins commerciales ou autres, sur support microforme, papier, électronique et/ou autres formats.

L'auteur conserve la propriété du droit d'auteur et des droits moraux qui protègent cette thèse. Ni la thèse ni des extraits substantiels de celle-ci ne doivent être imprimés ou autrement reproduits sans son autorisation.

---

In compliance with the Canadian Privacy Act some supporting forms may have been removed from this thesis.

Conformément à la loi canadienne sur la protection de la vie privée, quelques formulaires secondaires ont été enlevés de cette thèse.

While these forms may be included in the document page count, their removal does not represent any loss of content from the thesis.

Bien que ces formulaires aient inclus dans la pagination, il n'y aura aucun contenu manquant.

  
**Canada**

## ABSTRACT

The results of a parametrical experimental investigation of the energy separation performance of a micro-scale Ranque-Hilsch vortex tube are presented. The tube is 2 mm in diameter and constructed using a layered technique from multiple pieces of Plexiglas and aluminum. Four inlet slots, symmetrically located around the tube, form the vortex flow. The hydraulic diameter of each inlet slot is 229 microns. Three different orifice diameters for the cold exit are used in this experiment. They are 0.5, 0.8 and 1.1 mm. The multilayer technique enables the researcher to simply extend the length of the micro-scale vortex tube to any size ranging from 20 to 120 mm. The working fluid is filtered and dehumidified compressed air approximately at room temperature. The rate of the hot gas flow is varied by means of a control valve to achieve different values of cold mass fraction. The mass flow rates, temperatures and pressures of the supply and outlet flows are measured and the performance of the device presented in a dimensionless manner. The supply channel Reynolds numbers is varied over a considerable range which extends into the laminar regime in order to determine the minimum conditions for cooling.

Experiments conducted on a micro-scale vortex tube, for a fixed geometry and control valve setting, at low Reynolds numbers, based on the inlet tube hydraulic diameter and average velocity, exhibit an increase in dimensionless temperature in both the hot and the cold outlets as the Reynolds number increased from zero reaching maximum values before a Reynolds number of 500 and 800 respectively. In the case of the hot outlet, the dimensionless temperature decreases after reaching its maximum and achieves a minimum value at a Reynolds number below 1500. It then increases steadily with further increases in Reynolds number. The cold outlet dimensionless temperature decreases steadily after the maximum to become negative at a Reynolds number of approximately 1800. This implies that there is cooling effect at Reynolds numbers consistent with laminar flow. Except for very low Reynolds numbers the cold mass fraction is approximately constant as the Reynolds number increases for a fixed geometry and control valve setting. For smaller orifice diameter and hence smaller  $d_o/D$  ratio, the cold air mass fraction is decreased due to the increase of the resistance in the cold flow.

The cold air mass fraction also reduced with higher  $L/D$  ratio due to high resistance in the cold flow.

The performance of the micro-scale vortex tube is also investigated at a number of higher inlet pressures for different values of the cold air mass ratio. The inlet pressures considered are 200, 300 and 400 kPa at an average inlet temperature of 293.6 K and the cold air mass ratio is systematically varied from 0.05 to 0.95. An increase in the inlet pressure causes the values of the dimensionless cold temperature difference to increase over the whole range of the cold air mass fraction. Unstable operation is observed at small  $L/D$  that causes the shape of the dimensionless cold temperature difference versus cold mass flow fraction plot to be different than the conventional plot.

The effect of dimensionless tube length and cold exit orifice diameter on micro-scale vortex tube performance is found to be similar to that in the conventional devices.

## **DEDICATION**

To my beloved parents,  
my wife, my son Yaser and my daughters  
Zinah and Rana.

## ACKNOWLEDGEMENT

The author would like to acknowledge his sincere gratitude to Dr. A. Fartaj and Dr. G. W. Rankin for their valuable advice, outstanding supervision during the term of this research and for the time commitments, without which this work would never be achieved. It is a privilege to study and to work under their supervision.

The author also gratefully acknowledges the efforts of Mr. Timothy Bolger from the Technical Support Center (TSC) at the University of Windsor for his excellent work in constructing the micro-scale vortex tube.

Many thanks to my family for their support, encouragement and patience.

## TABLE OF CONTENTS

ABSTRACT	iii
DEDICATION	v
ACKNOWLEDGMENT	vi
LIST OF TABLES	x
LIST OF FIGURES	xi
NOMENCLATURE	xiv
CHAPTER	
1. INTRODUCTION	1
1.1 Background	1
1.2 Applications of Vortex Tube	5
1.3 Thesis Outline	6
2. LITERATURE REVIEW	7
2.1 Experimental Studies	7
2.1.1 Vortex Tube Geometry	8
2.1.2 The Internal Flow Field	10
2.1.3 Effect of Working Fluid	13
2.2 Theoretical Studies	15
2.3 Numerical Studies	19
2.4 Research Objective	20



3.	EXPERIMENTAL METHODOLOGY	21
3.1	The Micro-Scale Vortex Tube	21
3.2	Apparatus Description	21
3.2.1	Nozzle Section	22
3.2.2	Cold End Orifice Section	23
3.2.3	Extension Pieces	24
3.2.4	Hot End and Control Valve Section	24
3.2.5	Assembly	24
3.3	Instrumentation	26
3.3.1	Pressure Measurement	26
3.3.2	Temperature Measurement	27
3.3.3	Flow Rate Measurement	27
3.4	Experimental Facility	28
3.5	Experimental Methodology	29
3.5.1	Low Pressure Tests	29
3.5.2	High Pressure Tests	30
4.	RESULTS AND DISCUSSION	31
4.1	Results of the Low Pressure Tests	31
4.2	Results of the High Pressure Tests	39
4.3	Effect of Orifice Diameter	48
4.4	Effect of Tube Length	50

5	CONCLUSIONS AND RECOMMENDATIONS	52
5.1	Conclusions	52
5.2	Recommendations	53
	REFERENCES	54
APPENDIX A	Micro-Scale Vortex Tube Design Drawing	60
APPENDIX B	Experimental Uncertainty Analysis Calculations	63
APPENDIX C	Low Pressure Tests Results	69
APPENDIX D	High Pressure Tests Results	78
	VITA AUCTORIS	87

## LIST OF TABLES

Table 1	Optimum design parameters for Soni and Thomson [25]	10
Table 2	Correction used for temperature measurements	27

## LIST OF FIGURES

Figure 1	Vortex tube schematic drawing	2
Figure 2	Hot and cold rotating streamlines in a counter flow vortex tube	2
Figure 3	Sketch of the supposed flow pattern in a counter flow vortex tube	3
Figure 4	Typical performance curves of the vortex tube	4
Figure 5	Uniflow vortex tube with one opening at the hot end	4
Figure 6	Swirl velocity variation with radius	12
Figure 7	Effect of specific heat ratio, $k$ , on the maximum cold temperature drop [20]	14
Figure 8	Secondary flow of the vortex tube [18]	17
Figure 9	Expansion and contraction of turbulent eddies as they move radially	18
Figure 10	Ideal reversed Brayton cycle	19
Figure 11	Inlet nozzle section	23
Figure 12	Cold end orifice section	23
Figure 13	Longitudinal cross-sectional view of the vortex tube assembly	24
Figure 14	Expanded view of the micro-scale vortex tube	25
Figure 15	Vortex tube control volume	26
Figure 16	Schematic of the experiment setup	28
Figure 17	Dimensionless cold and hot temperatures vs. Reynolds number for $L/D = 10$	33
Figure 18	Dimensionless cold and hot temperatures vs. Reynolds number for $L/D = 30$	33

Figure 19	Dimensionless cold and hot temperatures vs. Reynolds number for $L/D = 50$	34
Figure 20	Cold mass ratio, $y_c$ , vs. Reynolds number for $L/D = 10$	35
Figure 21	Cold mass ratio, $y_c$ , vs. Reynolds number for $L/D = 30$	36
Figure 22	Cold mass ratio, $y_c$ , vs. Reynolds number for $L/D = 50$	36
Figure 23	Reynolds number as a function of the inlet pressure for $L/D=10$	37
Figure 24	Reynolds number as a function of the inlet pressure for $L/D=30$	38
Figure 25	Reynolds number as a function of the inlet pressure for $L/D=50$	38
Figure 26	Vortex tube performance for $L/D = 10$ and $d_c/D = 0.25$	40
Figure 27	Vortex tube performance for $L/D = 10$ and $d_c/D = 0.4$	41
Figure 28	Vortex tube performance for $L/D = 10$ and $d_c/D = 0.55$	41
Figure 29	Vortex tube performance for $L/D = 30$ and $d_c/D = 0.25$	42
Figure 30	Vortex tube performance for $L/D = 30$ and $d_c/D = 0.4$	43
Figure 31	Vortex tube performance for $L/D = 30$ and $d_c/D = 0.55$	43
Figure 32	Vortex tube performance for $L/D = 50$ and $d_c/D = 0.25$	44
Figure 33	Vortex tube performance for $L/D = 50$ and $d_c/D = 0.4$	44
Figure 34	Vortex tube performance for $L/D = 50$ and $d_c/D = 0.55$	45
Figure 35	Optimum cold air mass fraction vs. inlet pressure for $L/D = 10$	46
Figure 36	Optimum cold air mass fraction vs. inlet pressure for $L/D = 30$	47
Figure 37	Optimum cold air mass fraction vs. inlet pressure for $L/D = 50$	47
Figure 38	Optimum conditions vs. dimensionless orifice diameter for $L/D = 10$	48
Figure 39	Optimum conditions vs. dimensionless orifice diameter for $L/D = 30$	49
Figure 40	Optimum conditions vs. dimensionless orifice diameter for $L/D = 50$	49

Figure 41	Optimum conditions vs. dimensionless tube length for $d_o/D = 0.25$	50
Figure 42	Optimum conditions vs. dimensionless tube length for $d_o/D = 0.40$	51
Figure 43	Optimum conditions vs. dimensionless tube length for $d_o/D = 0.55$	51

## NOMENCLATURE

$c_p$	specific heat at constant pressure	$P$	pressure
$c_v$	specific heat at constant volume	$Pr$	Prandtl number
$D$	vortex tube inner diameter	$\dot{Q}$	Volumetric flow rate
$d_c$	cold exit (orifice) diameter	$r$	radius
$d_n$	slot holes diameter	$R$	gas constant
$h$	enthalpy	$Re$	Reynolds number
$k$	thermal conductivity	$T$	temperature
$L$	vortex tube length	$\Delta T$	temperature difference
$\dot{m}$	mass flow rate	$u$	axial velocity
$Ma$	Mach number	$w$	tangential velocity

### Greek symbols

$\rho$	density	$\eta$	efficiency
$\mu$	dynamic viscosity	$\nu$	kinematics viscosity

### Subscripts

$y$	Cold gas mass flow ratio	$c$	cold
$s$	static	$h$	hot
$t$	total	$o$	inlet

## CHAPTER 1 – INTRODUCTION

The development of new micro-fabrication techniques has led to a resurgence of research in micro-fluidic devices. The devices that have received most attention in the literature include pumps, valves, flow sensors and heat exchangers [1]. The performance of micro-scale Ranque-Hilsch tubes, non-moving part pneumatic devices that separate cold fluid from hot fluid for the purpose of cooling, has not received much attention. Traditionally, the vortex tube has been used in many low temperature applications where the efficiency is not the most important factor. A micro-scale Ranque-Hilsch tube in combination with a micro-fluidic pump has potential application in the cooling of electronic chips.

### 1.1 Background

The phenomenon of temperature separation occurring inside a cylindrical tube was reported for the first time by a French physicist, George J. Ranque who applied for a US patent in December 1932 [2] and subsequently presented a paper to the French Society of Physics in 1933 [3]. The discovery was further advanced, in 1947, by R. Hilsch [4] who published some details of the construction of the vortex tube along with the performance of the device for different tube diameters at various operating conditions. The vortex tube is a very simple device without moving parts (i.e. diaphragm, pistons, shafts, etc.) as shown in Figure 1.

In this arrangement a stream of a compressed gas (i.e.: air) is injected tangentially into the vortex tube having diameter  $D$  using one or more nozzles symmetrically located around the tube. The injected flow expands and accelerates at the entrance establishing a strong swirl flow which causes a region of increased pressure near the wall and a region of decreased pressure near the axis. The presence of an end wall alongside the inlet nozzles forces some of the injected gas to flow axially in a helical motion toward the far end of the tube (the hot end) where a control valve is located. If the control valve is open too much, a certain amount of out air is



drawn into the tube through the cold end opening and leaves the tube through the hot end. This is obviously not a desirable operating condition.

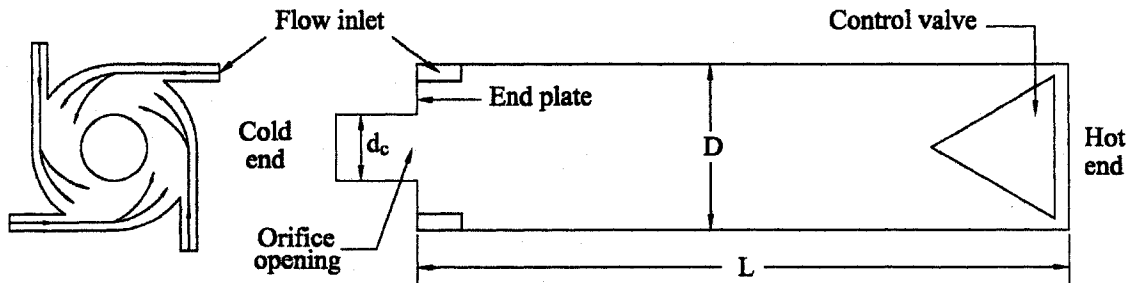


**Figure 1** Vortex tube schematic drawing

In the usual operation of this device, the flow through the hot end is restricted by partially closing the control valve. This causes some of the flow that had been directed to the far end of the tube to reverse direction along the center of the tube and leave the tube through the central orifice (Figure 2). The partial restriction of the flow leaving through the hot end causes even the low pressure at the center of the tube to be higher than atmospheric and hence flow exits the central orifice in the end wall. The gas escaping near the tube wall at the far end of the inlet nozzles has higher stagnation temperature than the incoming gas and the gas exiting through the central orifice has a lower stagnation temperature than the inlet gas.

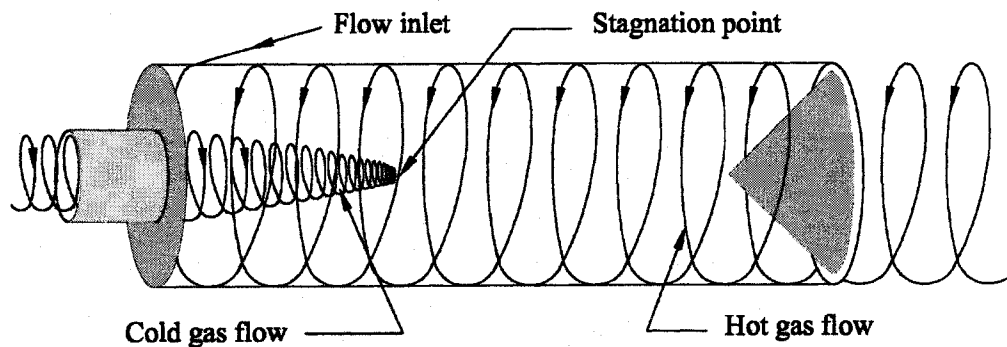


**Figure 2** Hot and cold rotating streamlines in a counter flow vortex tube

A possible flow pattern of the counter flow vortex tube proposed by Fulton [5] is shown in Figure 3. The outward flow of energy is represented by the radial arrows. The stagnation point that exists on the axis of the vortex tube indicates the starting point of reverse flow that represents the cold air stream which eventually leaves the tube through the orifice.

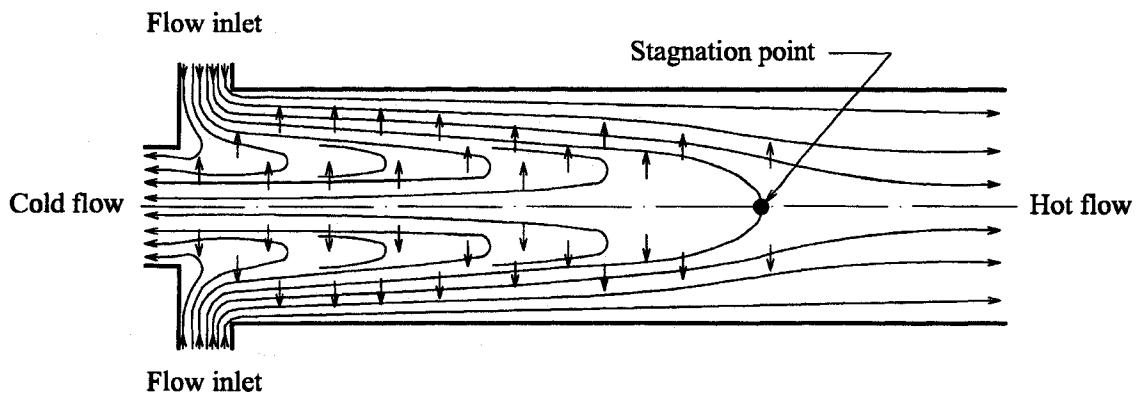


**Figure 3** Sketch of the supposed flow pattern in a counter flow vortex tube

A very low temperature flow can be made to exit from the cold end by operating the device at a supply pressure of a few atmospheres. For example, Hilsch [4] operated a 9.6 mm diameter tube using compressed air at approximately 600 kPa inlet pressure and 293 K inlet temperature to produce a cold stream temperature,  $T_c$ , of 245 K and a hot stream temperature,  $T_h$ , of 353 K. The temperatures of the hot and the cold stream are varied by properly changing the ratio of the cold mass flow rate to the total inlet mass flow rate,  $y_c$ , which can be regulated using the control valve located at the hot exit. The temperature difference of the hot flow,  $\Delta T_h = T_h - T_o$ , and the cold flow,  $\Delta T_c = T_c - T_o$ , can be plotted versus the cold mass fraction,  $y_c$ , to obtain the performance curve of the vortex tube as indicated in Figure 4.

An alternate design of the vortex tube is shown in Figure 5. Both the hot and the cold gas flow are exhausted through one side of the tube. The end wall adjacent to the inlet nozzles is completely sealed and the cold flow leaves the other end of the tube either through the same opening of the hot gas or from an opening within the control valve. The former type was used for flow field investigation only. However, it

has been observed by many investigators that this type of vortex tube, which is also called “uniflow”, has a poor performance compared to the equivalently proportioned counter flow vortex tube type.

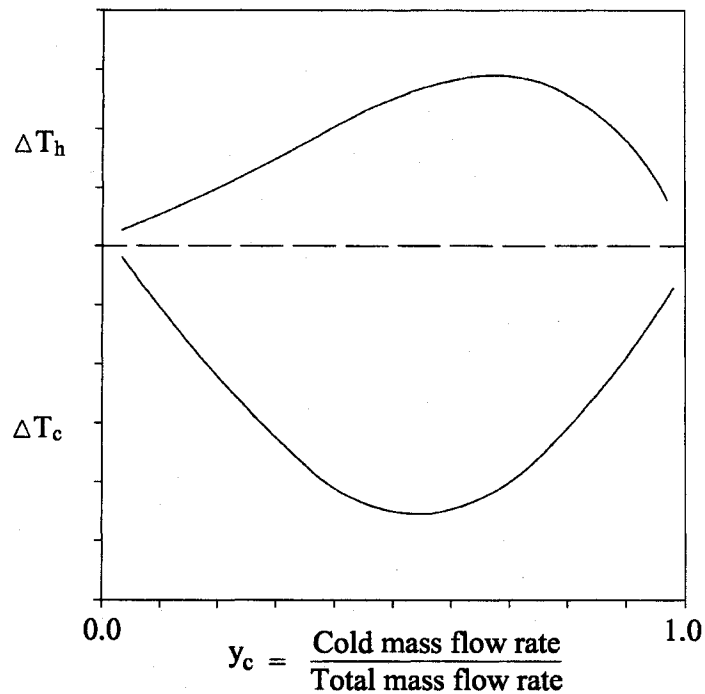


**Figure 4** Typical performance curves of the vortex tube

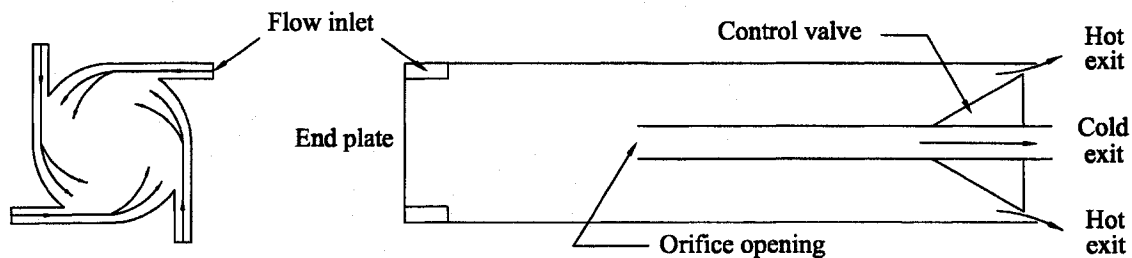


**Figure 5** Uniflow vortex tube with one opening at the hot end

Most of the previous investigators referred to the Ranque-Hilsch vortex tube effect as a temperature or energy separation process. This term will also be used in this work

although the terminology might not be quite accurate to describe the process. It is important to note that there are no hot and cold molecules to be separated from each other as imagined by James Clerk Maxwell [6]. In his thought experiment, Maxwell imagined a container filled with gas and separated by a wall into two compartments. A little “demon” guards a trap door between the two compartments, looking at oncoming molecules on both sides. Depending on their speeds, the demon opens or closes the door so that when a faster than average molecule flies from one compartment toward the door, the demon opens it, and the molecule will fly to the other compartment. Eventually, the molecules faster than average will be collected in one compartment and the slower one will be collected in the other compartment. Since average molecular speed corresponds to temperature, this will result in a temperature difference between the two compartments. The result is a hot, high pressure gas on one side, and a cold, low pressure gas on the other. Although the net effects of the Ranque-Hilsch vortex tube are similar to Maxwell demon, the effect of the former is to establish a total radial temperature gradient produced by energy transfer from the axis of the tube to the periphery and not to separate hot, fast moving molecules from slower, cold ones.

## **1.2 Applications of Vortex Tube**

Despite its low efficiency, the simplicity, robustness and the feature of no moving parts makes the vortex tube attractive for many low temperature applications (below zero degree Celsius) where the use of conventional cooling processes is not viable due to technical requirements. Such low temperature applications would include cooling machine parts, dehumidification of gas samples as well as cooling of electronic control enclosures and environmental chambers. There has also been an attempt [7,8] to replace the conventional expansion valve in a refrigeration cycle with the vortex tube.

### **1.3 Thesis Outline**

In Chapter 2, a literature review is presented covering the experimental, theoretical and numerical work previously conducted. Chapter 3 describes the design of the micro-scale vortex tube, the component details, the instrumentation used and the experimental setup as well as experiment methodology. The experimental results are presented in Chapter 4 followed by an extensive thermodynamic analysis and discussion. Detailed designs drawings of the micro-scale vortex tube, an uncertainty analysis as well as flow rate and Reynolds number calculations are included in the appendices.

## CHAPTER 2 - LITERATURE REVIEW

The most recent review of the literature related to the Ranque-Hilsch vortex tube is given in the dissertation by Gao [9]. Previous reviews [10,11 and 12] reveal hundreds of papers dealing with this topic.

In spite of the large volume of research that has been devoted to this subject over the years, there is still disagreement regarding the mechanism that accounts for the operation of this device. Although it has been shown that energy separation can occur in laminar flow [13,14 and 15] most explanations involve turbulent fluctuations [16]. Kurosaka [17] gives an acoustic streaming explanation while others claim that the operation is based on secondary flows and a thermodynamic refrigeration cycle [18].

The only study that was specifically directed towards micro-scale vortex tube devices was that of Dyskin and Kramarenko [19]. They reported experimentally determined performance characteristics (adiabatic efficiency) for vortex tubes operating with a pressure ratio,  $P_o/P_c$ , of 6 with diameters of 1, 2 and 3 mm. The corresponding mass flow rates were  $14.3 \times 10^{-5}$ ,  $40.0 \times 10^{-5}$  and  $94 \times 10^{-5}$  kg/sec respectively. Although details of the geometry are not given, an estimate of the inlet Reynolds numbers used for these cases yield values greater than 6000. It was, however, noted that the cooling effect decreased with decreasing flow rate. This is consistent with the speculation of Negm et al. [20] that the cooling effect should decrease with decreasing Reynolds number.

The previous investigations of the Ranque-Hilsch vortex tube can be divided basically into three main groups. These groups are experimental, theoretical, and numerical studies and they will be discussed briefly in the following sections.

### 2.1 Experimental Studies

The experimental studies are concerned with the effects of varying the geometry of the vortex tube components; focus on the details of the flow field inside the vortex tube and investigating the effect of using different working fluids other than air. Most of the experimental studies aim to determine the physical geometry of the tube required for optimum performance.

### 2.1.1 Vortex Tube Geometry

Following Hilsch's publication in 1947 [4], many investigators studied the effects of varying the vortex tube geometry such as tube diameter ( $D$ ), tube length ( $L$ ), orifice diameter ( $d_c$ ) and nozzle diameter ( $d_n$ ).

Dyskin and Kramarenko [19] found that by using a conical tube having  $3^\circ$  of tapered angle, the adiabatic efficiency was 10-12% lower than that when a cylindrical tube is used. Piralishvili and Polyayev [21] use what they called a "double circuit vortex tube" with a larger conical angle tube to improve the performance.

Keyes [22] found that the tube diameter is the most important geometrical variable influencing the vortex strength as the periphery Mach number increases with the reduction of the tube diameter. He reported that this improvement is due to a decrease in the turbulent wall shear as a result of the decrease in the tangential peripheral Reynolds number. The vortex tube diameters used in the study were 16, 25 and 50 mm.

Negam et al. [20] stated that the vortex tube performance depends only on Reynolds number for geometrically similar tubes and for the same operating conditions. They found that a vortex tube diameter gives the maximum cold temperature drop at different inlet pressures of 16 mm. Their finding agrees well with Hilsch [4] experiment conducted on 4.6, 9.6 and 17.6 mm tube diameters. They concluded that the tube performance improves with an increase in its diameter.

Many investigators reported that the tube length should be many times longer than the tube diameter for better temperature separation. Hilsch [4] for example found that the  $L/D$  ratio should be 50 for optimum performance. Saidi and Valipour [23] found that the optimum value for the tube length to the tube diameter ratio is  $20 \leq L/D \leq 55.5$ . Furthermore, they found that for  $L/D \leq 20$  the energy separation decreases leading to a decrease in both cold air temperature difference and efficiency. In the case of the micro-scale vortex tube, the optimum  $L/D$  ratio found by Dyskin and Kramarenko [19] was around 60. Contrary to what other investigators reported, Dornbrand [14] found that tube length need not be as long as what was believed necessary. Although for certain tube geometry, the  $L/D$  ratio used by him was 1.4, 2.6

and 3.8, he found, however, that the maximum efficiency would occur at  $L/D$  greater than 20-25.

There is more agreement on the orifice diameter,  $d_c$ , which should be around  $0.5D$  for maximum cold air temperature difference. Most of the previous studies found that the optimal orifice diameter and hence the  $d_c/D$  ratio would be in the range of 0.4 to 0.6. Dornbrand [14] found that if a shorter tube length is used with greater cold air mass ratio, a larger orifice diameter should be used to obtain maximum efficiency and a smaller orifice diameter to be used in case of low cold air mass ratio. He further investigated the effect of using a tapered orifice in diffusing the rotating flow to lower the back pressure. The results he obtained, however, do not show any appreciable gain in vortex tube performance. In explanation, he stated that either the rotating flow through the orifice diffuses efficiently without tapering it or the tapered orifice does not diffuse the rotating air.

Sublikin [24] concluded that the cold orifice diameter,  $d_c$ , is not an important parameter and has little effect on vortex tube performance.

The other parameter that influences the performance of the vortex tube is the inlet nozzle. Dornbrand [14] investigated five different types of nozzles. Among them are round tangent, round offset, and rectangular tangent. The round tangent nozzle gave the best results and a similar round nozzle which is offset by a very slight amount was the poorest. The optimum vortex tube performance was obtained at an equivalent nozzle diameter ratio,  $d_n/D$ , between 0.25 and 0.27. Sibulkin [24] reported that the inlet nozzle height is one of the important geometrical parameters having a significant effect on the vortex tube performance. He noticed that by increasing the inlet nozzle height both hot and cold temperature differences increase.

Soni and Thomson [25] conducted an extensive parametric study to describe the optimal performance. They utilized an empirical regression analysis to derive a functional relationship between maximum cold temperature drop and the independent design variables. Optimal design parameters obtained by them are shown in Table 1. They reported that to obtain maximum cold temperature drop a smaller nozzle diameter with a larger orifice diameter should be used.



**Table 1 Optimum design parameters for Soni and Thomson [25]**

Tube performance	Design Parameter			
	$\frac{\text{nozzle area}}{\text{tube area}}$	$\frac{\text{orifice area}}{\text{tube area}}$	$\frac{L}{D}$	$D$
Maximum $\Delta T_c$	$0.11 \pm 0.01$	$0.08 \pm 0.01$	$> 45$	26 mm
Maximum $\eta$	$0.084 \pm 0.001$	$0.145 \pm 0.035$	$> 45$	18 mm

Different types of material were used to construct the vortex tube. The most important factor in selecting the material is the surface roughness of the inner tube wall. As reported by Dornbrand [14], the vortex tube performance would decrease with an increase of the surface roughness. The material of construction of the vortex tube can be either steel, copper and aluminum or even a plastic or glass to allow flow visualization.

### 2.1.2 The Internal Flow Field

The desire to optimize the tube parameters for maximum cold temperature drop led to investigations regarding the mechanism behind the temperature separation inside the vortex tube. Investigations of the internal flow pattern and measurements of the velocity vector components, pressure and temperature distribution inside the vortex tube were conducted to shed some light on the mechanism of the energy separation. These can be used, at the same time, as a basis for the theoretical analysis of the vortex tube phenomenon. The earliest investigation of the flow field inside the vortex tube was the one conducted by Dornbrand [14] in 1948. He uses a 1 mm close end tube with a very small hole drilled on the wall near the closed end. A number of these tubes were inserted at specific locations along the tube length with the ability to be moved radially inside the vortex tube. This technique enabled a qualitative indication of the velocity field. He reported that the insertion of too many probes broke the vortex pattern. Other major investigations of this type were published by Hartnett and Eckert [26], Keyes [22] and Bruun [27]. The vast majority of this type of experiment utilize probes such as thermocouples to measure the temperature

distribution inside the vortex tube. To obtain the pressure distribution inside the vortex tube, a number of Pitot tubes are inserted at different sections along the length of the vortex tube with the capability to move the Pitot tube radially toward the axis of the vortex tube. Some investigators, such as Ahlborn and Groves [28], developed a technique to rotate the Pitot tube 360° around its axis to obtain the flow angles (or velocity vectors). In order to reduce the error caused by inserting these probes inside the vortex tube, most of the internal studies of the flow field were conducted on a relatively larger tube diameter. It should be noted, however, that the swirling flows are very sensitive to the disturbance created by inserting relatively large pressure probes. Furthermore, when these probes are inserted in a turbulent flow, they are subject to errors caused by turbulent fluctuations [29]. Therefore, more recent internal investigations by [9 and 29] utilize hot-wire anemometers to measure the velocity components. The advantages of the hot-wire probes over the pressure probes are its small size (causing minimal disturbance to the flow), excellent spatial resolution, good signal sensitivity and high frequency response which enables the study of turbulence [30]. Sibulkin [24] was the earliest investigator to utilize the hot-wire anemometer to measure the velocity in a uniflow and a counter flow vortex tube but could not obtain the circumferential velocity components. Fitouri et al. [29] utilized a single yaw hot-wire anemometer to measure the three velocity components and the turbulence intensity.

The results obtained from the internal study enabled the investigators to draw a map of the flow field inside the vortex tube. As reported by many investigators such as [26, 27 and 29], the tangential velocity distribution determined at different locations inside the vortex tube show that the flow in the inner region rotates like a rigid body (forced vortex). The magnitude of the velocity is constant at any point and is a function of the radius:

$$\frac{W}{r} = \text{constant} \quad (1)$$

where  $W$  is the tangential velocity and  $r$  is the distance from the center of the flow. In the outer region, the tangential velocity decreases due to wall shear stress and reaches zero at the wall. This region is referred to a “wall bounded” region.

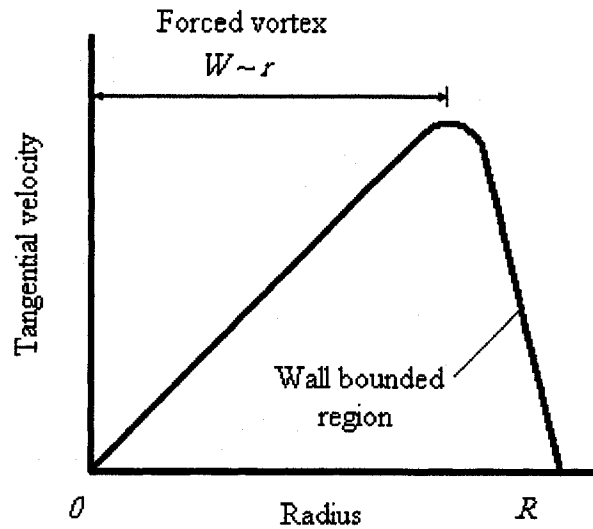


**Figure 6 Swirl velocity variations with radius**

It should be recalled, however, that the flow inside the vortex tube is three dimensional, confined and rotating at a high velocity so that inserting probes at any location could alter the flow field significantly causing inaccurate readings. As reported by Bruun [27], for instance, inserting any probe 30 to 40 mm radially in any of the ten cross sections along the vortex tube increased the total temperature of the cold stream measured in the cold outlet by 4 °C. Keys [22] mentioned that the data obtained by inserting a probe directly in the flow field is of uncertain validity due to the influence of the probe itself. An alternate solution to this problem is the use of non-contact measurement technique such as laser Doppler anemometer (LDA). This method requires the flow to be seeded in order to produce the necessary Doppler burst signals that are used to deduce the flow velocity. The ideal particles are small enough to accurately track the flow, yet large enough to produce an adequate signal to noise ratio (SNR) [31]. Real seed particles, however, are seldom ideal. By using the largest particles, the data is much more easily obtained and the measurements of the particle velocities are more accurate because of the improved SNR but the particles velocities are not representative of the fluid velocity. Although this technique constitutes some technical difficulties such as distortion of the optic beam due to it's interaction with the curved surface of the cylindrical chamber and the time required in setting up the

equipment, it is still considered the more accurate method of measuring the velocity components inside the tube.

### 2.1.3 Effect of Working Fluid

The vast majority of the work concerning the vortex tube used compressed air as the working fluid. A number of investigators, however, studied the effect of gas other than air. Keys [22] used nitrogen and helium instead of air. Linderstrom [32] used the vortex tube as a gas separator to separate a different composition of gas mixtures. He injected a mixture of oxygen and nitrogen, a mixture of oxygen and carbon dioxide and a mixture of oxygen and helium. A mixture of compressed gases flown into the vortex tube separate into individual gas streams by the effect of differential centrifugal forces acting on them. In their attempt to separate methane and nitrogen gases using vortex tubes, Kulkarni and Sardesai [33] found that there was partial gas separation leading to a higher concentration of methane at one exit in comparison to the inlet and a lower concentration at the other exit.

Ambrose [7] injected a saturated liquid of carbon dioxide in the vortex tube in an attempt to replace it with the throttling device used in the refrigeration cycle in order to increase the coefficient of performance of the refrigerator. He proposed a refrigeration cycle utilizing CO<sub>2</sub> as a refrigerant instead of Freon due to its high potential refrigeration gain at a fairly low pressure ratio. A large temperature difference was generated by expanding a saturated liquid carbon dioxide in the vortex tube but the temperature of the hot flow was not sufficiently high to permit heat rejection through the gas cooler.

In the experiment conducted by Stephan et al. [34], no temperature difference was found in the cold flow when air or oxygen is used as a working fluid. The results of their experiment, however, indicated that the cold temperature drop when helium is used as a working fluid is larger than that when air or oxygen is used. This is due to the fact that the molecular weight of the helium is much smaller than the molecular weight of air or oxygen.

The correlation mentioned in Figure 7 by Negam et al.[20] to predict the maximum cold temperature drop indicates that the specific heat ratio,  $c_p/c_v$ , has a significant influence on the performance of the vortex tube. It was found that gases with a higher specific heat ratio,  $k$ , have a better performance than the gases having a lower specific heat ratio.

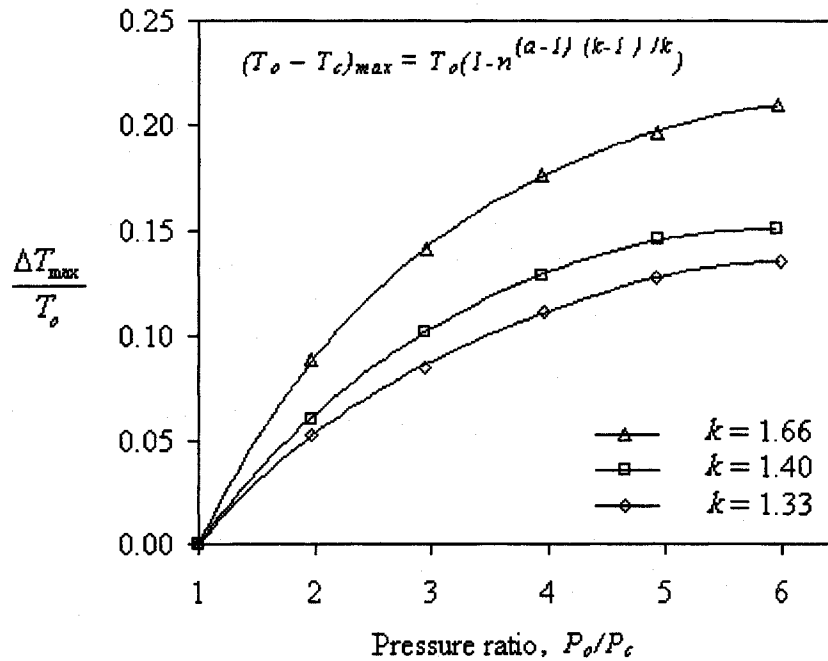


**Figure 7 Effect of specific heat ratio,  $k$ , on the maximum cold temperature drop [20]**

In the equation indicated in Figure 7,  $n$  is the pressure ratio,  $P_o/P_c$ ,  $a$  is the minimum change of specific entropy,  $\frac{(\Delta S_c)_{min}}{S}$ , reported by them to equal 0.67 and  $k$  is the specific heat ratio of the working fluid,  $\frac{c_p}{c_v}$ .

Balmer [35] injected liquid water at high inlet pressure (50 MPa) into a commercially available vortex tube. Although the results showed a significant temperature difference of about 15 °C between the cold and the hot flows, both flows temperature, however, was above the inlet water temperature. From his work, Balmer

concluded that the energy separation in these devices is not limited to compressible gases. Using the second law of thermodynamics, theoretical analysis establishes that net entropy producing temperature separation effect is also possible when incompressible liquids are used in the vortex tube.

## 2.2 Theoretical Studies

It is important to distinguish a change in the temperature of a fluid that is associated with a change in the fluid velocity from that due to work done or heat transfer from the fluid.

Consider the portion of fluid entering the vortex tube that is emitted from the cold exit. If there is no work done or heat transfer involved in the flow, application of the energy equation yields:

$$\begin{aligned} \text{internal} &+ \text{flow} &+ \text{kinetic} &= \\ \text{energy} &\text{work} &\text{energy} & \\ \text{enthalpy} &+ \text{kinetic} &= \text{constant} & \quad (2) \\ &\text{energy} & & \end{aligned}$$

$$h + \frac{u^2}{2} = \text{constant} \quad (3)$$

For a perfect gas:

$$h = c_p T \quad (4)$$

where  $c_p$  is the specific heat of the inlet air at constant pressure, taken as 1005 J/kg K.

Or:

$$T + \frac{u^2}{2c_p} = \text{constant} \quad (5)$$

The thermodynamic (or static temperature)  $T$  can therefore be seen to change if the fluid velocity changes even though no heat is transferred or work is done on the fluid.

The temperature change that is important in the vortex tube is one that is only due to heat transfer. Defining the total temperature as:

$$T_o = T + \frac{u^2}{2c_p} \quad (6)$$

the energy equation becomes  $T_o = \text{constant}$ . It will only change if heat is transferred or work done on the working fluid.

Following the qualitative description of Hilsch [4], many theoretical approaches were published in an attempt to analytically predict the distribution of velocity and temperature, and explain the energy transfer process. The theoretical analyses reported are either based on analytical simulations or on results obtained from the experimental work.

The explanation given by Ranque [2] attributes the energy separation process to the expansion of gas from a region of high pressure near the periphery to a low pressure in the region near the axis. Hilsch [4] presented the same thought in explaining the mechanism of the energy separation. He included the effect of the internal friction which causes the energy to flow from the axis region in the outward direction causing the temperature to increase in the periphery. Kassner and Knoernschild [13] explained that the cold temperature drop in the center region is due to the gas expansion and the hot temperature in the outer region due to the shear stresses that cause the flow in the inner region to be a forced vortex. A number of earlier theories suggested that the energy separation can occur in laminar flow as in the work presented by [14 and 15]. They considered the radial velocity instead of the tangential velocity in determining the Reynolds number.

In the two dimensional analytical model presented by Deissler and Perlmutter [16] and Reynolds [36] it was concluded that the turbulent mixing and turbulent shear work done on elements causes the heat transfer between flow layers by temperature and pressure gradients and hence causes the energy separation inside the vortex tube.

Kurosaka [17] suggested that the acoustic streaming of the vortex whistle is responsible for the Ranque-Hilsch effect. He explains that when the whistle is

inaudible, the steady state tangential velocity distribution in the radial direction is not in the form of a forced vortex and the steady state temperature is uniform. As the whistle becomes audible, the velocity profile converted to a forced vortex causing the temperature distribution to be separated into cold stream near the axis and hot stream near the periphery.

Ahlborn et al. [18] describe the Ranque-Hilsch energy separation phenomenon as a heat pump mechanism which is enabled by a secondary circulation flow imbedded into the primary vortex. There are three processes in the heat pump. All these processes exist in the vortex tube. These are the working fluid (1) as indicated in Figure 8 which moves heat between a high pressure region and a low pressure region, the fluid is compressed at a temperature higher than the surrounding temperature to give off heat (2) and the expanded working fluid is colder than it's surrounding to absorb heat (3). The processes of compression (4) and expansion (5) occurred due to random fluctuations.

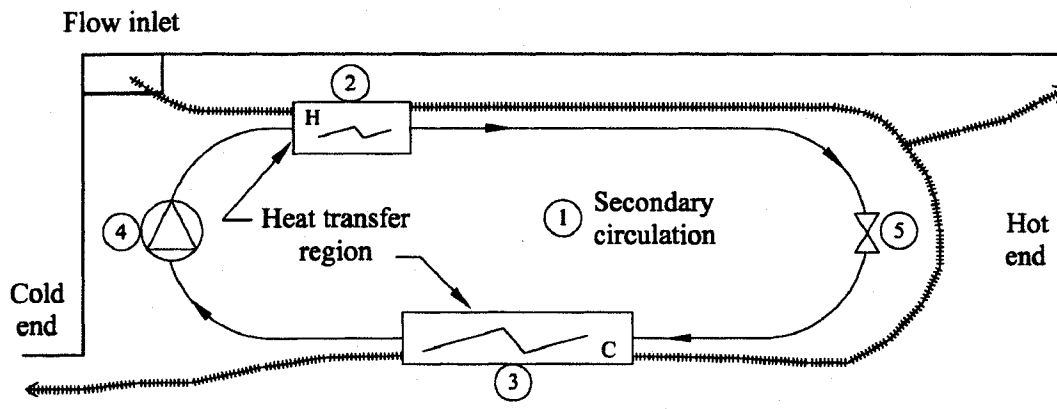


**Figure 8 Secondary flow of the vortex tube [18]**

Bruun [27] and Hinze [37] explained that the mechanism of the energy separation is mainly caused by adiabatic contraction and expansion of turbulent eddies in a centrifugal field. To explain this mechanism, particles are considered fluctuating between the high pressure and the low pressure region as shown in Figure 9. As the particles move from a low pressure region A to a higher pressure region B,



it will undergo an adiabatic compression and the temperature of the particles would increase to a level above the surrounding temperature. As a result, heat transfer will take place from the particles to the surrounding region at B increasing its temperature. At the same time, equivalent particles from the high pressure region B undergo an adiabatic expansion while moving to a lower pressure region A lowering its temperature to a level below the surrounding's temperature, causing the flow at that region to have a lower temperature. This process of adiabatic compression and expansion is similar to that which occurs in an ideal reverse Brayton cycle as shown in the T-s diagram in Figure 10. With the higher pressure difference between the axis of the tube and its periphery and with the higher level of fluctuation, the level of cooling would increase, lowering further the temperature of the flow leaving through the center of the tube.

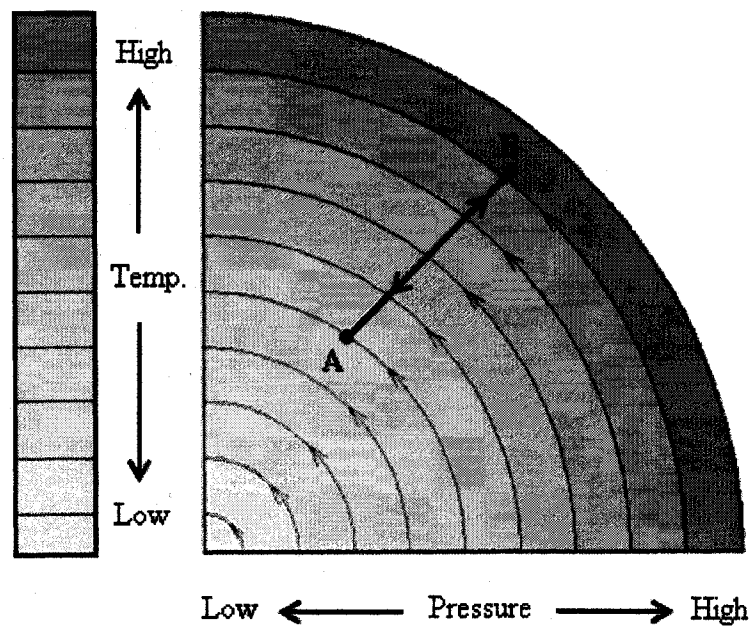


**Figure 9** Expansion and contraction of turbulent eddies as they move radially

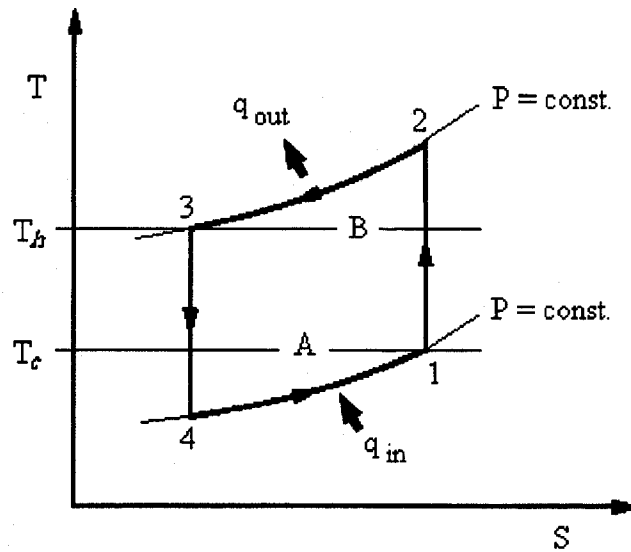


**Figure 10** Ideal reversed Brayton cycle

### 2.3 Numerical Studies

In the numerical studies conducted on vortex tubes, one of the computational fluid dynamics (CFD) packages such as FLUENT, CFX or STAR CD is used to solve the continuity, Navier–Stokes and energy equations. This allows prediction of the internal flow pattern, as well as temperature and pressure distribution inside the tube.

Cockerill [10] uses a two dimensional numerical model to investigate the flow field inside a uniflow and a counter flow vortex tube. The flow is assumed to be an axis-symmetry. He applied a number of modifications to the  $k-\epsilon$  model to account for the anisotropic flow inside the vortex tube. The computations give results for the swirl profiles that qualitatively comparable with the experiments conducted by him. The energy separations, however, are not predicted well. His numerical solutions show that the flow near the axis becomes warmer than the periphery.

Fröhlingsdorf and Unger [38] investigate the compressible and turbulent vortex tube flow numerically by modeling the Bruun experiment [27]. The numerical code used is CFX. The use of the  $k-\epsilon$  turbulence model leads to significant differences between measured and calculated tangential velocity profiles. By replacing the  $k-\epsilon$  turbulence model with the correlation reported by Keyes [22] in calculating the ratio

of the turbulent to laminar viscosity,  $\frac{\mu_T}{\mu_L}$ , a better approximation of the measured results were achieved. They found that by increasing the turbulent Prandtl number from 0.9 to 9.0 produces the same cold gas total temperature difference as in Bruun's experiment [27].

Bezprozvannykh and Mottl [39] report that various levels of complexity in turbulence modeling are suitable for vortex tube analysis. They use a three dimensional numerical model to investigate the energy separation for incompressible and compressible flows for water and air cases correspondingly. The commercial code used is FLUENT. For air as a working fluid, the maximum total temperature difference obtained,  $\Delta T = T_c - T_o$ , is 1 K only. For water, however, no temperature differences were obtained.

Behera et al. [40] implement a three dimensional numerical model in an approach of optimizing the design of the vortex tube using the  $k-\varepsilon$  turbulence model and the Star-CD commercial code. The numerical investigations enable them to obtain the three velocity components of the flow which is difficult to obtain experimentally due to disturbance of flow by measuring probes. The analyses show that the flow has forced and free vortex components. Optimum  $L/D$  ratio that delivered maximum cold temperature difference is found to be in the range of 20 to 30 and for optimum  $d_c/D$  is found to be 0.5.

## 2.4 Research Objective

The objective of this study is three fold:

1. To investigate the characteristics of a micro-scale vortex tube at low inlet pressure ranging from approximately 2.5 to 75 kPa and to obtain the critical inlet Reynolds number at which the cooling effect will be established.
2. To obtain the performance curves of the micro-scale vortex tube as a function of cold air mass ratio at higher inlet pressure values of 200, 300 and 400 kPa.
3. To determine the effect of  $L/D$  and  $d_c/D$  ratio on the performance of the micro-scale vortex tube.

## CHAPTER 3 – EXPERIMENTAL METHODOLOGY

This research is an investigation of a micro-scale vortex tube as an alternative cooling method for electronic micro-chip devices. To achieve this goal, a micro-scale vortex tube is designed, fabricated and tested. The setup is designed for flexible geometrical adjustment. This work provides detailed discussion on the various design parameters. Therefore, the main objective of this research is to experimentally investigate the characteristics of a micro-scale vortex tube at supply channel Reynolds numbers that extend from the laminar into the turbulent flow regime in order to determine the minimum operating conditions of these devices for cooling applications. In addition, the effects of tube length and cold outlet orifice size on the performance characteristics of micro-scale vortex tubes are determined. The experiments are conducted to determine the differences, if any, of the micro-scale vortex tube characteristics to conventional vortex tubes.

### **3.1 The Micro-Scale Vortex Tube**

Most of the previous experimental studies are conducted on fairly large tube diameters (i.e.: 10 – 25 mm) [10,20]. To reduce the effect of inserting measurement probes on the vortex flow pattern in the case of the internal studies, the diameter of the vortex tube used is even as large as 50 - 96 mm in some studies [22,26 and 27]. Investigating a micro-scale vortex tube has not been reported in detail yet. The only study that is specifically directed towards micro-scale vortex tube devices is that of Dyskin and Kramarenko [19]. They report experimentally determined performance characteristics (adiabatic efficiency) for vortex tubes operating with a pressure ratio of 6 with diameters of 1, 2 and 3 mm.

### **3.2 Apparatus Description**

For the purpose of this study, a 2 mm diameter vortex tube is designed and manufactured at the Technical Service Center (TSC) of the University of Windsor. The tube diameter is chosen to be the smallest possible that existing manufacturing

techniques permit. The design and the fabrication of such small a size vortex tube is necessarily different than the conventional one. A layered technique using multiple pieces of Plexiglas and aluminum is used for accurate machining of the inlet, orifice and control valve assembly. The design allows length increment changes hence different  $L/D$  ratios. The cross-sectional area of each piece has a dimension of 30 mm by 30 mm. The length of each piece varies according to its location within the assembly. In the following paragraphs, a detail description of the main parts of the micro-scale vortex tube is presented.

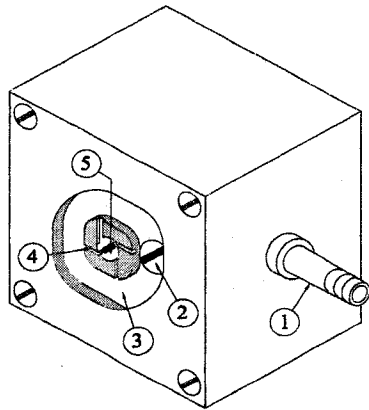
### 3.2.1 Nozzle Section

As the scope of this research is to investigate the vortex tube characteristics at supply channel Reynolds numbers that extend from the laminar into the turbulent flow regime, the supply air slots are designed to be very small to ensure a laminar flow in that region at low supply pressure. The hydraulic diameter of the supply channel is 229 microns. This is the smallest possible dimension that can be machined in the TSC of the University of Windsor. This gives a ratio of nozzle area,  $A_n$ , to the tube area,  $A_d$ , of 0.11 which is similar to that suggested by Soni and Thompson [25] to obtain a maximum cold temperature difference  $\Delta T_c$ .

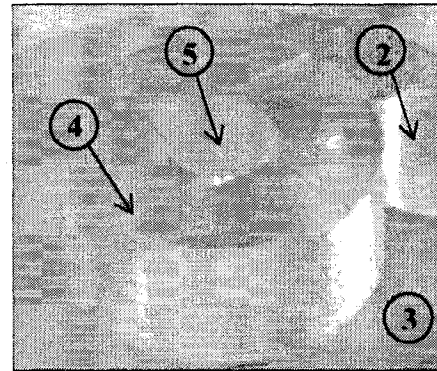
The main inlet nozzle section is machined from one piece made of Plexiglas material and having square cross section area of 30 by 30 mm and 20 mm length. As depicted in Figure 11, this piece consists of the inlet nozzle for the compressed air line (1) attached to the body of this section of the vortex tube. A 4 by 3 mm channel (3) is connected to the inlet nozzle (1) through a longitudinal hole (2). The channel (3) is provided to act as a pressurized manifold so that the flow enters the inlet slots (4) at a pressure and temperature very close to that measured at the inlet nozzle (1). The vortex is formed by four inlet slots (4) that are symmetrically located around the 2 mm tube diameter (5). The dimensions of each inlet slot (4) are 0.382 mm wide and 0.164 mm in height. The hydraulic diameter of the inlet slot,  $d_n$ , is calculated using the following formula:

$$d_n = \frac{4A}{\text{wetted perimeter}} \quad (7)$$

where  $A$  is the cross-sectional area of the inlet slot. The hydraulic diameter is found to be equal to 229 microns.



(a) Front view of the inlet nozzle section

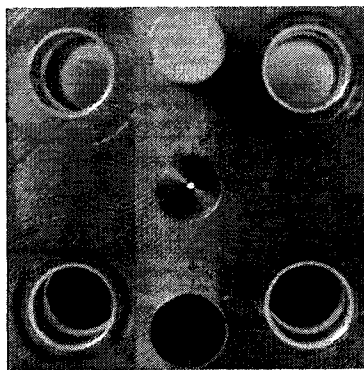


(b) Perspective view showing the details of the inlet nozzles

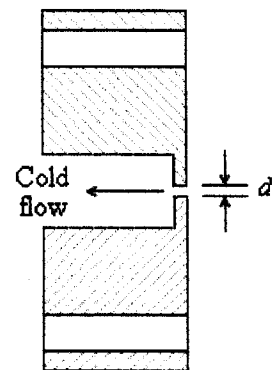
**Figure 11 Inlet nozzle section**

### 3.2.2 Cold End Orifice Section

Three different sizes of the cold orifice diameter are used in this research to investigate its effect over the vortex tube performance. These sizes are 0.5, 0.8 and 1.1 mm and give  $d_o/D$  ratios of 0.25, 0.4 and 0.55 respectively. The cold orifice piece forms one end of the vortex tube while the control valve piece forms the other end of the vortex tube. The material of construction is aluminum.



(a) Front view of the orifice section



(b) Side view of the orifice section

**Figure 12 Cold end orifice section**

Figure 12 shows the front and the side views of the cold end section. The three pieces are identical except for the size of the orifice diameter.

### 3.2.3 Extension Pieces

A number of extension pieces are fabricated to allow adjustment of the tube length. The material of construction for all pieces is Plexiglas. The lengths of the extension pieces are 5, 10 and 20 mm to give flexibility in selecting the tube length and hence the  $L/D$  ratio as shown in Figure 13.

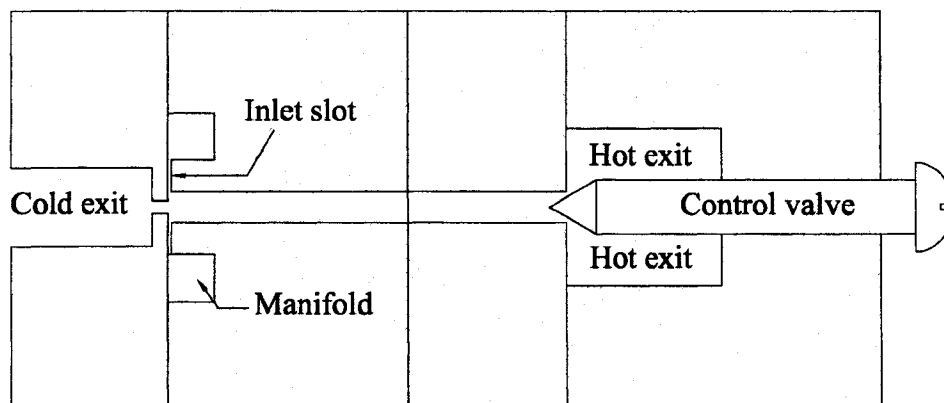


**Figure 13** Longitudinal cross-sectional view of the vortex tube assembly

### 3.2.4 Hot End and Control Valve Section

The hot section, as shown in Figure 13, consists of the control valve to adjust the amount of flow leaving the tube through that end. The block section is made of aluminum and the control valve is made of steel. The end of the control valve is tapered at  $60^\circ$ . A lock nut is provided to prevent the movement of the valve at a certain opening where desired.

### 3.2.5 Assembly

The most important point to be considered at this juncture is the alignment of the different parts of the vortex tube. The minimum number of pieces that can be used

to form a vortex tube with smallest length of 20 mm is three pieces - the main inlet nozzle piece, the cold and the hot end piece. The maximum numbers of pieces that can be used is seven to form a net tube length of 100 mm. Any eccentricity in the position of the cold end opening or the extension pieces may cause a significant disruption to the rotating flow. To avoid this problem, two stainless steel guide pins are used to align the multi-layers forming the vortex tube. The Plexiglas layers are sandwiched between two aluminum pieces which represents the hot and the cold end of the vortex tube as shown in Figure 14. Four bolts and nuts are used to hold the different pieces of the vortex tube and are passed through longitudinal holes at the corners of each piece. Design drawings showing the details of the micro-scale vortex tube using the multi-layer technique are shown in Appendix A.

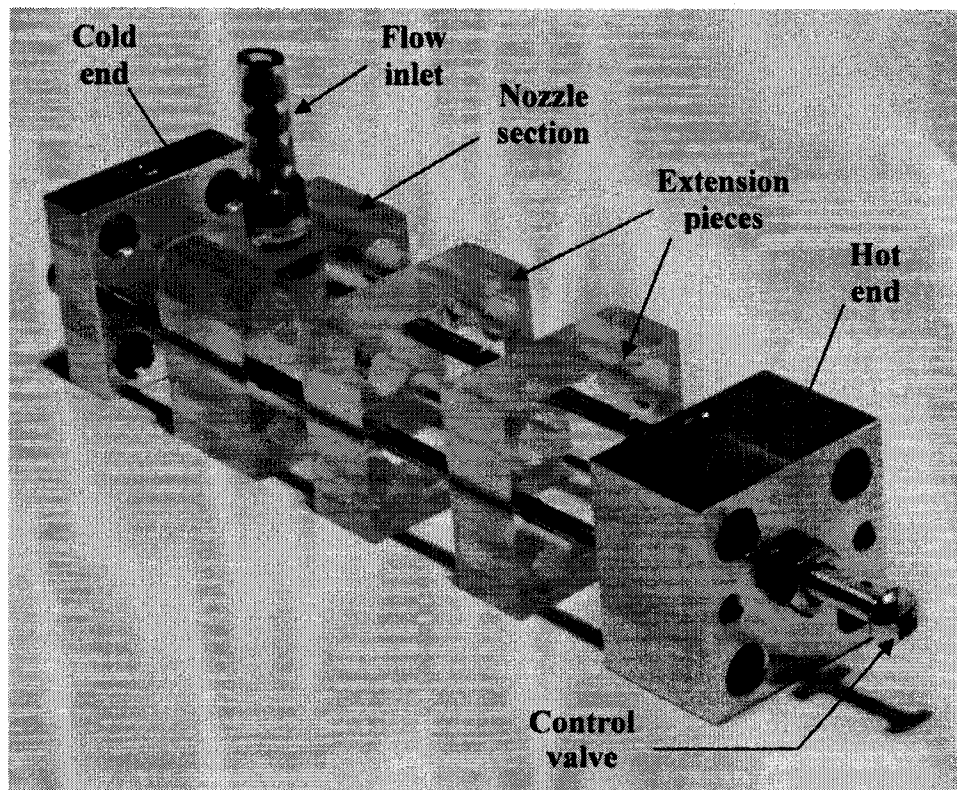


**Figure 14** Expanded view of the micro-scale vortex tube



### 3.3 Instrumentation

The vortex tube in this case is considered as a control volume having three boundaries as shown in Figure 15. The variables to be evaluated are the pressure, temperature, and mass flow rate of the inlet flow, cold and hot boundaries. The subscripts  $o$ ,  $c$  and  $h$  denotes for the inlet flow, cold and hot exit respectively.

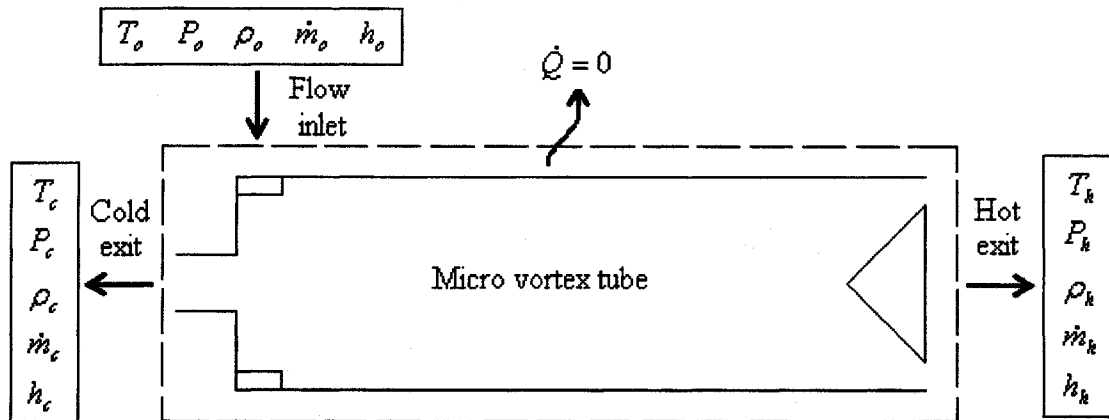


Figure 15 Vortex tube control volume

The three important inlet and exit flow quantities that need to be recorded during the experiment are the pressures, temperatures and the flow rates. The results obtained are eventually used to determine the performance of the vortex tube and to investigate the effect of geometry on the cold temperature drop. The following paragraph discusses the instrumentation used during the tests and the applicable calibration procedure.

#### 3.3.1 Pressure Measurement

Low supply inlet pressures ranging from 2 to 17.5 kPa are measured using a water manometer with an uncertainty of  $\pm 0.01$  kPa. Pressures in the range of 17.5 to 82 kPa are measured using a Bourdon tube gage with an uncertainty of  $\pm 1.7$  kPa and for higher supply pressures of 200, 300 and 400 kPa, a different Bourdon tube pressure gage is used that had an uncertainty of  $\pm 3.4$  kPa. The hot and cold flow

pressure measurements are obtained using a digital manometer with an uncertainty of  $\pm 0.01$  kPa.

### 3.3.2 Temperature Measurement

For the process of the energy separation in the vortex tube, the temperature of the cold and hot exit flow is the most important variable required as these values will be used to find the performance of the micro-scale vortex tube. The temperatures of the inlet, cold and hot air are measured using type - T (Copper Constantan) thermocouple probes. These thermocouples are calibrated using an ice bath and boiling water as temperature standards. The correction factors obtained from the correction curves are used to adjust the readings of the temperatures measured as shown in Table 2.

Table 2 Correction used for temperature measurements

Temperatures to be corrected	Correction factor
Temperature of the inlet flow, $T_o$	$T_o \times 1.0081$
Temperature of the cold flow, $T_c$	$T_c \times 1.0112 - 0.1011$
Temperature of the hot flow, $T_h$	$T_h \times 1.0071 + 0.1007$

### 3.3.3 Flow Rate Measurement

The volumetric flow rate,  $\dot{Q}$ , of air exiting the cold and the hot openings are measured using separate rotameters. The rotameters are calibrated while connected to the apparatus as shown in the experiment setup in Figure 16 so that both are subjected to the same working pressures as encountered in the experiment to avoid the need for corrections. The results of the cold and the hot exit flow are obtained. Assuming an ideal gas, the density of the hot and the cold gas are calculated using the equation of state:

$$\rho = \frac{P}{R T} \quad (8)$$

The mass flow rate,  $\dot{m}$ , leaving the cold and the hot ends are calculated from:

$$\dot{m} = \dot{Q} \rho \quad (9)$$

The total flow rate entering the apparatus is determined by the summation of the cold and the hot flow.

### 3.4 Experimental Facility

The experimental test facility used for this study is shown schematically in Figure 16. Dry and filtered compressed air is used throughout this experiment to avoid any condensation of the moisture in the compressed air due to the low cold air temperature exiting through the orifice. The air is dehumidified with a refrigerant dehumidification system. As indicated in Figure 16, the compressed air passes through a control valve (1), 5-micron air filter (2) and a pressure-regulating valve (3) before entering the vortex tube. A water manometer (4) is used to accurately measure the low supply pressure which ranges from 2 to 17.5 kPa. A pressure gage is used for the pressures above this range.

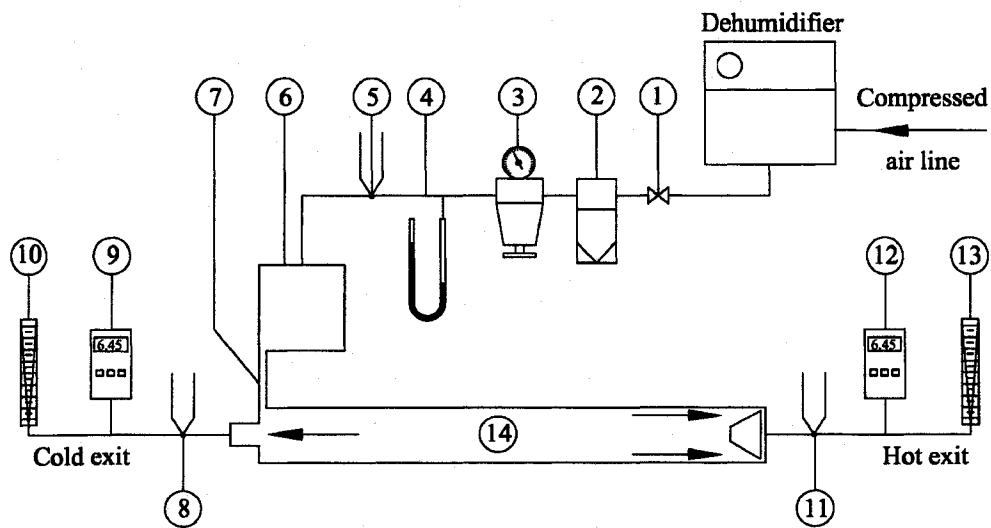


Figure 16 Schematic of the experiment setup

The temperatures of the inlet, cold and hot air are measured using type T thermocouple probes located at (5), (8) and (11) respectively. The compressed air is injected into the vortex tube through the manifold (6) and then the inlet slot (7). The cold exit pressure,  $P_c$ , and hot exit pressure,  $P_h$ , are measured using digital manometers (9) and (12). The volumetric flow rate of air exiting the cold and the hot openings are measured using rotameters (10) and (13).

### 3.5 Experimental Methodology

Two types of experimental tests are conducted to investigate the characteristic of the micro-scale vortex tube in this research. These are the low pressure test and the high pressure test. Each test is conducted at different tube length,  $L$ , orifice diameter,  $d_c$  and inlet pressure,  $P_o$ . A set of nine combinations of vortex tube geometrical parameters consisting of three different  $L/D$  ratios (10, 30 and 50) with three different  $d_c/D$  ratios (0.25, 0.4 and 0.55) form the geometry of the devices under investigation. The following paragraphs discuss the methodology and the aim of each test.

#### 3.5.1 Low Pressure Tests

In the first series of tests, the performance characteristics of the micro-scale vortex tubes are determined at low supply pressure and fixed geometry. This means that the control valve is arbitrarily opened to a certain setting and kept constant throughout the entire set of tests as the supply pressure is varied. The low supply pressures range from approximately 2.5 to 82 kPa.

The measured cold and hot air dimensionless temperatures leaving the vortex tube for various Reynolds numbers, based on the inlet slot of the supply air, are determined using the expression,  $\frac{T_c - T_o}{T_o}$  and  $\frac{T_h - T_o}{T_o}$  respectively. These parameters are chosen to eliminate the effect of the inlet air temperature.

The aim of this test is firstly to determine the critical Reynolds number at which a cold temperature drop will be established and secondly to observe changes in the cold mass fraction,  $y_c$ , with changes in Reynolds number for different tube

geometry with a fixed hot end valve setting. The inlet Reynolds number is determined from:

$$Re = \frac{\dot{m} d_n}{4 A \mu} \quad (10)$$

where  $\dot{m}$  is the air mass flow rate entering the vortex tube through one slot calculated using Equation (9),  $d_n$  is the equivalent diameter of the inlet slot and it is equal to 229 microns,  $A$  is the cross-sectional area of one inlet slot and found to be  $6.25 \times 10^{-8} \text{ m}^2$  and  $\mu$  is the viscosity of the inlet air taken as  $1.82 \times 10^{-5} \text{ kg/m.s}$ .

The resistance of the rotameters located at each of the hot and cold outlets combined with the low operating pressures in the experiments significantly alter the exit pressures of the cold and hot exits. Each is altered by a different amount which effectively creates a different exit pressure in each case. To avoid this problem, the flow of the cold or the hot stream is restricted using a flow restriction device in such a manner that the pressure of the cold and hot air exit is approximately equal.

### 3.5.2 High Pressure Tests

The second series of tests is conducted using the same tube geometrical combinations as in the low pressure test. In this case, however, the characteristic performance of the micro-scale vortex tube at higher inlet pressures and at different cold air mass ratio,  $y_c$ , is determined. The inlet pressure of the supply is 200, 300 and 400 kPa and the value of  $y_c$  varied from approximately 0.05 to 0.95 by adjusting the control valve at the hot end.

## CHAPTER 4 - RESULTS AND DISCUSSION

The results obtained from the low and high pressure tests are presented and discussed in this chapter. The uncertainties in the figures are indicated by the error bars unless they are less than the size of the symbol. Detailed calculations of the uncertainties are presented in Appendix B for reference. Details of the experimental results for low and high pressure tests are presented in Appendix C and Appendix D respectively.

### 4.1 Results of Low Pressure Tests

The temperatures measured using the thermocouples are assumed to be equal to the total temperature which can be justified as follows. The total temperature defined in Equation 6, the term  $u^2/2c_p$  represents the dynamic temperature of the flow. Within the range of the working pressure used in this experiment which is approximately 2.5 to 75 kPa, the cold and the hot exit velocities are found to be in the range of 0.15–1.84 m/s and 0.14 - 1.08 m/s respectively. The maximum dynamic temperatures calculated for both cold and hot temperature are found to be  $1.7 \times 10^{-3}$  and  $5.8 \times 10^{-4}$  K respectively and hence negligible compared to the static temperature.

The plots of dimensionless cold and hot air temperature as a function of the inlet Reynolds number for  $L/D = 10, 30$  and  $50$  are presented in Figures 17, 18 and 19 respectively. The minimum total flow rate is  $9.72 \times 10^{-6}$  kg/s which results in a Reynolds number of approximately 500. It can be seen that, at this low Reynolds number, both hot and cold exit temperatures are higher than the inlet temperature,  $T_o$ . The trend of the curves at Reynolds number below 500 is estimated as shown in the dashed line as it is known that all temperatures must be equal for the case of no flow. At this low Reynolds number, the vortex motion is not likely well established and the effect of the viscous term is the dominating factor. The viscous dissipation, therefore, causes the rise in the temperatures of both outlet streams. In the case of the hot outlet, the dimensionless temperature decreases after reaching its maximum at a Reynolds number of about 500 after which it achieves a minimum value at a Reynolds number of approximately 1200, 1300 and 1500 for  $L/D = 10, 30$  and  $50$  respectively. The

curve then increases steadily with further increase in Reynolds number. The cold outlet dimensionless temperature decreases steadily after reaching the maximum at a Reynolds number of about 800 to become negative at a Reynolds number of approximately 1800. In both the cases of hot and cold flow, the trend of increasing temperatures with Reynolds number is reversed at Reynolds numbers (approximately 500 for the hot flow and 800 for the cold flow) consistent with the critical Reynolds number estimated for tube length shorter than that required for fully developed flow which is common to micro-fluidic devices [1]. It is speculated that the reversal of temperature increase is due to the initiation of turbulence either in the supply nozzle or in the jet that forms in the vortex chamber just downstream of the supply nozzle.

The uncertainties in the Reynolds number are in the range of  $\pm 73$  to 196. While the uncertainty in both the dimensionless cold and hot temperature is found to be  $\pm 0.0019$ . It can be seen from Figures 17 through 19 that the cross-over Reynolds number and the curve shapes are approximately the same and they are within the data uncertainty. It can be concluded that the inlet nozzle geometry is most important factor as it affects the Reynolds number.

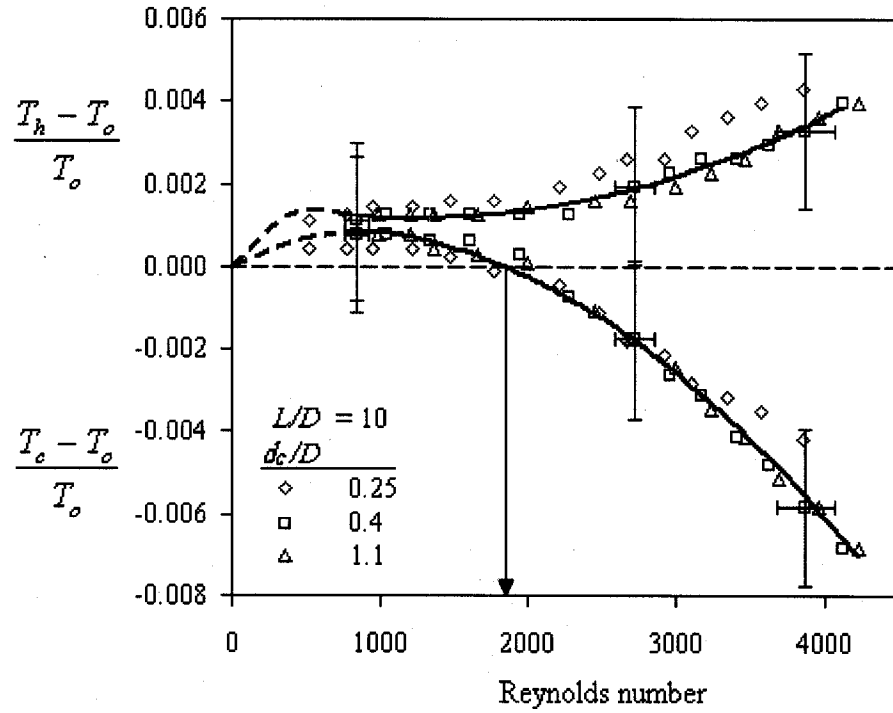


**Figure 17** Dimensionless cold and hot temperatures vs. Reynolds number for  $L/D = 10$

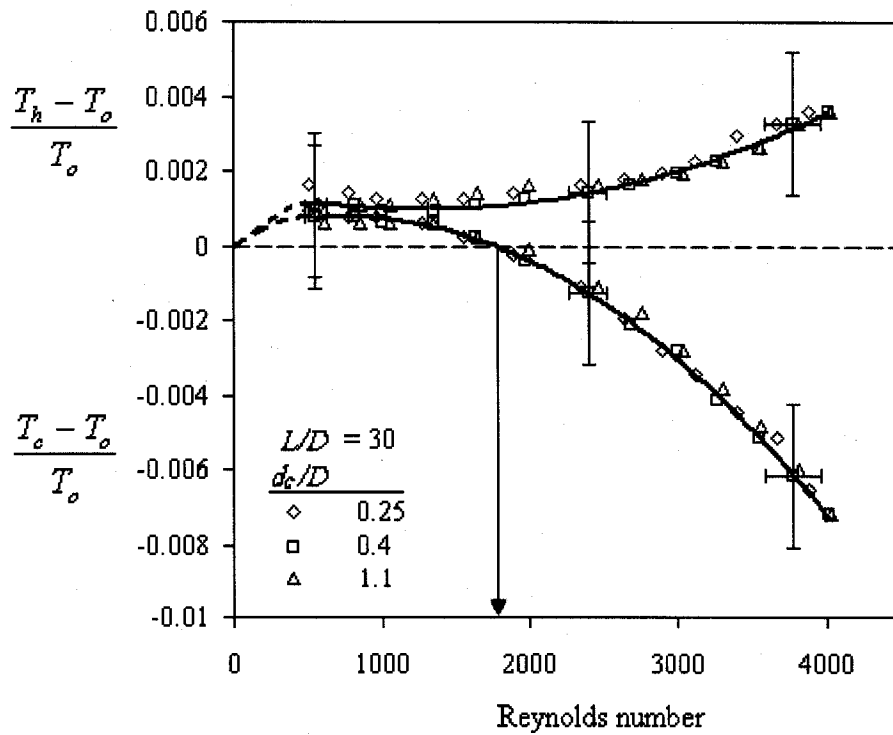


**Figure 18** Dimensionless cold and hot temperatures vs. Reynolds number for  $L/D = 30$



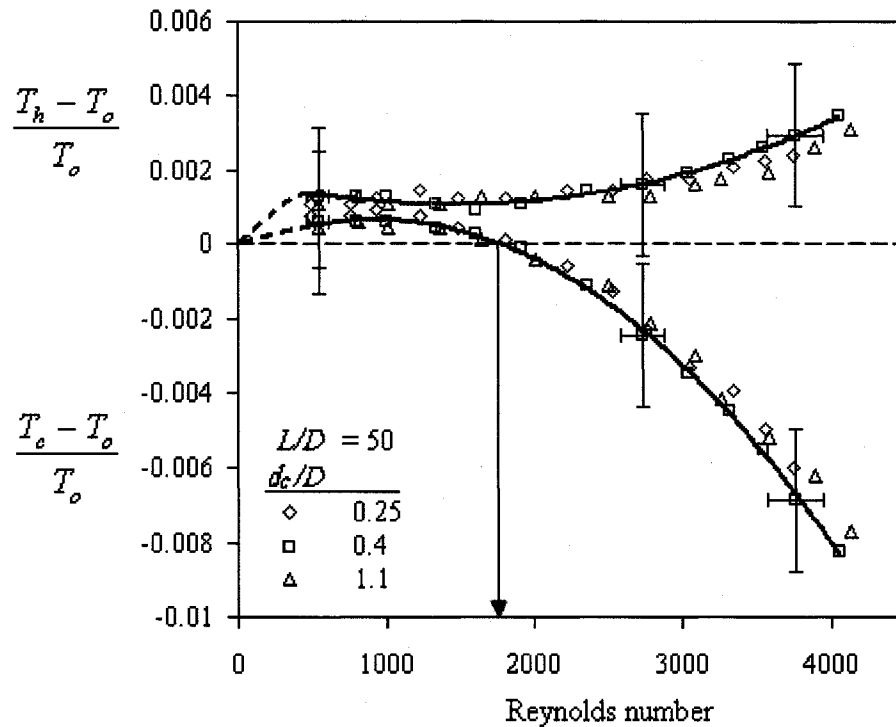


**Figure 19** Dimensionless cold and hot temperatures vs. Reynolds number for  $L/D = 50$

The effects of the orifice diameter and the tube length on the cold air mass ratio are shown in Figures 20 to 22. It should be recalled that this part of the test is conducted at an arbitrary fixed hot control valve opening. One would expect that the cold air mass fraction,  $y_c$ , for such a case would remain the same if the resistance to flow out the cold and hot end is constant. It is clearly shown from the data obtained, however, that:

- For Reynolds number below approximately 2000, the value of cold air mass fraction,  $y_c$ , decreases with an increase of the Reynolds number due to flow resistance changing. It is constant for Reynolds number values above 2000. This is similar to the behavior of other fluid mechanic quantities such as drag coefficient and friction factor.
- For smaller orifice diameter and hence smaller  $d_o/D$  ratio, the cold air mass fraction is decreased. This is likely due to the increase of the resistance in the cold flow.

- The cold air mass fraction also reduced with higher values of  $L/D$  ratio. This variation is not as obvious as in the case of  $d_c/D$ . An increase in the  $L/D$  value changes the internal flow pattern allowing the cold air to travel toward the hot end before reversing direction and passing through cold exit. This increased cold flow path would an increase in resistance.

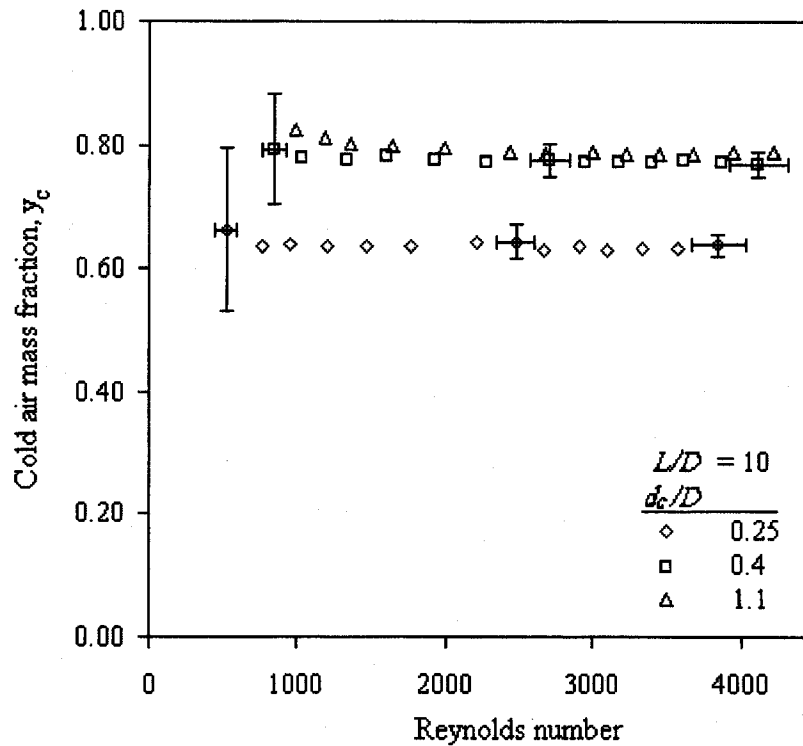


**Figure 20** Cold mass ratio,  $y_c$ , vs. Reynolds number for  $L/D = 10$

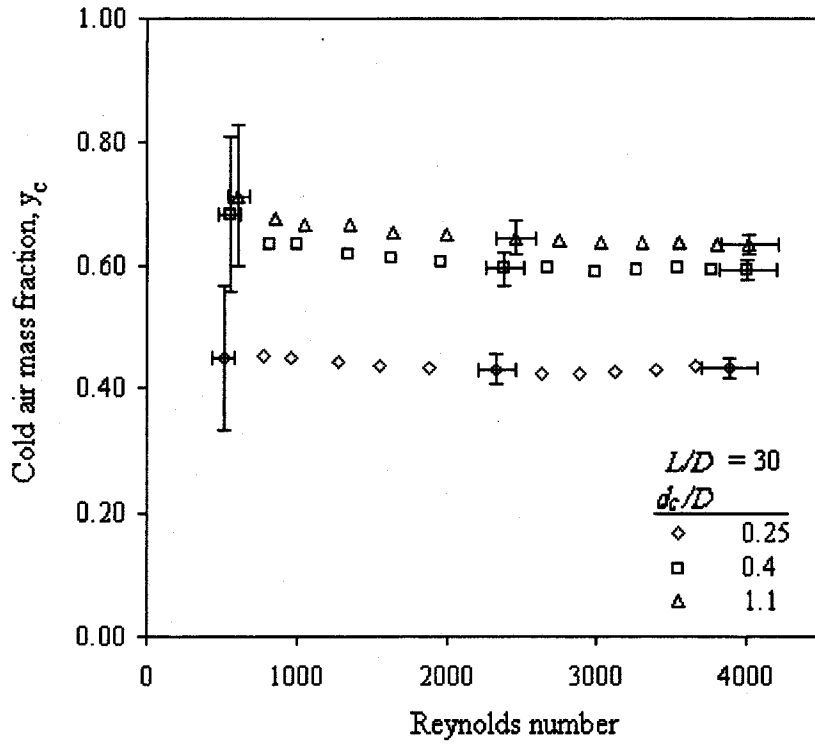


Figure 21 Cold mass ratio,  $y_c$ , vs. Reynolds number for  $L/D = 30$

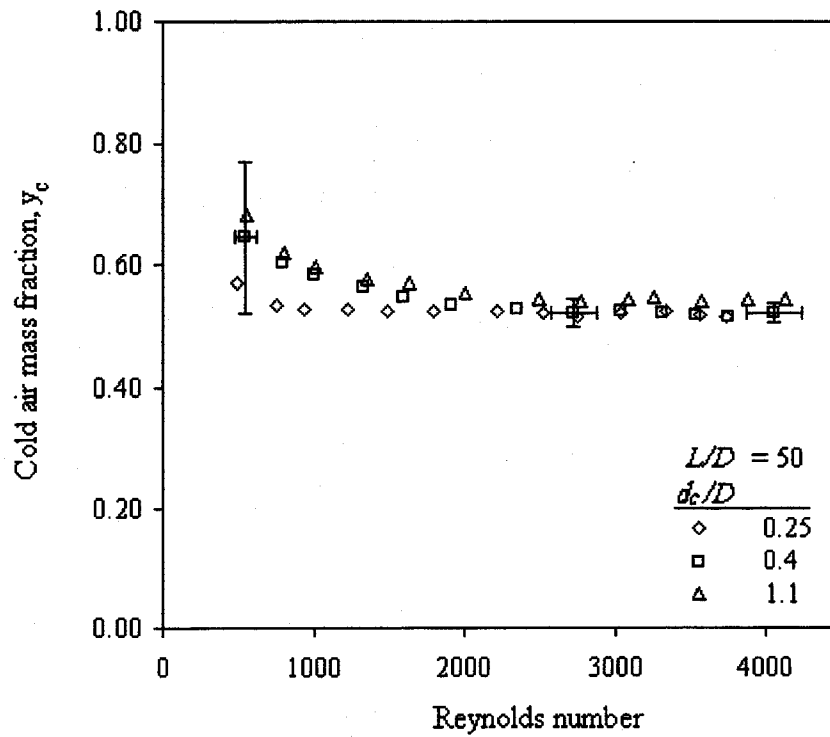
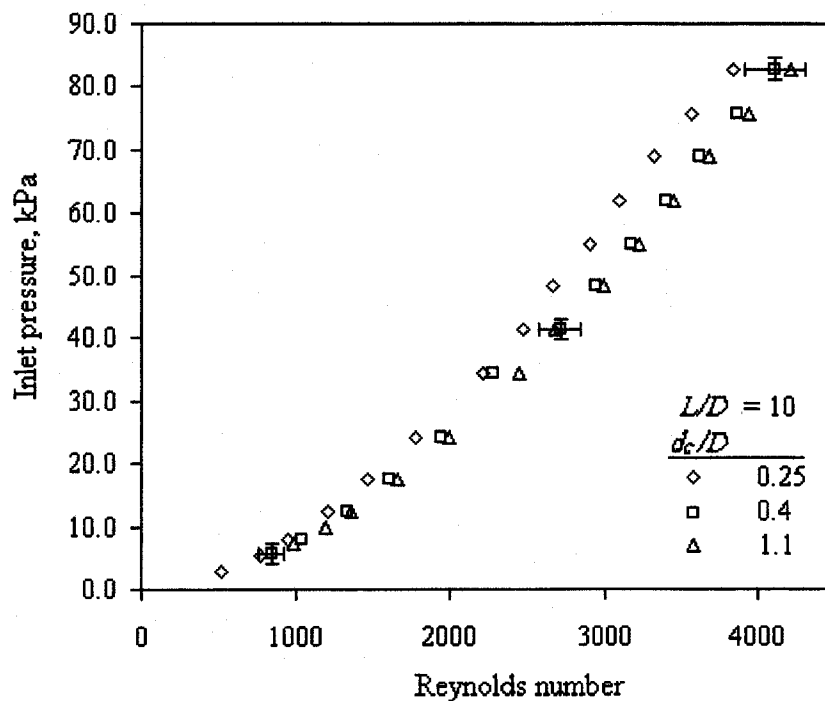
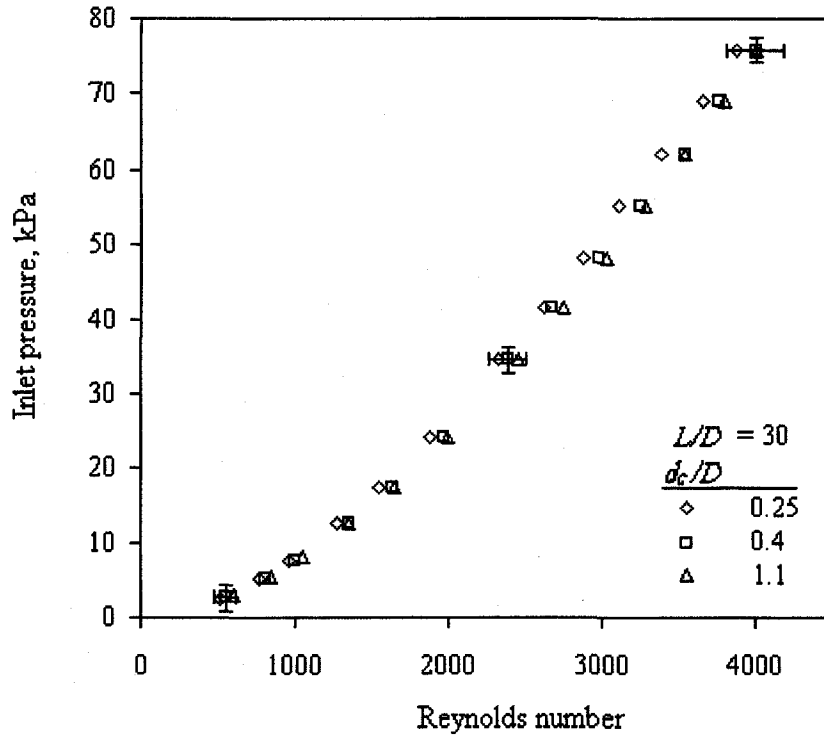


Figure 22 Cold mass ratio,  $y_c$ , vs. Reynolds number for  $L/D = 50$

The change of the inlet Reynolds number with increasing supply pressure is shown in Figures 23 to 25. They are as expected with supply pressure increasing with Reynolds number. This reflects the total resistance of the flow through both hot and cold air outlets. In general, for the same inlet pressure, there was a slight shift to the right of the curve in the Reynolds number as the  $d_c/D$  increases. This is as expected as decreasing  $dc$  has the effect of increasing the total resistance. It would be expected that increasing the  $L/D$  ratio would also increase the pressure required for any Reynolds number. For the shortest  $L/D$  ratio, a higher pressure is however required to achieve the same Reynolds number value obtained for longer  $L/D$  ratio. This anomaly may be due to the pressure fluctuation observed for this case and mentioned later.



**Figure 23** Reynolds number as a function of the inlet pressure for  $L/D=10$



**Figure 24** Reynolds number as a function of the inlet pressure for  $L/D=30$

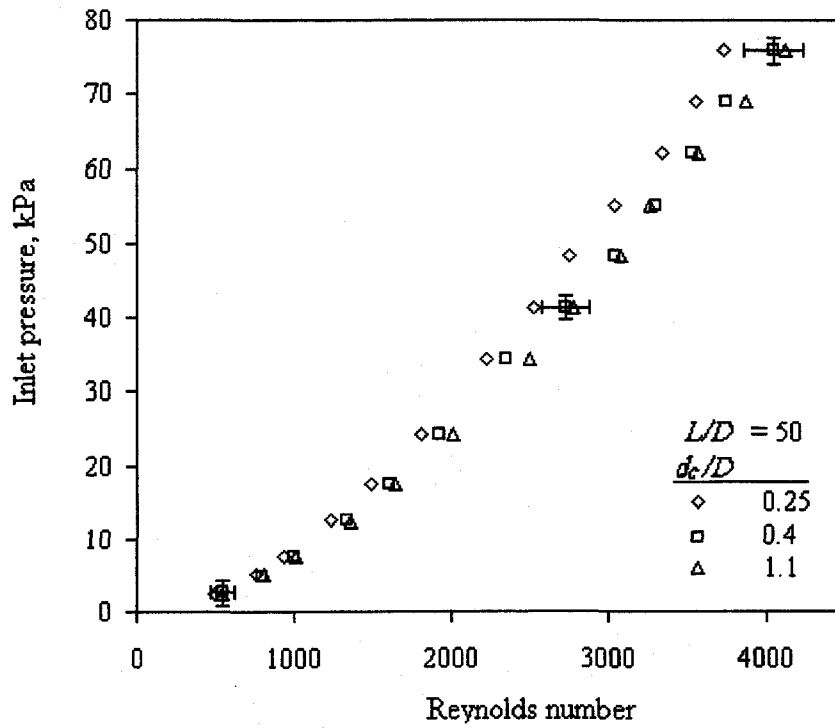


**Figure 25** Reynolds number as a function of the inlet pressure for  $L/D=50$

## 4.2 Results of High Pressure Tests

When investigating the vortex tube as a cooling device, researchers are more interested in obtaining the value of the cold flow temperature. However, both the cold flow as well as the hot flow temperature measurements will be presented in this research. The objective of the second part of the experiment is to investigate the operating characteristics of the micro-scale vortex tube utilizing the same tube geometry for the first part of the test at a higher inlet supply pressure and by varying the cold air mass fraction. The inlet pressures considered here are 200, 300 and 400 kPa. Details of the experimental results are presented in Appendix D. The cold air mass ratio is systematically varied from approximately 0.05 to 0.95 by means of the control valve located at the hot end exit. The cold and hot air flow dimensionless temperatures are presented in Figures 26 to 34. The cold flow dimensionless temperature is represented by the lower curves while the upper curves for the hot flow dimensionless temperature.

For the smallest  $L/D$  ratio, the dimensionless hot and cold temperature as a function of the cold air mass ratio and the inlet pressure as a parameter are shown in Figures 26 to 28. The symbols in these particular sets of curves represent data points collected at different cold air mass ratio and different inlet pressures and the lines are interpolating splines. The best fit curve is found not to be a good choice to represent the variation in the cold and the hot flow temperatures for this particular tube geometry. It can be clearly seen for  $L/D = 10$  and for the three different  $dc/D$  ratios, for the value of the cold mass fraction of approximately 0.05, which represents the lowest cold flow rate leaving the orifice opening, the temperature measured is lower than the inlet air temperature due to the effect of the energy separation. From Figure 26 at 200 kPa inlet pressure, when the value of  $y_c$  is increased, the temperature of the cold flow drops until it reaches its lowest value at  $y_c = 0.38$ . With the slight increase of  $y_c$ , a sharp increase in the cold flow temperature is observed (which is more obvious with the 300 and 400 kPa inlet pressure) is also associated with a slight drop in the hot flow temperature. The sharp increase occurs at larger values of the cold air mass fraction as the inlet pressure increases. This is associated with an increase in fluctuations in the measured pressures and flow rates. It is believed that the flow

instability phenomenon which occurs at a certain value of  $y_c$  causes radial mixing between the cold and hot flow temperatures. The instability needs further investigation for proper explanation. This case is only observed with the shortest tube length of  $L/D$  equal to 10. By further increasing the value of  $y_c$ , the cold flow dimensionless temperature increases and approaches zero as  $y_c$  approaches 1.

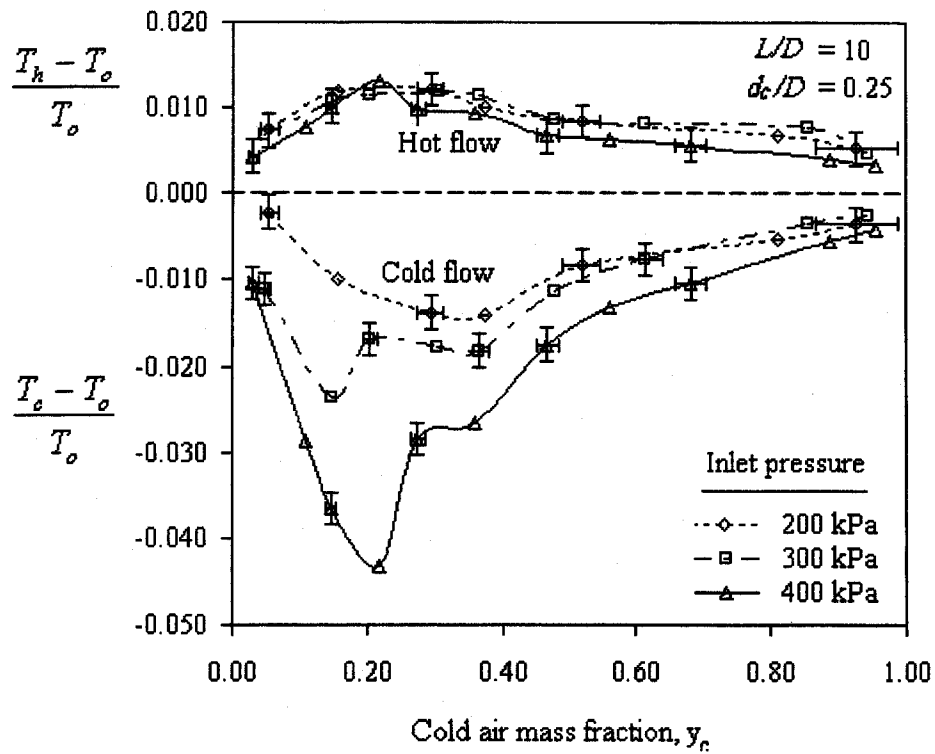


**Figure 26** Vortex tube performance for  $L/D = 10$  and  $d_c/D = 0.25$

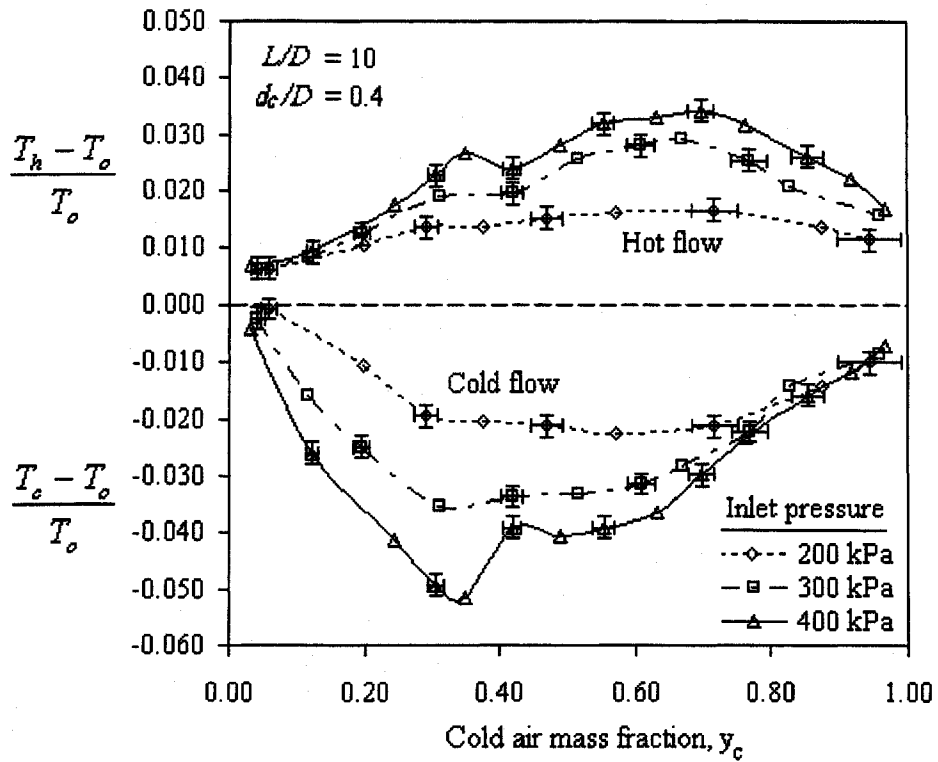


Figure 27 Vortex tube performance for  $L/D = 10$  and  $d_c/D = 0.4$

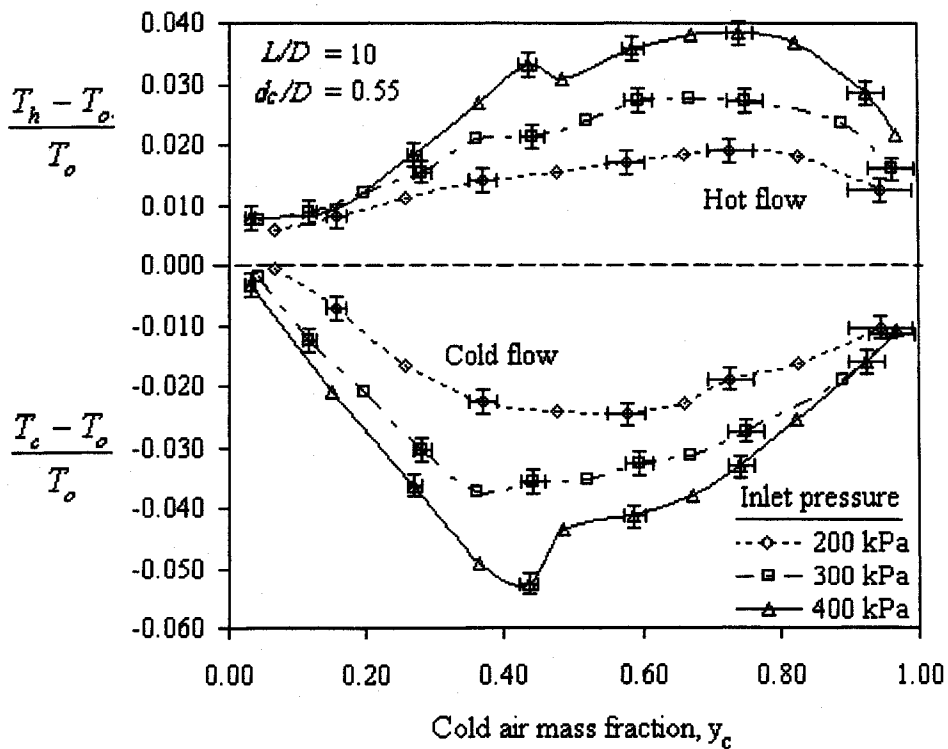
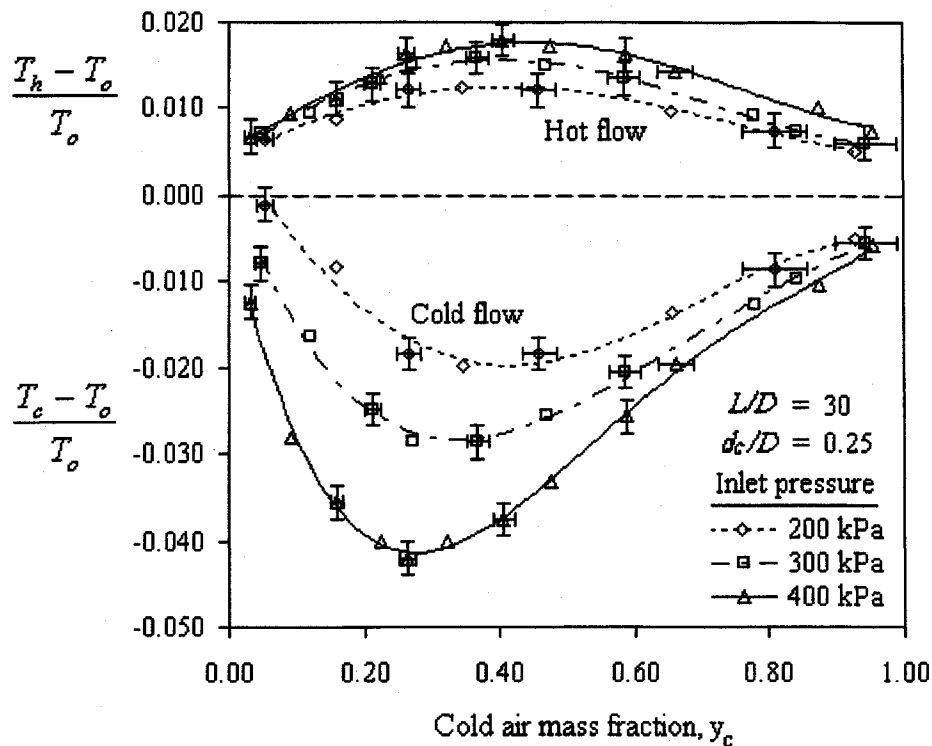


Figure 28 Vortex tube performance for  $L/D = 10$  and  $d_c/D = 0.55$



The results obtained for larger  $L/D$  ratios (Figures 29 to 34) show a smooth variation of the cold and the hot flow temperature for different inlet pressures and different values of  $y_c$ . No sharp increase in the cold flow temperature is observed. As a general observation, an increase in the inlet pressure is seen to cause the values of the dimensionless cold temperature difference to increase over the whole range of the cold air mass fraction. Furthermore, it is found that the cold air mass ratio corresponding to the lowest cold air stream temperature decreases with the increasing of the supply pressure for similar tube geometry. Except for  $d_c/D = 0.25$ , it is not expected for  $y_c$  to reach the value of 0.3 as observed in conventional vortex tubes [41 and 42]. When the smallest orifice diameter is used, however, the  $y_c$  value obtained is found to be in the range of 0.2 to 0.4. This difference in the value of  $y_c$  appears to be related to the relative size of the inlet nozzle hydraulic diameter to the size of the orifice diameter used. Similarly, the maximum hot air temperatures seen to be at values of cold mass ratio different than those for the conventional devices.



**Figure 29** Vortex tube performance for  $L/D = 30$  and  $d_c/D = 0.25$

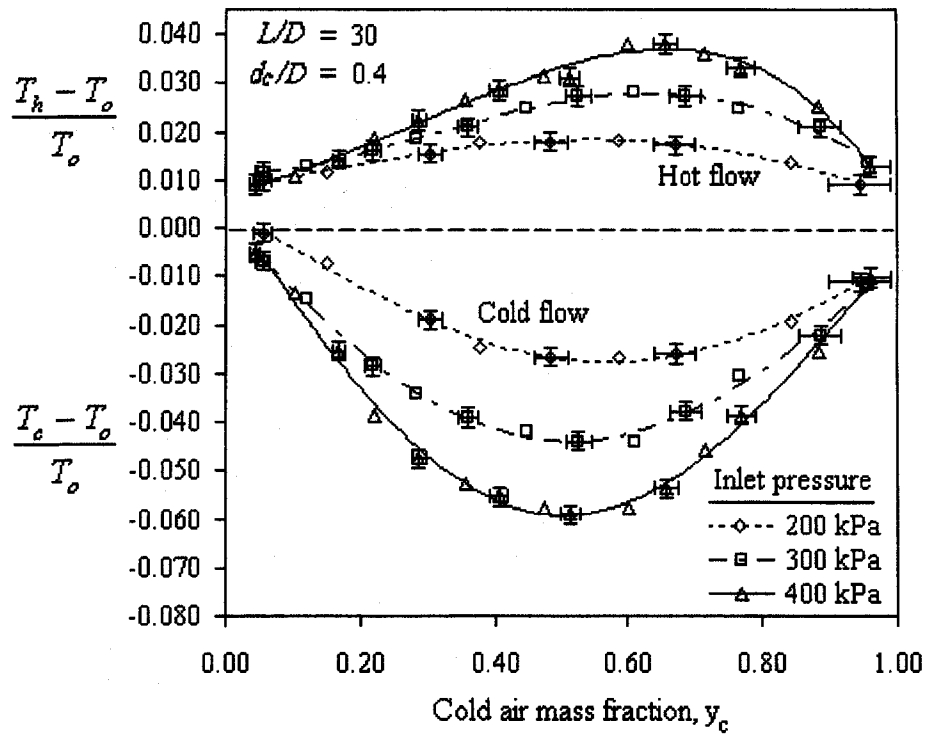


Figure 30 Vortex tube performance for  $L/D = 30$  and  $d_c/D = 0.4$

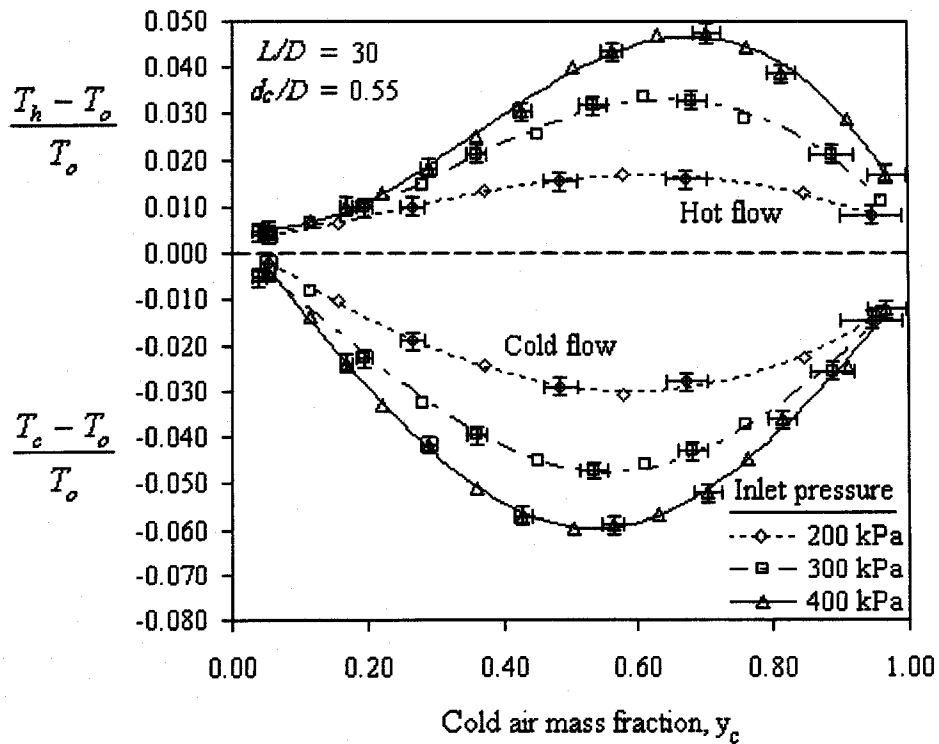


Figure 31 Vortex tube performance for  $L/D = 30$  and  $d_c/D = 0.55$

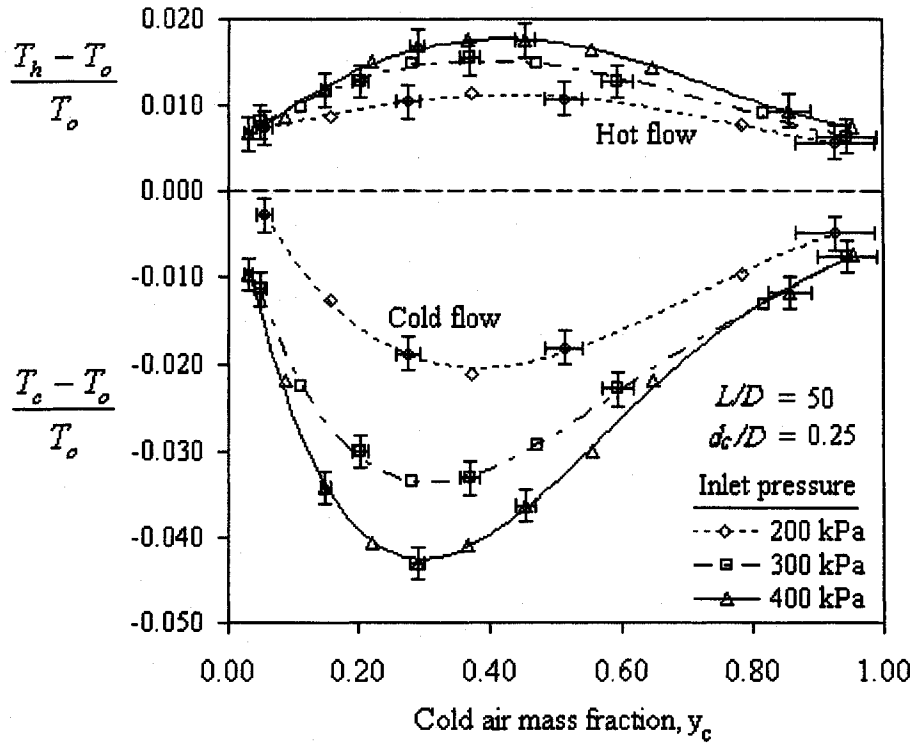


Figure 32 Vortex tube performance for  $L/D = 50$  and  $d_c/D = 0.25$

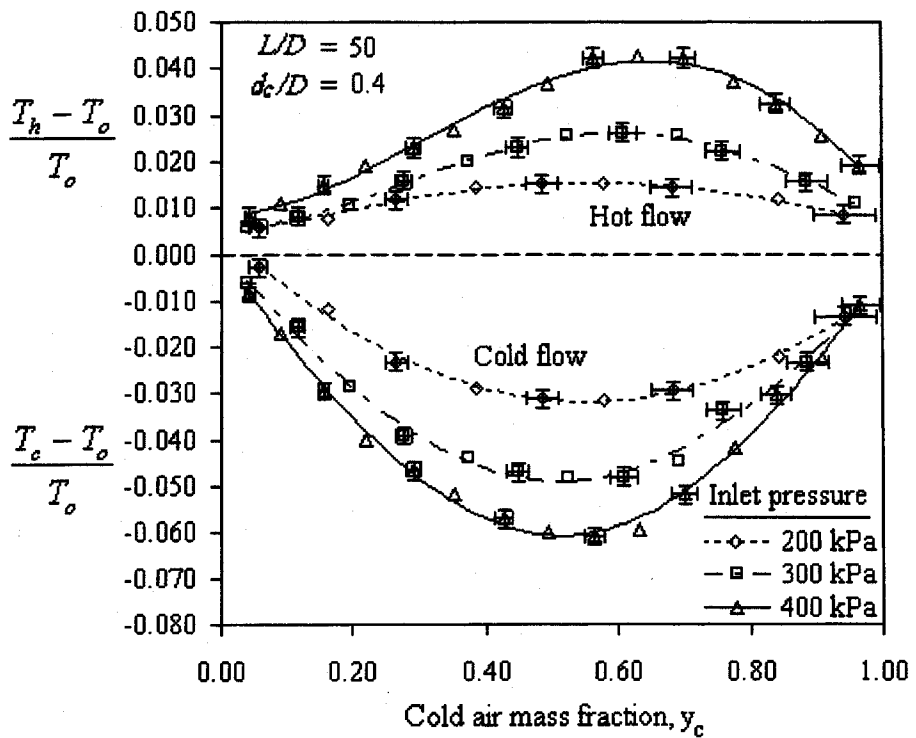
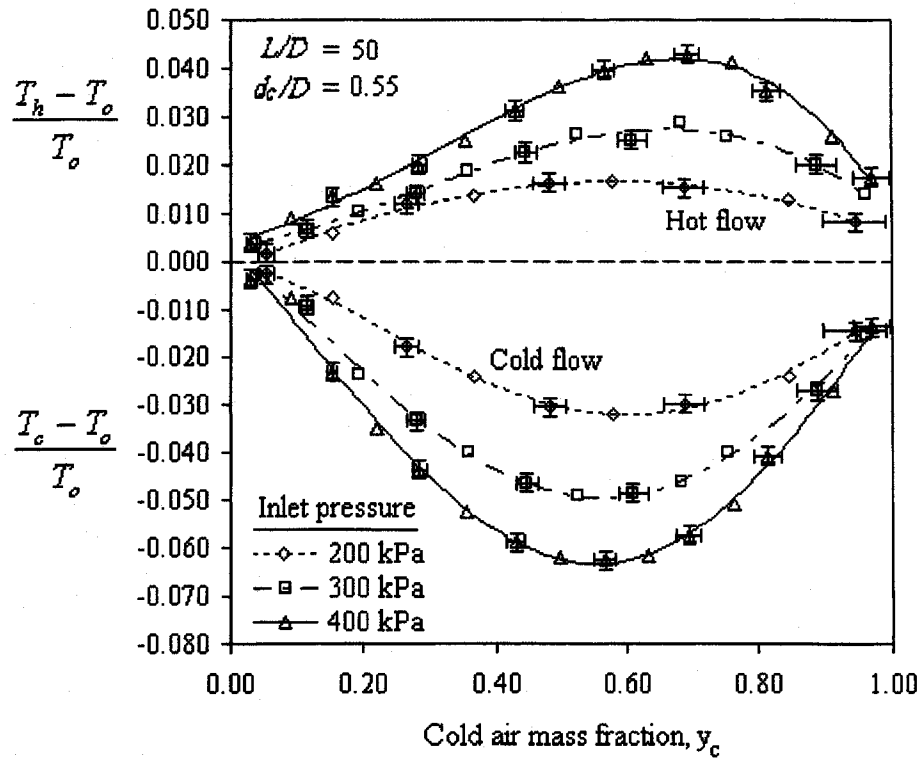
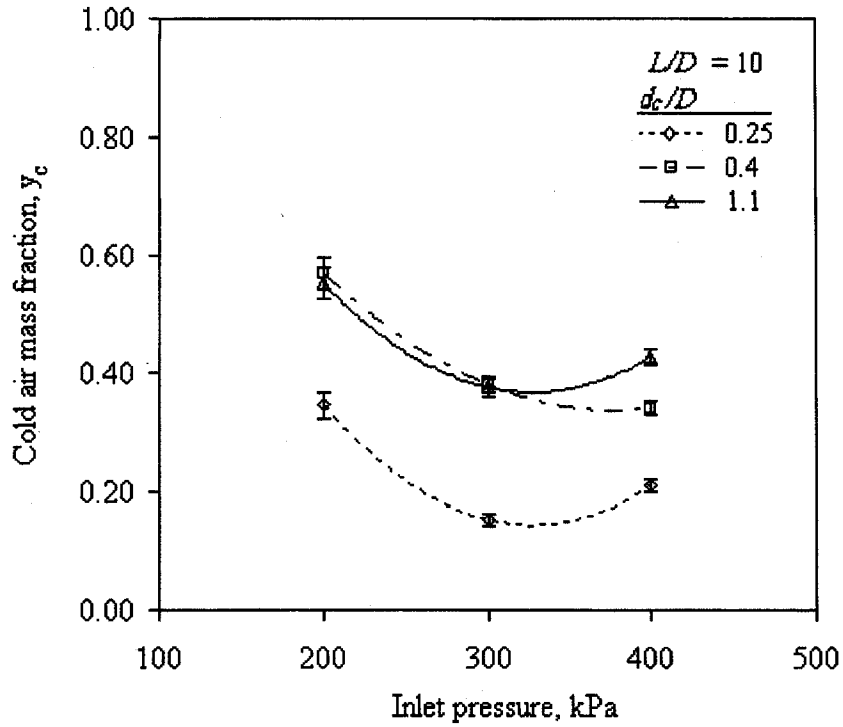


Figure 33 Vortex tube performance for  $L/D = 50$  and  $d_c/D = 0.4$



**Figure 34 Vortex tube performance for  $L/D = 50$  and  $d_c/D = 0.55$**

The optimum values of the cold air mass fraction,  $y_c$ , correspond to the lowest cold flow temperature and are presented in Figures 35 through 37. For  $L/D = 10$  and  $d_c/D = 0.25$  and  $1.1$ , the trend of the optimum cold air mass fraction change is similar (Figure 35). For  $d_c/D = 0.4$ , the value of the optimum cold air mass fraction is within the error bar of that for  $d_c/D = 1.1$  at  $200$  and  $300$  kPa inlet pressure, however, is different at an inlet pressure of  $400$  kPa. This may be due to the instabilities mentioned previously.



**Figure 35 Optimum cold air mass fraction vs. inlet pressure for  $L/D = 10$**

For  $L/D = 30$ , the optimum cold air mass fraction value changes in an approximately linear manner with the inlet pressure (Figure 36). The cases corresponding to  $L/D = 50$  are shown in Figure 37. The trends are also approximately linear with the slope approaching zero for large  $d_c/D$  values.

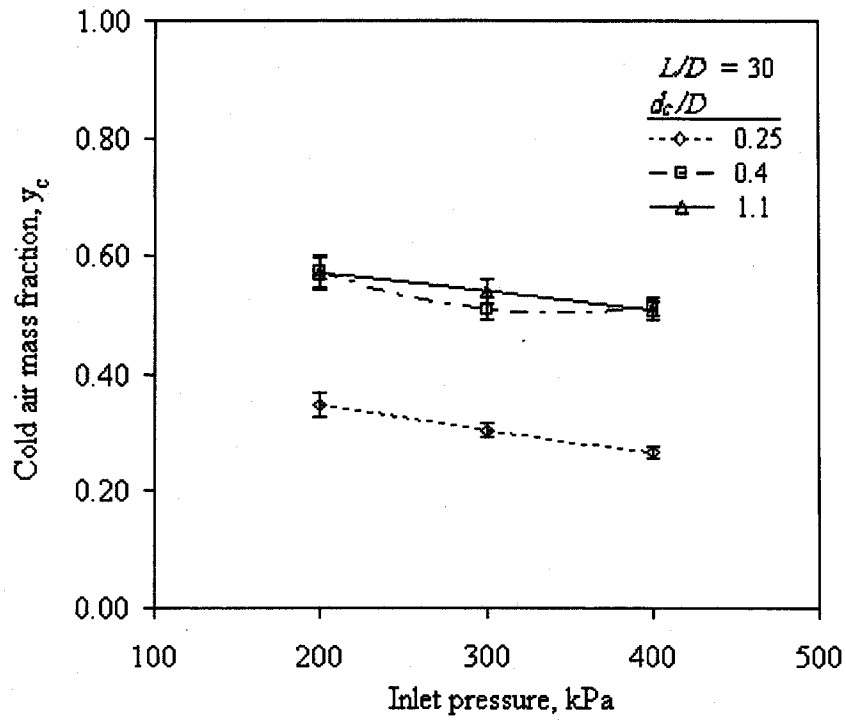


**Figure 36** Optimum cold air mass fraction vs. inlet pressure for  $L/D = 30$

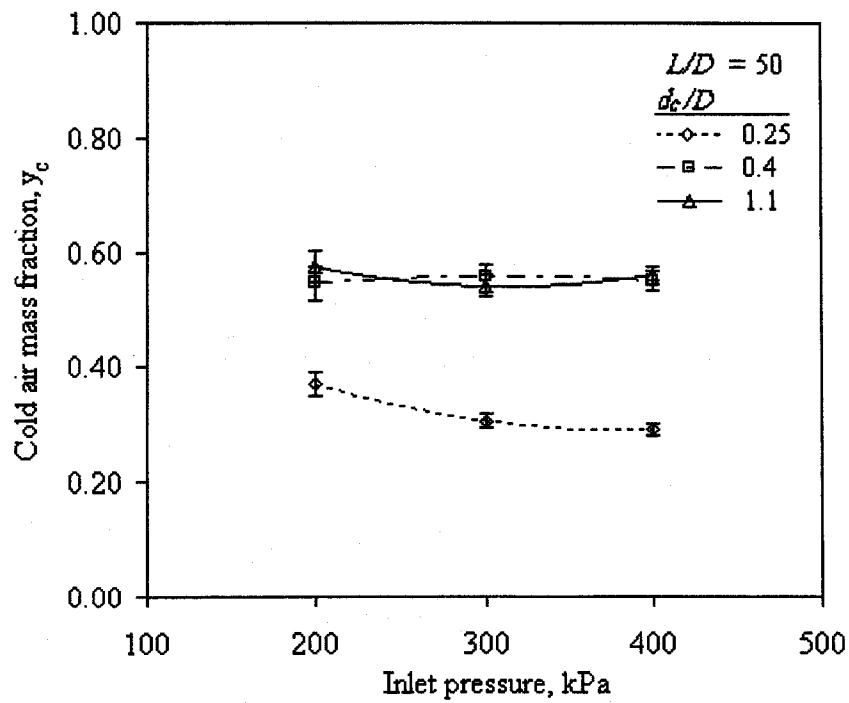


**Figure 37** Optimum cold air mass fraction vs. inlet pressure for  $L/D = 50$

### 4.3 Effect of Orifice Diameter

Figures 38 to 40 show the optimum dimensionless cold temperature performance of the micro-scale vortex tube for different sizes of the orifice diameter. In all cases the dimensionless cold temperature decreases with increasing  $d_c/D$  ratio reaching constant values at  $d_c/D$  in the range of 0.5 to 0.55. All the results obtained in optimizing the orifice diameter,  $d_c$ , are in good agreement with the conventional vortex tube [10,23]

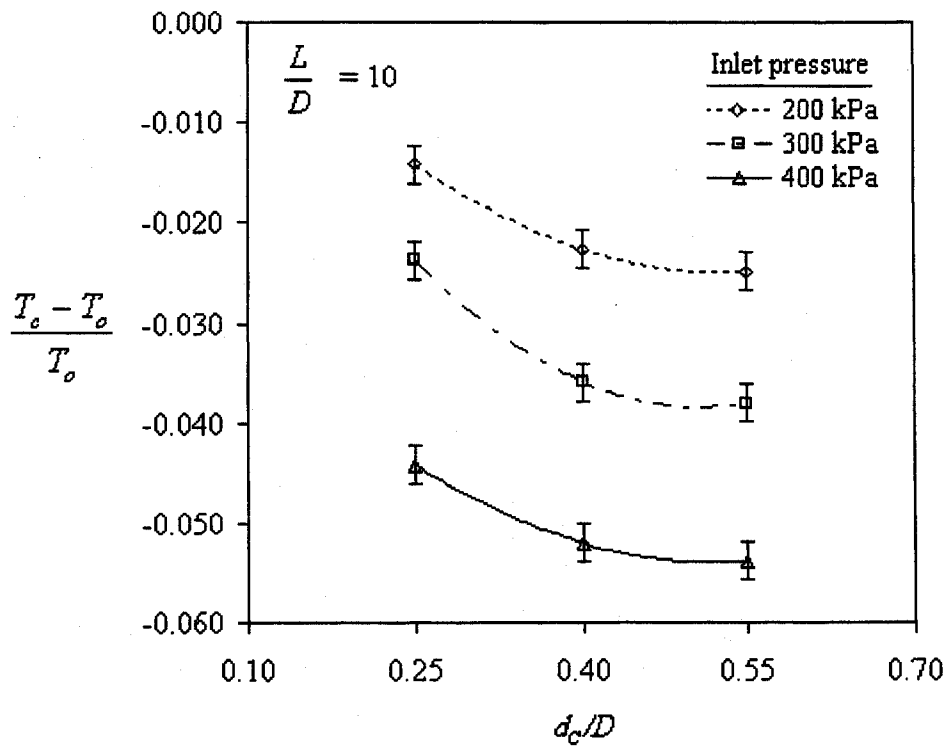


**Figure 38** Optimum conditions vs. dimensionless orifice diameter for  $L/D = 10$

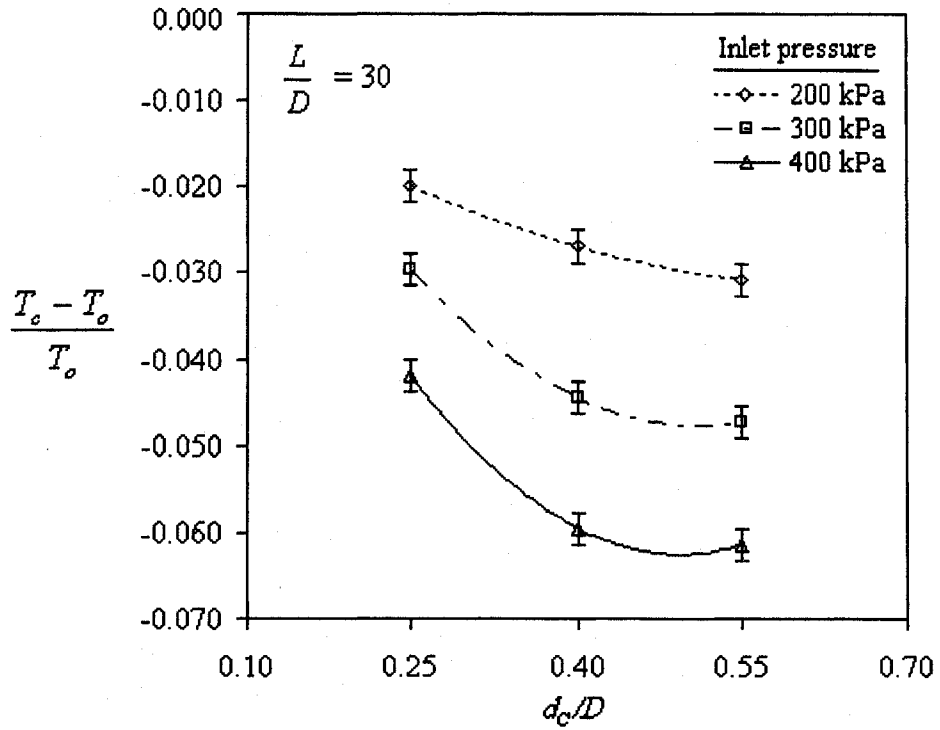


**Figure 39** Optimum conditions vs. dimensionless orifice diameter for  $L/D = 30$

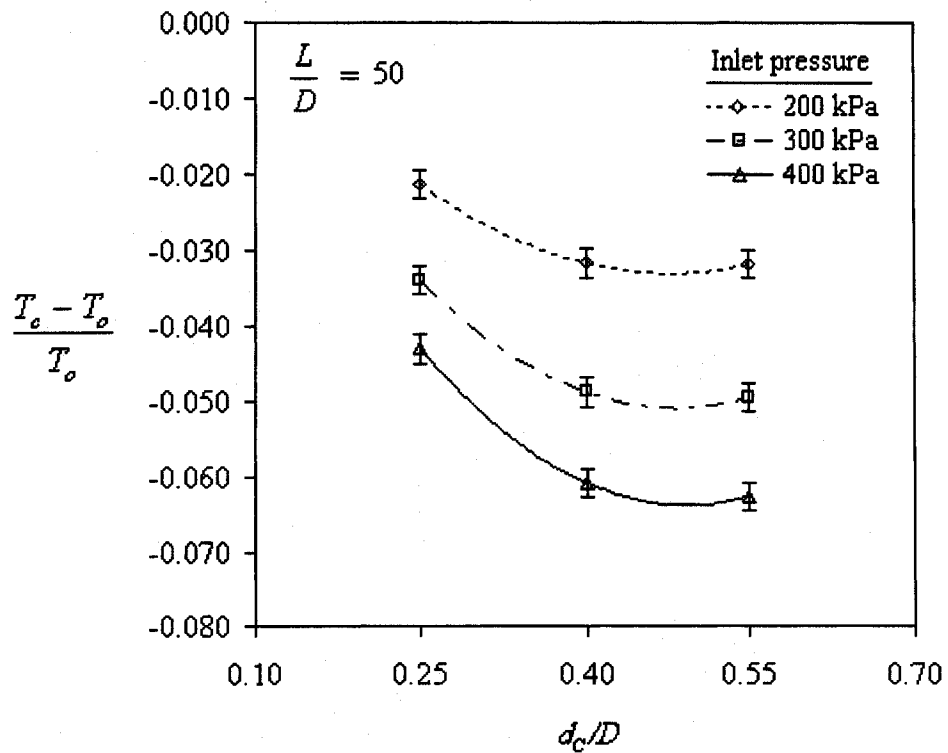


**Figure 40** Optimum conditions vs. dimensionless orifice diameter for  $L/D = 50$



#### 4.4 Effect of Tube Length

The effects the  $L/D$  ratio on optimum dimensionless cold temperature are shown in Figures 41 to 43. Except for a vortex tube with  $d_c/D = 0.25$  operated at 400 kPa inlet pressure, it can be generally observed that the maximum  $L/D$  ratio of 50 gives the maximum cold temperature drop. Although the curves do not indicate a mathematical optimum tube length, by looking to curve's trend, it can be inferred that increasing the  $L/D$  ratio beyond 50 will not be of great advantage. The results of the  $L/D$  value obtained are in a close agreement to that reported by Dyskin and Kramarenko [19] who also conducted their experiment on a micro-scale vortex tube.

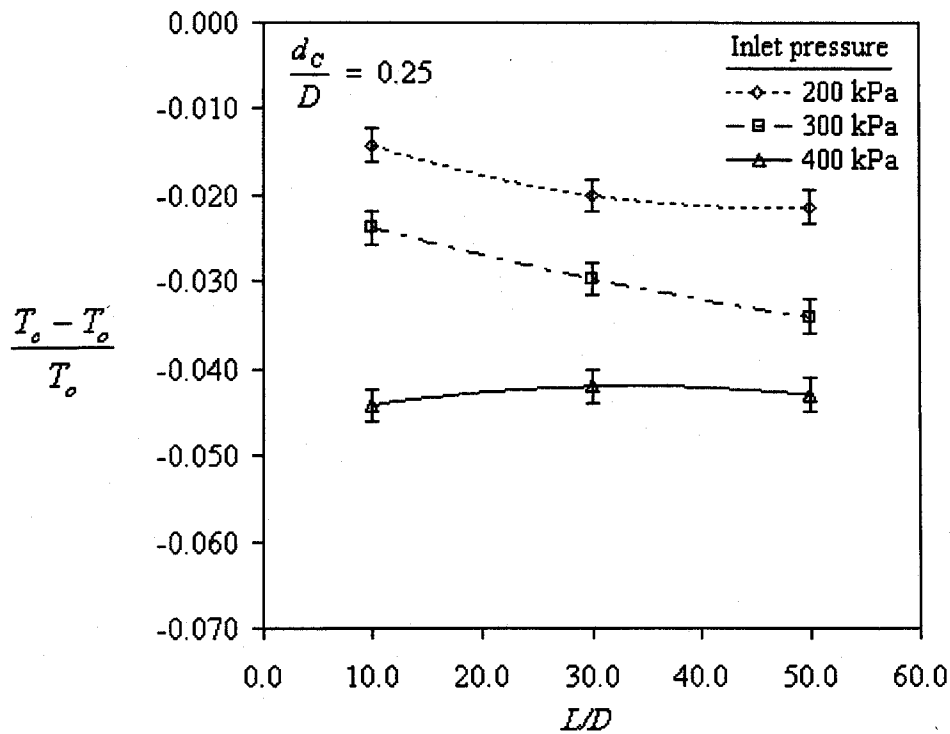


**Figure 41** Optimum conditions vs. dimensionless tube length for  $d_c/D = 0.25$

The cold temperature drop obtained at 400 kPa inlet pressure, 0.25  $d_c/D$  and 10  $L/D$  ratio was lower than that obtained for a larger  $L/D$  ratio. This inconsistency with the other results obtained at different tube's geometry may be attributed to the higher level of fluctuation taking place with that tube geometry as mentioned previously.

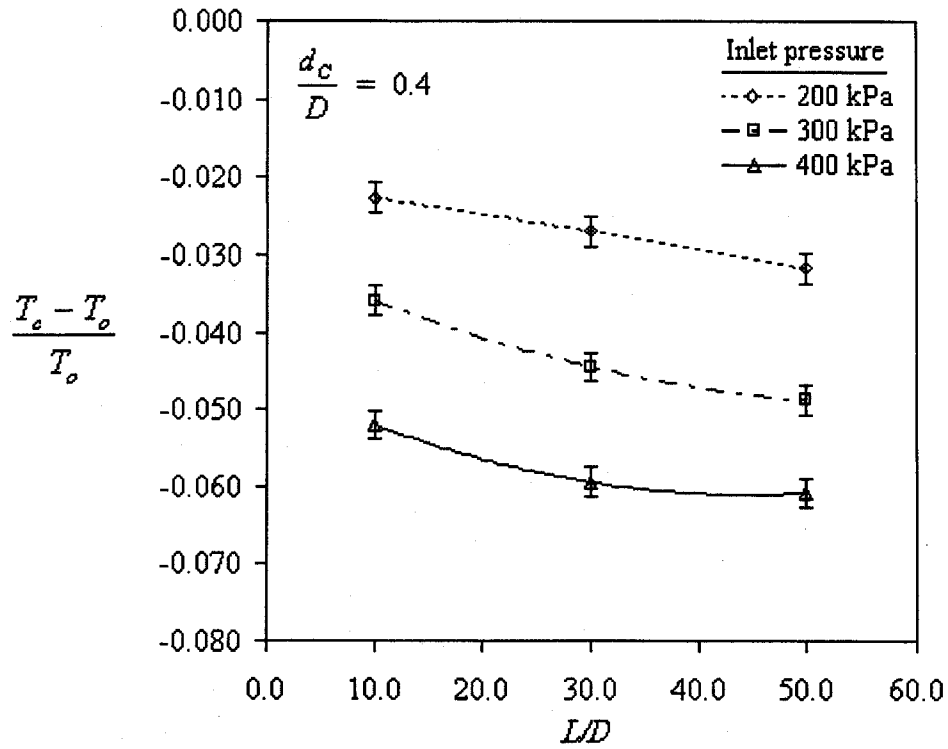


**Figure 42** Optimum conditions vs. dimensionless tube length for  $d_c/D = 0.40$

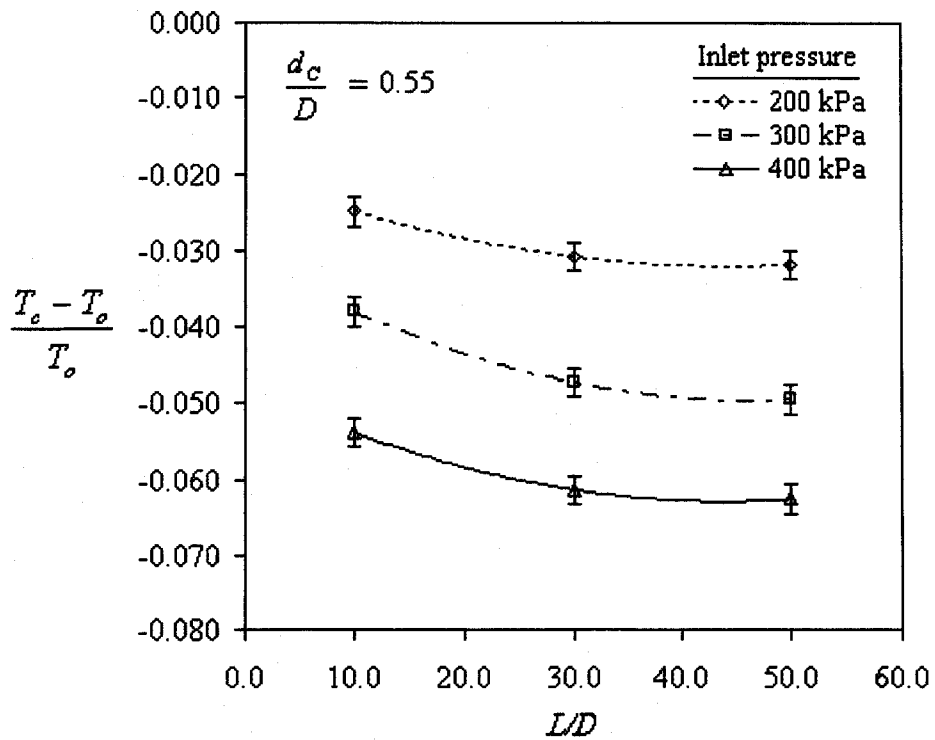


**Figure 43** Optimum conditions vs. dimensionless tube length for  $d_c/D = 0.55$

## CHAPTER 5 – CONCLUSIONS AND RECOMMENDATIONS

### 5.1 Conclusions

The performance characteristics of a micro-scale vortex tube are presented over a wide range of working pressure, different cold air mass ratio as well as different vortex tube length and orifice diameter. The following conclusions may be drawn:

1. Experiments conducted on the micro-scale vortex tube with fixed geometry at low Reynolds numbers have shown that:
  - Dimensionless temperature increases in both the cold and the hot air flows as the Reynolds number increases from zero and reaches maximum values before a Reynolds number of approximately 500 and 800 for the hot and cold flow respectively.
  - The cold outlet dimensionless temperature decreases steadily after the maximum to become negative at a Reynolds number in the order of 2000. This implies that the cooling effect occurs at inlet Reynolds numbers consistent with turbulent flow.
  - Except for low Reynolds numbers (i.e.: less than 2000) the cold mass fraction is approximately constant as the Reynolds number increases.
2. The experiment conducted to determine the performance curves of the micro-scale vortex tube at high inlet pressure indicate:
  - The optimum cold air mass fraction,  $y_c$ , is not constant and tends to be higher when compared with the conventional vortex tube.

- The effects of  $L/D$  and  $d_o/D$  ratios are similar to that in the conventional devices.
- Unstable operation is observed at small  $L/D$  and high inlet pressure.

## **5.2 Recommendations**

A further investigation of the flow instability noticed at small  $L/D$  and high inlet pressure is recommended in order to obtain more information on its nature of the flow.

It would be useful to instrument the micro-scale vortex tube with pressure transducer capable of measuring the pressure fluctuations that occur during that instability.

## REFERENCES

- [1] **P. Gravesen, J. Branebjerg and O.S. Jensen**, Microfluidics—a review. *J. Micromech. Microeng.*, 1993, **3**, pp. 168-182.
- [2] **G. J. Ranque**, Method and apparatus for obtaining from a fluid under pressure two currents of fluids at different temperatures. Application date December 6, 1932. U.S. patent number 1,952,281.
- [3] **G. J. Ranque**, Expériences sur la détente giratoire avec production simultanées d'un échappement d'air chaud et d'un échappement d'air froid, *Le journal de physique et le Radium*, 1933, **4**, pp. 112-115.
- [4] **R. Hilsch**, The use of expansion gases in centrifugal field as a cooling process. *The Review of Scientific Instruments*, 1947, **18**(2), pp. 108-113.
- [5] **C. D. Fulton**, Ranque's tube, *Refrigeration Engineering*, 1950, **5**, pp. 473 – 479.
- [6] **J. C. Maxwell**, *Theory of Heat*, Longman, Tenth Edition, London, UK, 1891, pp. 338-339.
- [7] **C. Ambrose**, Flash expansion in a Ranque-Hilsch vortex tube of a saturated liquid, Master thesis, 1964, Mechanical Engineering Department, University of Toronto.
- [8] **F. Hooper, C. Ambrose**. An improved expansion process for the vapor refrigeration cycle, *The 4<sup>th</sup> Canadian Congress of Applied Mechanics*, 1973, pp. 811 – 812.

- [9] **C. Gao**, Experimental study on the Ranque-Hilsch vortex tube, Ph.D. Dissertation, 2005, Department of Applied Physics, Eindhoven University of Technology, The Netherlands.
- [10] **T. Cockerill**, Thermodynamics and fluid mechanics of a Ranque-Hilsch vortex tube, Masters Thesis, 1998, Department of Engineering, University of Cambridge, England.
- [11] **R. Westley**, A bibliography and survey of the vortex tube, Cranfield College Note 9, 1954, College of Aeronautics.
- [12] **Y. Soni**, A parametric study of the Ranque-Hilsch tube. Ph.D. Dissertation, 1973 University of Idaho Graduate School, Idaho, U.S.A.
- [13] **R. Kassner and E. Knoernschild**, Friction laws and energy transfer in circular flow, Wright-Patterson Air Force Base, 1948, Technical Report No. F-TR-2198-ND.
- [14] **H. Dornbrand**, Theoretical and experimental study of vortex tube. Wright-Patterson Air Force Base, 1950, Technical Report No. 6123.
- [15] **R. G. Deissler and M. Perlmutter**, An analysis of the energy separation in laminar and turbulent compressible vortex flows. Heat Transfer and Fluid Mechanics Institute, 1958, Stanford University Press, pp. 40-53.
- [16] **R. G. Deissler and M. Perlmutter**, Analysis of the flow and energy separation in a turbulent vortex. *Int. J. Mass and Heat Transfer*, 1960, **1**, pp. 173-191.
- [17] **M. Kurosaka**, Acoustic streaming in swirling flow and the Ranque-Hilsch (vortex-tube) effect, *Journal of Fluid Mechanics*, 1982, **124**, pp.139–172.

- [18] **B. Ahlborn, J. Keller and E. Rebhan**, The heat pump in vortex tube, *Journal of Non-Equilibrium Thermodynamics*, 1998, **23**, pp.159-165.
- [19] **M. Dyskin and P. Kramarenko**, Energy characteristics of vortex micro tube, Translated from *Inzhenerno-Fizicheskii Zhurnal*, 1984, **47** (6), pp. 903-905.
- [20] **M. Negm, A. Seraj and S. Abull Ghani**, Generalized correlations for the process of energy separation in vortex tube, *Modeling, Simulation and Control*, ASME Press, 1988, **14** (4), pp. 47-64.
- [21] **Sh. A. Piralishvili and V. M. Polyaev**, Flow and thermodynamic characteristics of energy separation in a double-circuit vortex tube – An experimental investigation, *Experimental Thermal and Fluid Science*, 1996, **12**, pp. 399-410.
- [22] **J. J. Keyes, Jr**, An experiment study of gas dynamics in high velocity vortex flow, *Proceedings of the Heat Transfer and Fluid Mechanics Institute*, 1960, Stanford University, Oak Ridge National Laboratory, Tennessee, pp 31-46.
- [23] **M. H. Saidi and M. S. Valipour**, Experimental modeling of vortex tube refrigerator, *Applied Thermal Engineering*, 2003, **23**, pp. 1971-1980.
- [24] **M. Sibulkin**, Unsteady, viscous, circular flow, Part 3, Application to the Ranque-Hilsch vortex tube, *J. Fluid Mech.*, 1961, **12**, pp. 269 – 293.
- [25] **Y. Sonl and W. J. Thompson**, Optimal design of the Ranque-Hilsch vortex tube, *Transaction of ASME, Journal of Heat Transfer*, May 1975, pp. 316-317.

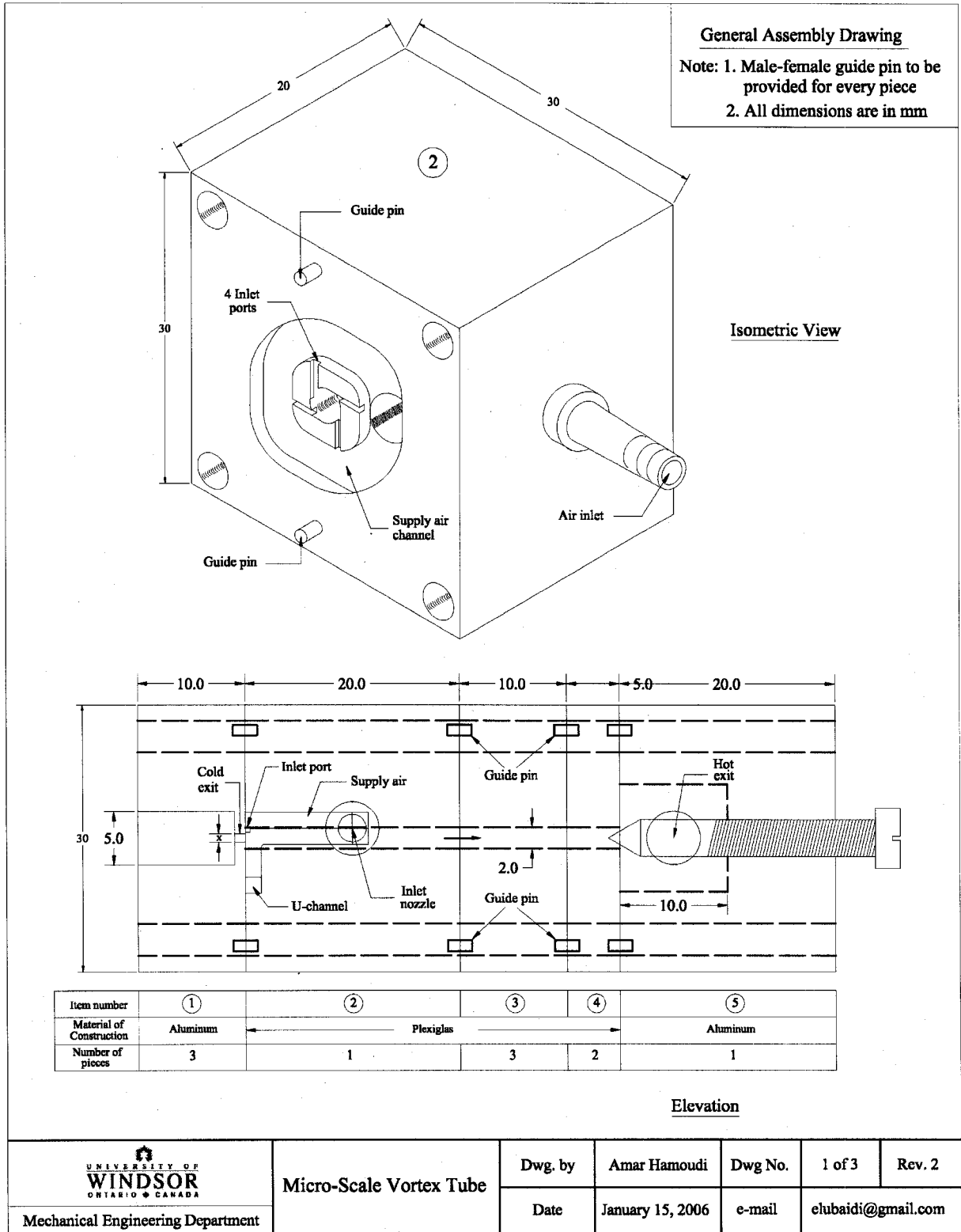
- [26] **J. P. Hartnett and E. R. Eckert.** Experimental study of the velocity and temperature distribution in a high velocity vortex type flow, Publication of the Heat Transfer Laboratory, University of Minnesota, Minneapolis, Minn., May 1957, pp. 751-758.
- [27] **H. Bruun.** Experimental investigation of the energy separation in vortex tube, Journal of Mechanical Engineering Science, 1969, **11** (6), pp. 567-582.
- [28] **B. Ahlborn and S. Groves.** Secondary flow in a vortex tube, Fluid Dynamic Research, 1997, **21**, pp. 73-86.
- [29] **F. Fitouri, M. Khan, H. Bruun,** A multi-position hot wire technique for the study of swirling flows in vortex chambers, Experimental Thermal and Fluid Science, 1995, **10**, pp. 142 – 151.
- [30] **E. Doebelin,** Measurement Systems: Application and Design 4<sup>th</sup> Ed., McGraw-Hill, 1990, New York, NY, Chapter 7, Section 1.
- [31] **R.C. Rudoff and W. D. Bachalo,** Seed particle response and size characterization in high-speed flows, Laser anemometry - Advances and applications, 1991, Proceedings of the 4<sup>th</sup> International Conference, Cleveland, OH, US, pp. 443-447
- [32] **C. Linderstrom-Lang,** Gas separation in the Ranque-Hilsch vortex tube, International Journal of Heat and Mass Transfer, 1964, **7**, pp. 1195 – 1206.
- [33] **M. R. Kulkarni and C. R. Sardesai,** Enrichment of Methane concentration via separation of gases using vortex tubes, Journal of Energy Engineering, 2002, **128** (1), pp. 1-12.
- [34] **K. Stephan, S. Lin, M. Durst, F. Huang, D. Seher,** A similarity relation for energy separation in a vortex tube, International Journal of Heat and Mass Transfer, 1984, **27** (6), pp. 911-920.



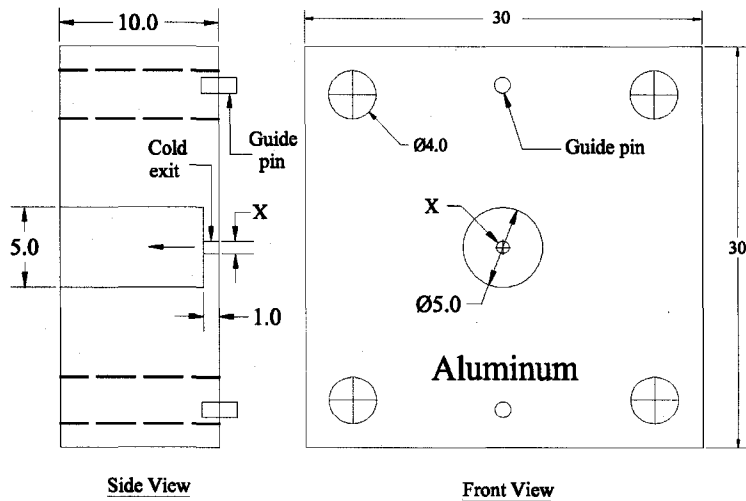
- [35] **R. T. Balmer**, Pressure-driven Ranque-Hilsch temperature separation in liquids, *Journal of Fluids Engineering*, 1988, **110** (2), pp. 161-164.
- [36] **A. J. Reynolds**, Energy flow in a vortex tube, *Z. Angew. Math. Phys.*, 1961, **12**, pp. 343–356.
- [37] **O. Hinze**, *Turbulence*, McGraw-Hill Series in Mechanical Engineering. 1975, McGraw-Hill, New York, NY, Second edition.
- [38] **W. Fröhlingsdorf and H. Unger**, Numerical investigation of the compressible flow and the energy separation in the Ranque-Hilsch vortex tube. *International Journal of Heat and Mass Transfer*, 1999, **42**, pp. 415-422.
- [39] **V. Bezprozvannykh and H. Mottl**, The Ranque-Hilsch Effect: CFD Modeling, The Eleventh Annual Conference of the CFD Society of Canada, Vancouver, BC, May 2003.
- [40] **U. Behera, P. Paul, S. Kasthuriengan, R. Karunanithi, S. Ram, K. Dinesh, S. Jacob**, CFD analysis and experimental investigations towards optimizing the parameters of Ranque–Hilsch vortex tube, *International Journal of Heat and Mass Transfer*, 2005, **48**, pp. 1961–1973.
- [41] **B. A. Shannak**, Temperature separation and friction losses in vortex tube, *Heat and Mass Transfer*, 2004, **40**, pp. 779–785.
- [42] **K. Stephan, S. Lin, M. Durst, F. Huang and D. Seher**. An investigation of energy separation in a vortex tube. *International Journal of Heat and Mass Transfer*, 1983, **26**, pp. 341-348.

- [43] **M. Moran, H. Shapiro, B. Munson and D. DeWitt**, Introduction to thermal system engineering, John Wiley & Sons, Indianapolis, IN, USA, 2002, Ch.7, pp 161-162.
- [44] **R. Figiolo and D. Beasley**, Theory and design for mechanical measurements, John Wiley & Sons, Indianapolis, IN, USA, 1991.
- [45] **S. Kline and F. McClintock**, Describing uncertainties in single-sample experiments”, Mechanical Engineering (1953), **75**, pp. 3-8.

# Appendix A – Micro-Scale Vortex Tube Design Drawing

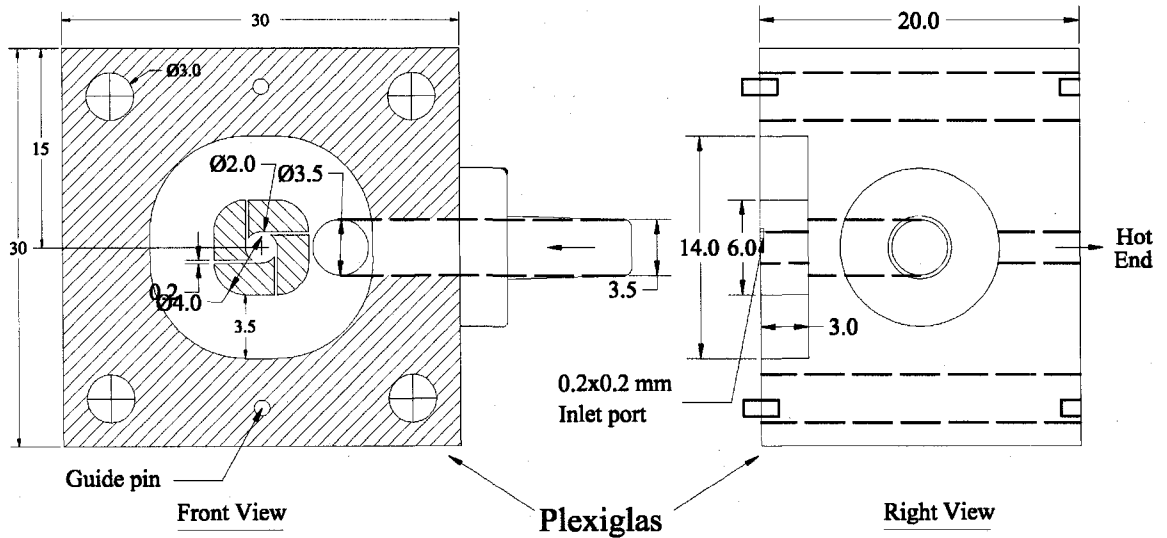



Item number	①
Material of Construction	Aluminum
Number of pieces	3
Orifice opening (X)	
X	0.7 mm
X	0.8 mm
X	0.9 mm

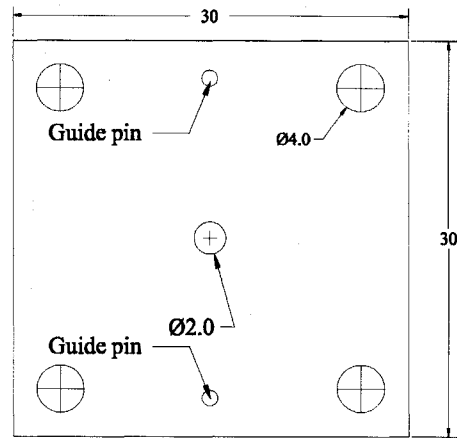
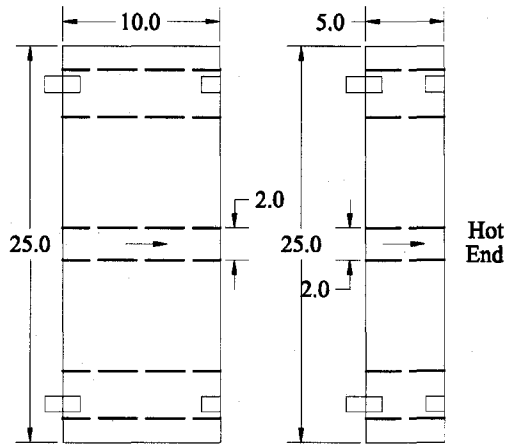


Item number	②
Material of Construction	Plexiglas
Number of pieces	1

Note: 1. Male-female guide pin to be provided for every piece  
 2. All dimensions are in mm

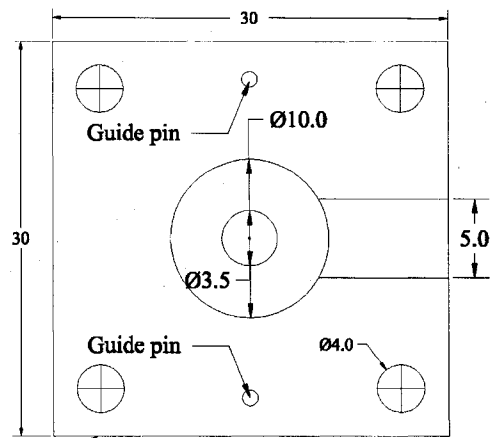
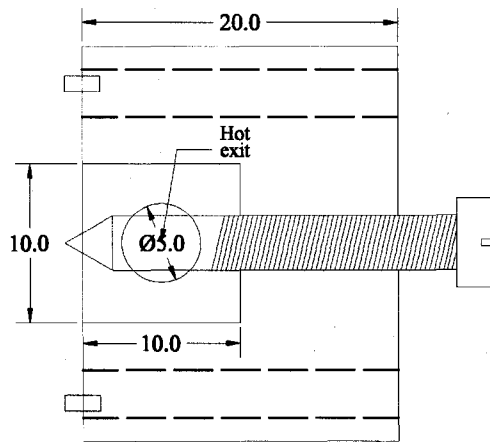
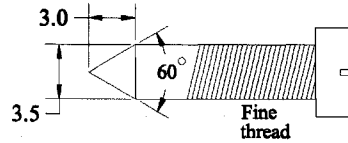



 UNIVERSITY OF WINDSOR ONTARIO • CANADA Mechanical Engineering Department	Micro-Scale Vortex Tube	Dwg. by	Amar Hamoudi	Dwg No.	2 of 3	Rev. 2
		Date	January 15, 2006	e-mail	elubaidi@gmail.com	



Item number	③		④
Material of Construction	Plexiglas		Plexiglas
Number of pieces	3		2

Item number	⑤
Material of Construction	Aluminum
Number of pieces	1



 <b>UNIVERSITY OF WINDSOR</b> ONTARIO • CANADA Mechanical Engineering Department	<b>Micro-Scale Vortex Tube</b>	Dwg. by	Amar Hamoudi	Dwg No.	3 of 3	Rev. 2
		Date	January 15, 2006	e-mail	clubaidi@gmail.com	

## Appendix B – Experimental Uncertainty Analysis Calculations

All major factors affecting the measurement accuracy are discussed in this section. With the precision of the measuring devices for each variable such as temperature, pressure and flow rates are known; the measurements uncertainty associated with each variable can be estimated. This method is based on the theoretical relationship of each variable.

The uncertainties of the instruments used are calculated using the formula given by Figiola and Beasley [44]:

$$u_d = \pm \sqrt{u_o^2 + u_c^2} \quad (11)$$

where  $u_c$  is the summation of errors in the instrument and are calculated using the following formula:

$$u_c = \pm \sqrt{e_1^2 + e_2^2 + \dots + e_K^2} \quad (12)$$

The method of Kline and McClintock [45] is used to determine the propagation of uncertainties.

### 1. Pressure Instruments

Three pressures gages having different ranges are used in this experiment. The low range (0 – 17.5 kPa) has an uncertainty of  $\pm 0.01$  kPa, the medium range (0 - 206.0 kPa), an uncertainty of  $\pm 1.7$  kPa and the high range pressure gage (0 – 413 kPa), an uncertainty of  $\pm 3.4$  kPa. The uncertainty of the barometric pressure gage is  $\pm 0.07$  kPa.

## 2. Temperature Instruments

The temperatures of the inlet, cold and hot air are measured using type - T (Copper Constantan) thermocouple probes. The increment and the accuracy of these devices are  $\pm 0.1$  °C and  $\pm 0.4$ °C respectively. The resolution,  $u_o$ , is calculated from:

$$u_o = \pm \frac{1}{2} \text{increment} \quad (13)$$

Therefore, the uncertainty for each of these devices is:

$$u_d = \pm \sqrt{0.05^2 + 0.4^2} = \pm 0.4 \text{ °C}$$

## 3. Uncertainty in Dimensionless Temperature

In order to estimate the uncertainty in dimensionless cold flow temperature,  $\frac{T_c - T_o}{T_o}$ , the Kline and McClintock method [45] is used:

$$U_{U_c} = \sqrt{\left(\frac{\partial U_c}{\partial T_c} u_{Tc}\right)^2 + \left(\frac{\partial U_c}{\partial T_o} u_{To}\right)^2} \quad (14)$$

$$U_{U_c} = \sqrt{\left(\frac{u_{Tc}}{T_o}\right)^2 + \left(\frac{T_c \times u_{To}}{T_o^2}\right)^2} \quad (15)$$

where  $U_c = \frac{T_c - T_o}{T_o} = \frac{T_c}{T_o} - 1$ , and  $\frac{\partial U_c}{\partial T_c} = \frac{1}{T_o}$

Equation 23 can also be used to calculate the uncertainty in the hot flow dimensionless temperature. The estimated uncertainty values for the hot and cold flow dimensionless temperature are presented in Appendix B and C. They are also

indicated in the graphs for the low and high pressure tests in forms of error bars. For the low and high pressure tests, however, the uncertainty in the cold and hot dimensionless temperature is  $\pm 0.0019$ .

#### 4. Uncertainty in Flow Rate Measurements

Four rotameters are used in measuring the hot and cold flow rate. The uncertainties in each of them are:

- Rotameter 1 =  $\pm 8.33 \times 10^{-7} \text{ m}^3/\text{sec}$
- Rotameter 2 =  $\pm 8.33 \times 10^{-7} \text{ m}^3/\text{sec}$
- Rotameter 3 =  $\pm 1.67 \times 10^{-6} \text{ m}^3/\text{sec}$
- Rotameter 4 =  $\pm 5.83 \times 10^{-6} \text{ m}^3/\text{sec}$

Rotameters 1 and 2 were used together to measure the total flow rate entering the micro-scale device in the low pressure tests. Therefore, the uncertainty is:

$$u_d = \pm \sqrt{(8.33 \times 10^{-7})^2 + (8.33 \times 10^{-7})^2}$$

$$= \pm 1.178 \times 10^{-6} \text{ m}^3/\text{sec}$$

For the high pressure tests, rotameters 3 and 4 are used together to measure the total flow rate. Therefore, the uncertainty is:

$$u_d = \pm \sqrt{(1.67 \times 10^{-6})^2 + (5.83 \times 10^{-6})^2}$$

$$= \pm 6.06 \times 10^{-6} \text{ m}^3/\text{sec}$$

#### 5. Uncertainty in Tube Geometry Measurements

The micro-scale vortex tube, manufactured at the University of Windsor, has a tolerance of  $\pm 0.013 \text{ mm}$ . Therefore, the uncertainty in  $d_c/D$  ratio is:



$$\frac{U_{d_c/D}}{d_c/D} = \sqrt{\left(\frac{U_{d_c}}{d_c}\right)^2 + \left(\frac{U_D}{D}\right)^2} \quad (16)$$

The uncertainty in the  $d_c/D$  ratio is found to be  $\pm 0.007$ . They are not indicated in Figures 37 through 39 because they are within the size of the symbol of the  $d_c/D$ . Applying the same above method, the uncertainty in the  $L/D$  ratio is:

$$\frac{U_{L/D}}{L/D} = \sqrt{\left(\frac{U_L}{L}\right)^2 + \left(\frac{U_D}{D}\right)^2} \quad (17)$$

The uncertainties in the  $L/D$  ratio are found to be in the range of  $\pm 0.065$  to  $0.325$  mm. There is also no indication of the uncertainties in Figures 40 through 42 because the error bars for such a small values are smaller than the symbol representing the  $L/D$  values.

## 6. Uncertainty in Air Viscosity Calculations

From viscosity data taken from Moran et al. [43], the variation of viscosity with temperatures was found to have a slope of  $5 \times 10^{-8}$  kg/m.s. K in the temperature range of these experiments. Since the temperature of the inlet air varied within 4 K, then the uncertainty in viscosity is:

$$4 \times 5 \times 10^{-8} = \pm 2 \times 10^{-7} \text{ kg/m.s}$$

## 7. Uncertainty in Air Density Calculations

The uncertainty in the inlet air density,  $\rho = \frac{P_o}{R T_o}$ , is calculated as follow:

$$U_\rho = \sqrt{\left(\frac{\partial \rho}{\partial P} \times U_P\right)^2 + \left(\frac{\partial \rho}{\partial T} \times U_T\right)^2} \quad (18)$$

$$U_{\rho} = \rho \sqrt{\left(\frac{U_P}{P}\right)^2 + \left(\frac{U_T}{T}\right)^2} \quad (19)$$

Assuming that the uncertainty in the gas constant,  $R$ , is negligible this gives an uncertainty in density of  $\pm 2.3 \times 10^{-3} \text{ kg/ m}^3$ .

## 8. Reynolds Number calculations, $Re$

The Reynolds number is defined as:

$$Re = \frac{\dot{m} d_n}{4 A \mu} \quad (20)$$

where  $d_n$  is the hydraulic diameter of the inlet nozzle and  $A$  is the cross-sectional area of the inlet nozzle. The propagation of uncertainties to Reynolds number is calculated using the method of Kline and McClinton [45]:

$$\frac{U_{Re}}{Re} = \sqrt{\left(\frac{U_{\rho}}{\rho}\right)^2 + \left(\frac{U_{\dot{Q}}}{\dot{Q}}\right)^2 + \left(\frac{U_{dn}}{dn}\right)^2 + \left(\frac{U_{\mu}}{\mu}\right)^2} \quad (21)$$

The uncertainties to Reynolds number are presented in Appendix C and D. It is also indicated as an error bars in the graphs of the Reynolds number versus dimensionless temperature, inlet pressure and the cold air mass fraction. They are found in the range of  $\pm 74$  to 196.

## 9. Uncertainty in Cold Air Mass Fraction

The uncertainty in the cold mass flow rate,  $\dot{m}_c$ , as a function of the air flow rate,  $\dot{Q}_c$ , and the gas density,  $\rho$  is:

$$U_{\dot{m}_c} = \sqrt{\left(\frac{\partial \dot{m}_c}{\partial \dot{Q}_c} U_{\dot{Q}_o}\right)^2 + \left(\frac{\partial \dot{m}_c}{\partial \rho_c} U_{\rho_c}\right)^2} \quad (22)$$

For the low pressure tests, the value is  $\pm 10^{-6}$  kg/s and for the high pressure tests it is  $\pm 2 \times 10^{-6}$  kg/s.

The uncertainty in the inlet mass flow rate,  $\dot{m}_o$ , is:

$$U_{\dot{m}_o} = \sqrt{\left(\frac{\partial \dot{m}_o}{\partial \dot{Q}_o} U_{\dot{Q}_o}\right)^2 + \left(\frac{\partial \dot{m}_o}{\partial \rho_o} U_{\rho_o}\right)^2} \quad (23)$$

It is found to be  $\pm 1.4 \times 10^{-6}$  kg/s for the low pressure tests and  $\pm 7.3 \times 10^{-6}$  kg/s for the high pressure tests. Therefore, for the cold air mass fraction,  $y_c$ , it is:

$$U_{y_c} = \sqrt{\left(\frac{\partial y_c}{\partial \dot{m}_c} U_{\dot{m}_c}\right)^2 + \left(\frac{\partial y_c}{\partial \dot{m}_o} U_{\dot{m}_o}\right)^2} \quad (24)$$

Since  $y_c = \frac{\dot{m}_c}{\dot{m}_o}$ , then the above equation can be written in

$$U_{y_c} = \sqrt{\left(\frac{U_{\dot{m}_c}}{\dot{m}_o}\right)^2 + \left(\frac{\partial \dot{m}_c}{\partial \dot{m}_o^2} U_{\dot{m}_o}\right)^2} \quad (25)$$

The uncertainties in the cold air mass fraction for the low and high pressure tests are presented in Appendix C and D respectively. The values for the low pressure tests are within  $\pm 0.01$  to  $0.13$  while for the high pressure tests are within  $\pm 0.007$  to  $0.046$ .

**Table C.1** Low pressure test for tube length,  $L = 20$  mm and tube orifice diameter,  $d_c = 0.5$  mm

Inlet condition				Cold exit				Hot exit				$y_c$	Uncertainty results			
$P_o$ (kPa)	$T_o$ (°K)	Flow (kg/s) $\times 10^{-5}$	$Re$	Flow (kg/s) $\times 10^{-5}$	$P_c$ (kPa)	$T_c$ (°K)	$\frac{T_c - T_o}{T_o}$	Flow (kg/s) $\times 10^{-5}$	$P_h$ (kPa)	$T_h$ (°K)	$\frac{T_h - T_o}{T_o}$		$\frac{T_c - T_o}{T_o}$	$\frac{T_h - T_o}{T_o}$	$y_c$	$Re$
2.8	298.1	1.04	522	0.69	0.16	298.2	0.0004	0.35	0.16	298.4	0.0011	0.66	0.0019	0.0019	0.131	74
5.5	298.1	1.53	772	0.97	0.16	298.2	0.0004	0.56	0.16	298.4	0.0013	0.64	0.0019	0.0019	0.087	78
7.9	298.1	1.89	952	1.21	0.17	298.2	0.0004	0.68	0.17	298.5	0.0014	0.64	0.0019	0.0019	0.071	82
12.5	298.1	2.41	1214	1.53	0.17	298.2	0.0004	0.88	0.17	298.5	0.0014	0.63	0.0019	0.0019	0.055	88
17.5	298.1	2.93	1475	1.87	0.18	298.1	0.0003	1.06	0.17	298.5	0.0016	0.64	0.0019	0.0019	0.046	95
24.1	298.1	3.52	1774	2.25	0.18	298.0	-0.0001	1.28	0.17	298.5	0.0016	0.64	0.0019	0.0019	0.038	104
34.5	298.1	4.40	2215	2.83	0.35	297.9	-0.0004	1.57	0.35	298.6	0.0019	0.64	0.0019	0.0019	0.031	119
41.4	298.1	4.93	2481	3.17	0.35	297.7	-0.0011	1.76	0.35	298.7	0.0023	0.64	0.0019	0.0019	0.027	129
48.3	298.1	5.30	2670	3.34	0.36	297.5	-0.0018	1.96	0.36	298.8	0.0026	0.63	0.0019	0.0019	0.025	135
55.2	298.1	5.79	2915	3.68	0.36	297.4	-0.0021	2.11	0.36	298.8	0.0026	0.64	0.0019	0.0019	0.023	145
62.1	298.1	6.17	3108	3.89	0.37	297.2	-0.0028	2.28	0.37	299.0	0.0033	0.63	0.0019	0.0019	0.022	152
68.9	298.1	6.64	3344	4.20	0.38	297.1	-0.0031	2.44	0.37	299.1	0.0036	0.63	0.0019	0.0019	0.020	161
75.8	298.1	7.11	3581	4.51	0.38	297.0	-0.0035	2.60	0.37	299.2	0.0040	0.63	0.0019	0.0019	0.019	170
82.7	298.1	7.66	3856	4.90	0.39	296.8	-0.0042	2.77	0.39	299.3	0.0043	0.64	0.0019	0.0019	0.018	181

Table C.2 Low pressure test for tube length,  $L = 20$  mm and tube orifice diameter,  $d_c = 0.8$  mm

Inlet condition				Cold exit				Hot exit				$y_c$	Uncertainty results			
$P_o$ (kPa)	$T_o$ (°K)	Flow (kg/s) $\times 10^{-5}$	$Re$	Flow (kg/s) $\times 10^{-5}$	$P_c$ (kPa)	$T_c$ (°K)	$\frac{T_c - T_o}{T_o}$	Flow (kg/s) $\times 10^{-5}$	$P_h$ (kPa)	$T_h$ (°K)	$\frac{T_h - T_o}{T_o}$		$\frac{T_c - T_o}{T_o}$	$\frac{T_h - T_o}{T_o}$	$y_c$	$Re$
5.7	298.5	1.68	846	1.33	0.17	298.7	0.0008	0.35	0.16	298.8	0.0011	0.79	0.0019	0.0019	0.088	79
8.0	298.5	2.06	1039	1.61	0.17	298.7	0.0008	0.45	0.17	298.8	0.0013	0.78	0.0019	0.0019	0.071	84
12.5	298.5	2.67	1342	2.07	0.18	298.6	0.0006	0.59	0.17	298.8	0.0013	0.78	0.0019	0.0019	0.055	91
17.4	298.5	3.20	1612	2.50	0.18	298.6	0.0006	0.70	0.18	298.8	0.0013	0.78	0.0019	0.0019	0.046	99
24.1	298.5	3.86	1941	2.99	0.35	298.5	0.0003	0.86	0.35	298.8	0.0013	0.78	0.0019	0.0019	0.038	110
34.5	298.5	4.53	2280	3.50	0.36	298.2	-0.0008	1.03	0.36	298.8	0.0013	0.77	0.0019	0.0019	0.033	121
41.4	298.5	5.40	2717	4.19	0.37	297.9	-0.0018	1.21	0.37	299.0	0.0019	0.78	0.0019	0.0019	0.027	137
48.3	298.5	5.87	2954	4.54	0.38	297.7	-0.0026	1.33	0.37	299.1	0.0023	0.77	0.0019	0.0019	0.025	146
55.2	298.5	6.32	3180	4.88	0.39	297.5	-0.0031	1.43	0.39	299.2	0.0026	0.77	0.0019	0.0019	0.023	155
62.1	298.5	6.78	3415	5.24	0.40	297.2	-0.0041	1.55	0.40	299.2	0.0026	0.77	0.0019	0.0019	0.022	164
68.9	298.5	7.21	3631	5.59	0.41	297.0	-0.0048	1.62	0.41	299.3	0.0030	0.78	0.0019	0.0019	0.021	172
75.8	298.5	7.70	3877	5.95	0.42	296.7	-0.0058	1.75	0.42	299.4	0.0033	0.77	0.0019	0.0019	0.019	182
82.7	298.5	8.2	4126	6.31	0.43	296.4	-0.0069	1.89	0.42	299.6	0.0040	0.77	0.0019	0.0019	0.018	192

**Table C.3 Low pressure test for tube length,  $L = 20$  mm and tube orifice diameter,  $d_c = 1.1$  mm**

Inlet condition				Cold exit				Hot exit				$y_c$	Uncertainty results			
$P_o$ (kPa)	$T_o$ (°K)	Flow (kg/s) $\times 10^{-5}$	Re	Flow (kg/s) $\times 10^{-5}$	$P_c$ (kPa)	$T_c$ (°K)	$\frac{T_c - T_o}{T_o}$	Flow (kg/s) $\times 10^{-5}$	$P_h$ (kPa)	$T_h$ (°K)	$\frac{T_h - T_o}{T_o}$		$\frac{T_c - T_o}{T_o}$	$\frac{T_h - T_o}{T_o}$	$y_c$	Re
7.3	298.7	1.97	994	1.63	0.17	298.9	0.0008	0.35	0.17	299.0	0.0013	0.82	0.0019	0.0019	0.077	83
9.9	298.7	2.38	1200	1.93	0.18	298.9	0.0008	0.45	0.17	299.0	0.0013	0.81	0.0019	0.0019	0.063	87
12.4	298.7	2.71	1364	2.18	0.18	298.8	0.0004	0.53	0.18	299.0	0.0013	0.80	0.0019	0.0019	0.055	92
17.5	298.7	3.29	1659	2.63	0.19	298.7	0.0003	0.66	0.19	299.0	0.0013	0.80	0.0019	0.0019	0.045	101
24.1	298.7	3.97	1997	3.16	0.35	298.7	0.0001	0.81	0.35	299.1	0.0014	0.80	0.0019	0.0019	0.038	112
34.5	298.7	4.87	2450	3.84	0.37	298.3	-0.0011	1.03	0.37	299.1	0.0016	0.79	0.0019	0.0019	0.031	127
41.4	298.7	5.34	2686	4.19	0.38	298.1	-0.0018	1.15	0.37	299.1	0.0016	0.78	0.0019	0.0019	0.028	136
48.3	298.7	5.97	3005	4.70	0.38	297.9	-0.0024	1.27	0.39	299.2	0.0019	0.79	0.0019	0.0019	0.025	148
55.2	298.7	6.43	3238	5.06	0.39	297.6	-0.0035	1.38	0.40	299.3	0.0023	0.79	0.0019	0.0019	0.023	157
62.1	298.7	6.90	3472	5.41	0.40	297.4	-0.0041	1.49	0.40	299.4	0.0026	0.78	0.0019	0.0019	0.022	166
68.9	298.7	7.35	3699	5.77	0.41	297.1	-0.0052	1.58	0.41	299.6	0.0033	0.78	0.0019	0.0019	0.020	175
75.8	298.7	7.87	3962	6.21	0.42	296.9	-0.0058	1.66	0.42	299.7	0.0036	0.79	0.0019	0.0019	0.019	186
82.7	298.7	8.4	4229	6.63	0.44	296.6	-0.0068	1.77	0.44	299.8	0.0040	0.79	0.0019	0.0019	0.018	196

**Table C.4 Low pressure test for tube length,  $L = 60$  mm and tube orifice diameter,  $d_c = 0.5$  mm**

Inlet condition				Cold exit				Hot exit				$y_c$	Uncertainty results			
$P_o$ (kPa)	$T_o$ (°K)	Flow (kg/s) $\times 10^{-5}$	$Re$	Flow (kg/s) $\times 10^{-5}$	$P_c$ (kPa)	$T_c$ (°K)	$\frac{T_c - T_o}{T_o}$	Flow (kg/s) $\times 10^{-5}$	$P_h$ (kPa)	$T_h$ (°K)	$\frac{T_h - T_o}{T_o}$		$\frac{T_c - T_o}{T_o}$	$\frac{T_h - T_o}{T_o}$	$y_c$	$Re$
2.5	298.6	1.01	510	0.46	0.17	298.9	0.0009	0.56	0.17	299.1	0.0016	0.45	0.0019	0.0019	0.116	74
5.0	298.7	1.54	777	0.70	0.18	298.9	0.0008	0.84	0.17	299.1	0.0014	0.45	0.0019	0.0019	0.076	78
7.5	298.7	1.93	970	0.87	0.18	298.9	0.0008	1.06	0.19	299.0	0.0013	0.45	0.0019	0.0019	0.061	82
12.5	298.7	2.53	1275	1.12	0.20	298.8	0.0006	1.41	0.20	299.0	0.0013	0.44	0.0019	0.0019	0.046	89
17.5	298.7	3.08	1552	1.35	0.22	298.7	0.0003	1.74	0.22	299.0	0.0013	0.44	0.0019	0.0019	0.038	97
24.1	298.7	3.75	1885	1.63	0.23	298.6	-0.0002	2.12	0.24	299.1	0.0014	0.44	0.0019	0.0019	0.031	108
34.5	298.7	4.65	2340	2.01	0.26	298.3	-0.0011	2.64	0.26	299.1	0.0016	0.43	0.0019	0.0019	0.025	123
41.4	298.7	5.23	2633	2.22	0.29	298.1	-0.0019	3.01	0.29	299.2	0.0018	0.42	0.0019	0.0019	0.022	134
48.3	298.7	5.74	2890	2.44	0.31	297.8	-0.0028	3.30	0.30	299.2	0.0019	0.42	0.0019	0.0019	0.020	144
55.2	298.7	6.20	3121	2.64	0.32	297.6	-0.0035	3.56	0.32	299.3	0.0023	0.43	0.0019	0.0019	0.019	152
62.1	298.7	6.76	3403	2.90	0.35	297.3	-0.0045	3.86	0.35	299.5	0.0030	0.43	0.0019	0.0019	0.017	163
68.9	298.7	7.29	3670	3.18	0.36	297.1	-0.0052	4.11	0.35	299.6	0.0033	0.44	0.0019	0.0019	0.016	174
75.8	298.7	7.73	3890	3.35	0.36	296.7	-0.0065	4.38	0.36	299.7	0.0036	0.43	0.0019	0.0019	0.015	183

**Table C.5 Low pressure test for tube length,  $L = 60$  mm and tube orifice diameter,  $d_c = 0.8$  mm**

Inlet condition				Cold exit				Hot exit				$y_c$	Uncertainty results			
$P_o$ (kPa)	$T_o$ (°K)	Flow (kg/s) $\times 10^{-5}$	Re	Flow (kg/s) $\times 10^{-5}$	$P_c$ (kPa)	$T_c$ (°K)	$\frac{T_c - T_o}{T_o}$	Flow (kg/s) $\times 10^{-5}$	$P_h$ (kPa)	$T_h$ (°K)	$\frac{T_h - T_o}{T_o}$		$\frac{T_c - T_o}{T_o}$	$\frac{T_h - T_o}{T_o}$	$y_c$	Re
2.6	298.8	1.09	550	0.75	0.17	299.0	0.0008	0.35	0.17	299.1	0.0011	0.68	0.0019	0.0019	0.126	74
5.1	298.8	1.63	819	1.03	0.19	299.0	0.0008	0.59	0.19	299.1	0.0011	0.64	0.0019	0.0019	0.082	79
7.5	298.8	2.00	1009	1.27	0.20	298.9	0.0006	0.74	0.20	299.0	0.0009	0.63	0.0019	0.0019	0.066	83
12.5	298.8	2.69	1352	1.66	0.22	298.9	0.0006	1.02	0.22	299.0	0.0009	0.62	0.0019	0.0019	0.049	92
17.4	298.8	3.24	1632	1.99	0.24	298.8	0.0003	1.26	0.24	299.1	0.0011	0.61	0.0019	0.0019	0.040	100
24.1	298.8	3.92	1971	2.37	0.27	298.6	-0.0004	1.55	0.26	299.1	0.0013	0.61	0.0019	0.0019	0.033	111
34.5	298.8	4.76	2394	2.83	0.35	298.4	-0.0013	1.93	0.35	299.2	0.0014	0.59	0.0019	0.0019	0.027	125
41.4	298.8	5.33	2683	3.17	0.36	298.1	-0.0021	2.16	0.36	299.2	0.0016	0.59	0.0019	0.0019	0.024	136
48.3	298.8	5.95	2994	3.51	0.36	297.9	-0.0028	2.44	0.36	299.3	0.0019	0.59	0.0019	0.0019	0.022	148
55.2	298.8	6.49	3269	3.85	0.37	297.5	-0.0041	2.64	0.37	299.4	0.0023	0.59	0.0019	0.0019	0.020	158
62.1	298.8	7.06	3556	4.20	0.37	297.2	-0.0052	2.87	0.37	299.5	0.0026	0.59	0.0019	0.0019	0.018	169
68.9	298.8	7.49	3772	4.44	0.38	296.9	-0.0062	3.05	0.38	299.7	0.0033	0.59	0.0019	0.0019	0.017	178
75.8	298.8	7.98	4018	4.73	0.38	296.6	-0.0072	3.26	0.39	299.8	0.0036	0.59	0.0019	0.0019	0.016	188



**Table C.6 Low pressure test for tube length,  $L = 60$  mm and tube orifice diameter,  $d_c = 1.1$  mm**

Inlet condition				Cold exit				Hot exit				$y_c$	Uncertainty results			
$P_o$ (kPa)	$T_o$ (°K)	Flow (kg/s) $\times 10^{-5}$	$Re$	Flow (kg/s) $\times 10^{-5}$	$P_c$ (kPa)	$T_c$ (°K)	$\frac{T_c - T_o}{T_o}$	Flow (kg/s) $\times 10^{-5}$	$P_h$ (kPa)	$T_h$ (°K)	$\frac{T_h - T_o}{T_o}$		$\frac{T_c - T_o}{T_o}$	$\frac{T_h - T_o}{T_o}$	$y_c$	$Re$
3.0	298.6	1.21	611	0.87	0.17	298.7	0.0006	0.35	0.17	298.8	0.0009	0.71	0.0019	0.0019	0.116	75
5.5	298.6	1.69	853	1.14	0.19	298.7	0.0006	0.55	0.19	298.9	0.0011	0.67	0.0019	0.0019	0.081	80
8.0	298.6	2.10	1056	1.40	0.20	298.7	0.0006	0.70	0.20	298.9	0.0011	0.67	0.0019	0.0019	0.065	84
12.5	298.6	2.69	1356	1.80	0.22	298.7	0.0006	0.90	0.22	298.9	0.0013	0.67	0.0019	0.0019	0.051	92
17.4	298.6	3.28	1651	2.14	0.25	298.6	0.0003	1.14	0.25	299.0	0.0014	0.65	0.0019	0.0019	0.041	100
24.1	298.6	3.98	2001	2.58	0.28	298.5	-0.0001	1.40	0.29	299.0	0.0016	0.65	0.0019	0.0019	0.034	112
34.5	298.6	4.90	2468	3.16	0.35	298.2	-0.0011	1.74	0.35	299.0	0.0016	0.65	0.0019	0.0019	0.027	128
41.4	298.6	5.47	2756	3.50	0.36	298.0	-0.0018	1.97	0.36	299.1	0.0018	0.64	0.0019	0.0019	0.025	139
48.3	298.6	6.04	3039	3.85	0.37	297.7	-0.0028	2.19	0.37	299.1	0.0019	0.64	0.0019	0.0019	0.022	149
55.2	298.6	6.57	3307	4.19	0.37	297.4	-0.0038	2.37	0.37	299.2	0.0023	0.64	0.0019	0.0019	0.020	160
62.1	298.6	7.07	3560	4.51	0.38	297.1	-0.0048	2.56	0.37	299.3	0.0026	0.64	0.0019	0.0019	0.019	170
68.9	298.6	7.57	3812	4.81	0.38	296.8	-0.0060	2.76	0.39	299.5	0.0033	0.64	0.0019	0.0019	0.018	180
75.8	298.6	8.00	4029	5.08	0.39	296.4	-0.0072	2.93	0.39	299.6	0.0036	0.63	0.0019	0.0019	0.017	188

**Table C.7 Low pressure test for tube length,  $L = 100$  mm and tube orifice diameter,  $d_c = 0.5$  mm**

Inlet condition				Cold exit				Hot exit				$y_c$	Uncertainty results			
$P_o$ (kPa)	$T_o$ (°K)	Flow (kg/s) $\times 10^{-5}$	Re	Flow (kg/s) $\times 10^{-5}$	$P_c$ (kPa)	$T_c$ (°K)	$\frac{T_c - T_o}{T_o}$	Flow (kg/s) $\times 10^{-5}$	$P_h$ (kPa)	$T_h$ (°K)	$\frac{T_h - T_o}{T_o}$		$\frac{T_c - T_o}{T_o}$	$\frac{T_h - T_o}{T_o}$	$y_c$	Re
2.5	298.9	0.97	489	0.56	0.16	299.1	0.0008	0.42	0.17	299.2	0.0011	0.57	0.0019	0.0019	0.131	73
5.1	298.9	1.50	757	0.80	0.18	299.1	0.0008	0.70	0.17	299.2	0.0011	0.54	0.0019	0.0019	0.082	78
7.5	298.9	1.86	939	0.99	0.19	299.2	0.0009	0.88	0.19	299.3	0.0013	0.53	0.0019	0.0019	0.066	81
12.5	298.9	2.45	1234	1.30	0.20	299.1	0.0008	1.15	0.20	299.3	0.0014	0.53	0.0019	0.0019	0.050	88
17.5	298.9	2.97	1493	1.56	0.22	299.0	0.0004	1.40	0.22	299.3	0.0013	0.53	0.0019	0.0019	0.042	96
24.1	298.9	3.58	1804	1.89	0.24	298.9	0.0001	1.70	0.24	299.3	0.0013	0.53	0.0019	0.0019	0.034	105
34.5	298.9	4.43	2228	2.32	0.27	298.7	-0.0006	2.10	0.26	299.3	0.0014	0.52	0.0019	0.0019	0.028	119
41.4	298.9	5.02	2525	2.62	0.29	298.5	-0.0013	2.40	0.29	299.3	0.0014	0.52	0.0019	0.0019	0.025	130
48.3	298.9	5.47	2754	2.83	0.35	298.2	-0.0023	2.64	0.35	299.4	0.0018	0.52	0.0019	0.0019	0.023	138
55.2	298.9	6.05	3048	3.17	0.36	297.9	-0.0033	2.89	0.36	299.4	0.0018	0.52	0.0019	0.0019	0.020	150
62.1	298.9	6.66	3354	3.51	0.36	297.7	-0.0040	3.15	0.36	299.5	0.0021	0.53	0.0019	0.0019	0.019	161
68.9	298.9	7.09	3568	3.68	0.36	297.4	-0.0050	3.41	0.36	299.6	0.0023	0.52	0.0019	0.0019	0.017	170
75.8	298.9	7.45	3752	3.86	0.37	297.1	-0.0060	3.60	0.37	299.6	0.0024	0.52	0.0019	0.0019	0.017	177

**Table C.8 Low pressure test for tube length,  $L = 100$  mm and tube orifice diameter,  $d_c = 0.8$  mm**

Inlet condition				Cold exit				Hot exit				$y_c$	Uncertainty results			
$P_o$ (kPa)	$T_o$ (°K)	Flow (kg/s) $\times 10^{-5}$	Re	Flow (kg/s) $\times 10^{-5}$	$P_c$ (kPa)	$T_c$ (°K)	$\frac{T_c - T_o}{T_o}$	Flow (kg/s) $\times 10^{-5}$	$P_h$ (kPa)	$T_h$ (°K)	$\frac{T_h - T_o}{T_o}$		$\frac{T_c - T_o}{T_o}$	$\frac{T_h - T_o}{T_o}$	$y_c$	Re
2.6	298.1	1.09	547	0.70	0.18	298.2	0.0006	0.38	0.179	298.4	0.0013	0.65	0.0019	0.0019	0.124	74
5.0	298.1	1.59	800	0.96	0.19	298.2	0.0006	0.63	0.189	298.4	0.0013	0.60	0.0019	0.0019	0.082	79
7.5	298.1	1.99	1000	1.16	0.20	298.2	0.0006	0.83	0.199	298.4	0.0013	0.58	0.0019	0.0019	0.065	83
12.5	298.1	2.65	1336	1.50	0.22	298.2	0.0004	1.16	0.217	298.4	0.0011	0.56	0.0019	0.0019	0.048	91
17.4	298.1	3.19	1607	1.76	0.23	298.1	0.0003	1.44	0.234	298.3	0.0009	0.55	0.0019	0.0019	0.039	99
24.1	298.1	3.81	1920	2.04	0.25	298.0	-0.0001	1.77	0.254	298.4	0.0011	0.54	0.0019	0.0019	0.033	109
34.5	298.1	4.68	2358	2.48	0.29	297.7	-0.0011	2.21	0.286	298.5	0.0014	0.53	0.0019	0.0019	0.027	124
41.4	298.1	5.43	2731	2.84	0.35	297.3	-0.0025	2.59	0.354	298.5	0.0016	0.52	0.0019	0.0019	0.023	138
48.3	298.1	6.05	3046	3.18	0.36	297.0	-0.0035	2.87	0.359	298.6	0.0019	0.53	0.0019	0.0019	0.021	150
55.2	298.1	6.59	3320	3.45	0.36	296.7	-0.0045	3.14	0.364	298.7	0.0023	0.52	0.0019	0.0019	0.019	160
62.1	298.1	7.05	3551	3.66	0.37	296.4	-0.0055	3.39	0.369	298.8	0.0026	0.52	0.0019	0.0019	0.018	169
68.9	298.1	7.48	3763	3.87	0.37	296.0	-0.0069	3.61	0.374	298.9	0.0030	0.52	0.0019	0.0019	0.017	178
75.8	298.1	8.07	4064	4.22	0.38	295.6	-0.0082	3.85	0.376	299.1	0.0035	0.52	0.0019	0.0019	0.015	190

**Table C.9 Low pressure test for tube length,  $L = 100$  mm and tube orifice diameter,  $d_c = 1.1$  mm**

Inlet condition				Cold exit				Hot exit				$y_c$	Uncertainty results			
$P_o$ (kPa)	$T_o$ (°K)	Flow (kg/s) $\times 10^{-5}$	Re	Flow (kg/s) $\times 10^{-5}$	$P_c$ (kPa)	$T_c$ (°K)	$\frac{T_c - T_o}{T_o}$	Flow (kg/s) $\times 10^{-5}$	$P_h$ (kPa)	$T_h$ (°K)	$\frac{T_h - T_o}{T_o}$		$\frac{T_c - T_o}{T_o}$	$\frac{T_h - T_o}{T_o}$	$y_c$	Re
2.5	298.2	1.10	552	0.75	0.17	298.3	0.0004	0.35	0.17	298.5	0.0011	0.68	0.0019	0.0019	0.126	74
5.0	298.2	1.62	814	1.00	0.18	298.3	0.0006	0.61	0.18	298.5	0.0013	0.62	0.0019	0.0019	0.082	79
7.5	298.2	2.02	1015	1.21	0.19	298.3	0.0004	0.81	0.19	298.5	0.0011	0.60	0.0019	0.0019	0.064	83
12.5	298.2	2.70	1360	1.56	0.21	298.3	0.0004	1.14	0.21	298.5	0.0011	0.58	0.0019	0.0019	0.047	92
17.4	298.2	3.27	1646	1.87	0.23	298.2	0.0001	1.40	0.23	298.5	0.0013	0.57	0.0019	0.0019	0.039	100
24.1	298.2	4.00	2012	2.22	0.26	298.0	-0.0004	1.78	0.26	298.5	0.0013	0.56	0.0019	0.0019	0.032	112
34.5	298.2	4.96	2499	2.72	0.30	297.8	-0.0011	2.25	0.30	298.5	0.0013	0.55	0.0019	0.0019	0.025	129
41.4	298.2	5.53	2784	3.00	0.35	297.5	-0.0021	2.53	0.35	298.5	0.0013	0.54	0.0019	0.0019	0.023	140
48.3	298.2	6.14	3093	3.34	0.35	297.3	-0.0030	2.80	0.35	298.6	0.0016	0.54	0.0019	0.0019	0.021	151
55.2	298.2	6.50	3274	3.57	0.36	296.9	-0.0042	2.94	0.36	298.7	0.0018	0.55	0.0019	0.0019	0.019	158
62.1	298.2	7.13	3590	3.86	0.37	296.6	-0.0052	3.27	0.37	298.7	0.0019	0.54	0.0019	0.0019	0.018	171
68.9	298.2	7.73	3891	4.21	0.37	296.3	-0.0062	3.52	0.37	298.9	0.0026	0.54	0.0019	0.0019	0.016	183

**Table D.1 High pressure test for tube length,  $L = 20$  mm and tube orifice diameter,  $d_c = 0.5$  mm**

Inlet condition				Cold exit				Hot exit				$y_c$	Uncertainty results				
$P_o$	$T_o$ (°K)	Flow (kg/s) $\times 10^{-4}$	$Re$	Flow (kg/s) $\times 10^{-5}$	$P_c$ (kPa)	$T_c$ (°K)	$\frac{T_c - T_o}{T_o}$	Flow (kg/s) $\times 10^{-5}$	$P_h$ (kPa)	$T_h$ (°K)	$\frac{T_h - T_o}{T_o}$		$\frac{T_c - T_o}{T_o}$	$\frac{T_h - T_o}{T_o}$	$m_c \times 10^{-6}$	$m_o \times 10^{-6}$	$y_c$
200 (kPa)	296.7	1.59	7989	0.86	1.22	296.1	-0.0021	15.00	1.25	298.9	0.0074	0.05	0.0019	0.0019	2.022	7.281	0.013
	296.7	1.64	8249	2.55	1.16	293.8	-0.0100	13.83	1.15	300.2	0.0118	0.16	0.0019	0.0019	2.037	7.263	0.014
	296.7	1.58	7948	4.64	1.02	292.7	-0.0137	11.15	1.05	300.3	0.0121	0.29	0.0019	0.0019	2.044	7.283	0.019
	296.7	1.57	7924	5.89	0.99	292.6	-0.0141	9.85	0.97	299.7	0.0101	0.37	0.0019	0.0019	2.045	7.304	0.022
	296.7	1.51	7617	7.84	0.85	294.3	-0.0083	7.29	0.85	299.2	0.0084	0.52	0.0019	0.0019	2.033	7.303	0.028
	296.7	1.25	6283	10.10	1.04	295.2	-0.0052	2.34	1.00	298.7	0.0067	0.81	0.0019	0.0019	2.034	7.334	0.05
	296.7	1.18	5925	10.90	0.97	295.7	-0.0035	0.86	0.97	298.3	0.0054	0.93	0.0019	0.0019	2.031	7.329	0.06
300 (kPa)	296.7	2.21	11144	1.05	1.86	293.5	-0.0110	21.09	1.87	298.7	0.0067	0.05	0.0019	0.0019	2.053	7.338	0.009
	296.7	2.25	11343	3.30	1.68	289.7	-0.0236	19.23	1.67	299.9	0.0108	0.15	0.0019	0.0019	2.077	7.326	0.01
	296.7	2.18	10988	4.47	1.56	291.8	-0.0168	17.36	1.59	300.1	0.0115	0.2	0.0019	0.0019	2.061	7.319	0.012
	296.7	2.19	11023	6.66	1.39	291.5	-0.0178	15.24	1.39	300.2	0.0118	0.3	0.0019	0.0019	2.062	7.327	0.014
	296.7	2.18	10976	7.95	1.26	291.4	-0.0182	13.86	1.27	300.1	0.0115	0.36	0.0019	0.0019	2.061	7.333	0.015
	296.7	2.02	10157	9.65	1.05	293.4	-0.0113	10.53	1.05	299.3	0.0087	0.48	0.0019	0.0019	2.046	7.327	0.02
	296.7	1.89	9514	11.60	0.91	294.5	-0.0076	7.30	0.9	299.1	0.0081	0.61	0.0019	0.0019	2.039	7.32	0.026
	296.7	1.62	8172	13.90	1.05	295.7	-0.0035	2.34	1.05	299	0.0077	0.86	0.0019	0.0019	2.039	7.331	0.041
	296.7	1.51	7626	14.30	1.02	296	-0.0025	0.86	1.02	298.1	0.0047	0.94	0.0019	0.0019	2.037	7.329	0.048
400 (kPa)	296.9	2.91	14626	0.89	2.83	293.9	-0.0103	28.17	2.79	298.2	0.0043	0.03	0.0019	0.0019	2.069	7.422	0.007
	296.9	2.89	14524	3.17	2.55	288.4	-0.0287	25.69	2.52	299.2	0.0077	0.11	0.0019	0.0019	2.104	7.404	0.008
	296.8	2.91	14656	4.27	2.40	286.0	-0.0365	24.85	2.39	299.8	0.0101	0.15	0.0019	0.0019	2.119	7.401	0.008
	296.8	2.87	14454	6.23	2.19	284.0	-0.0434	22.48	2.17	300.7	0.0132	0.22	0.0019	0.0019	2.132	7.402	0.009
	296.8	2.80	14098	7.70	1.92	288.4	-0.0284	20.30	1.92	299.7	0.0098	0.28	0.0019	0.0019	2.095	7.395	0.01
	296.8	2.72	13671	9.76	1.65	288.9	-0.0267	17.40	1.64	299.6	0.0094	0.36	0.0019	0.0019	2.089	7.395	0.012
	296.8	2.48	12485	12.00	1.30	291.7	-0.0175	13.24	1.30	298.8	0.0067	0.47	0.0019	0.0019	2.066	7.375	0.016
	296.8	2.40	12081	13.00	1.09	293.0	-0.0130	10.55	1.10	298.7	0.0064	0.56	0.0019	0.0019	2.057	7.359	0.019
	296.8	2.29	11534	16.00	0.96	293.8	-0.0103	7.32	0.95	298.5	0.0057	0.68	0.0019	0.0019	2.054	7.353	0.024
	296.8	1.95	9793	17.30	1.06	295.2	-0.0055	2.18	1.07	298	0.0040	0.89	0.0019	0.0019	2.052	7.351	0.035
	296.8	1.91	9616	18.00	1.03	295.6	-0.0042	0.86	1.05	297.8	0.0033	0.96	0.0019	0.0019	2.051	7.344	0.038

**Table D.2 High pressure test for tube length,  $L = 20$  mm and tube orifice diameter,  $d_c = 0.8$  mm**

Inlet condition				Cold exit				Hot exit				$y_c$	Uncertainty calculations				
$P_o$	$T_o$ (°K)	Flow (kg/s) $\times 10^{-4}$	Re	Flow (kg/s) $\times 10^{-5}$	$P_c$ (kPa)	$T_c$ (°K)	$\frac{T_c - T_o}{T_o}$	Flow (kg/s) $\times 10^{-5}$	$P_h$ (kPa)	$T_h$ (°K)	$\frac{T_h - T_o}{T_o}$		$\frac{T_c - T_o}{T_o}$	$\frac{T_h - T_o}{T_o}$	$m_c \times 10^{-6}$	$m_o \times 10^{-6}$	$y_c$
200 (kPa)	296.3	1.63	8193	0.95	1.35	296.1	-0.0008	15.33	1.32	298.2	0.0064	0.06	0.0019	0.0019	2.02	7.30	0.013
	296.3	1.64	8275	3.24	1.15	293.2	-0.0107	13.20	1.15	299.4	0.0105	0.20	0.0019	0.0019	2.04	7.29	0.015
	296.3	1.67	8388	4.85	1.04	290.5	-0.0196	11.81	1.05	300.3	0.0135	0.29	0.0019	0.0019	2.06	7.30	0.018
	296.3	1.68	8447	6.30	0.99	290.2	-0.0206	10.48	0.97	300.4	0.0139	0.38	0.0019	0.0019	2.06	7.32	0.020
	296.3	1.66	8333	7.77	0.92	290.0	-0.0213	8.78	0.92	300.8	0.0152	0.47	0.0019	0.0019	2.06	7.33	0.024
	296.3	1.69	8491	9.62	0.83	289.6	-0.0226	7.25	0.82	301.1	0.0162	0.57	0.0019	0.0019	2.07	7.35	0.028
	296.3	1.69	8517	12.15	0.75	290.0	-0.0213	4.77	0.75	301.2	0.0166	0.72	0.0019	0.0019	2.07	7.38	0.034
	296.3	1.59	8010	13.92	0.98	292.2	-0.0141	2.00	0.97	300.3	0.0135	0.87	0.0019	0.0019	2.06	7.40	0.043
	296.3	1.57	7892	14.83	0.95	293.4	-0.0100	0.85	0.95	299.7	0.0115	0.95	0.0019	0.0019	2.05	7.38	0.046
300 (kPa)	296.6	2.10	10557	0.87	1.96	295.9	-0.0025	20.10	1.94	298.5	0.0064	0.04	0.0019	0.0019	2.04	7.34	0.010
	296.5	2.23	11240	2.59	1.85	291.9	-0.0158	19.74	1.77	299.0	0.0084	0.12	0.0019	0.0019	2.06	7.34	0.010
	296.4	2.24	11297	4.37	1.66	289.0	-0.0250	18.07	1.62	300.1	0.0125	0.19	0.0019	0.0019	2.08	7.33	0.011
	296.4	2.29	11503	7.16	1.36	286.0	-0.0352	15.69	1.37	302.1	0.0189	0.31	0.0019	0.0019	2.10	7.34	0.014
	296.4	2.25	11321	9.41	1.18	286.5	-0.0335	13.08	1.20	302.3	0.0196	0.42	0.0019	0.0019	2.10	7.36	0.017
	296.4	2.28	11453	11.74	1.07	286.6	-0.0332	11.01	1.07	304.1	0.0257	0.52	0.0019	0.0019	2.10	7.37	0.019
	296.4	2.32	11658	14.11	0.95	287.1	-0.0315	9.05	0.95	304.8	0.0281	0.61	0.0019	0.0019	2.10	7.38	0.021
	296.4	2.37	11916	15.89	0.88	288.0	-0.0284	7.78	0.87	305.1	0.0291	0.67	0.0019	0.0020	2.09	7.39	0.023
	296.4	2.32	11694	17.89	0.98	289.8	-0.0223	5.34	0.97	304.0	0.0254	0.77	0.0019	0.0019	2.09	7.41	0.026
	296.4	2.32	11658	19.18	1.03	292.3	-0.0141	3.98	1.02	302.6	0.0206	0.83	0.0019	0.0019	2.08	7.39	0.028
296.4	2.06	10389	19.79	0.97	293.9	-0.0086	0.85	1.00	301.1	0.0159	0.96	0.0019	0.0019	2.07	7.38	0.036	
400 (kPa)	296.2	2.82	14179	0.88	2.42	295.0	-0.0042	27.29	2.44	298.3	0.0071	0.03	0.0019	0.0019	2.05	7.39	0.007
	296.2	2.85	14364	3.51	2.20	288.5	-0.0260	25.03	2.23	299.0	0.0094	0.12	0.0019	0.0019	2.10	7.39	0.008
	296.1	2.75	13824	6.69	1.92	283.9	-0.0414	20.77	1.92	301.3	0.0176	0.24	0.0019	0.0019	2.13	7.38	0.010
	296.1	2.89	14550	8.85	1.75	281.5	-0.0493	20.06	1.73	302.9	0.0227	0.31	0.0019	0.0019	2.14	7.39	0.011
	296.0	2.92	14701	10.24	1.61	280.7	-0.0517	18.96	1.59	304.0	0.0268	0.35	0.0019	0.0020	2.15	7.39	0.012
	296.0	2.86	14385	11.97	1.44	284.5	-0.0390	16.61	1.44	303.2	0.0241	0.42	0.0019	0.0019	2.12	7.39	0.013
	296.0	2.89	14571	14.21	1.27	284.0	-0.0408	14.74	1.27	304.4	0.0282	0.49	0.0019	0.0020	2.13	7.41	0.015
	296.1	2.90	14579	16.03	1.19	284.6	-0.0390	12.93	1.17	305.6	0.0319	0.55	0.0019	0.0020	2.12	7.41	0.016
	296.1	2.91	14633	18.39	1.02	285.4	-0.0363	10.68	1.02	306.0	0.0333	0.63	0.0019	0.0020	2.12	7.42	0.018
	296.1	2.91	14650	20.33	1.15	287.3	-0.0298	8.77	1.15	306.3	0.0343	0.70	0.0019	0.0020	2.12	7.43	0.019
	296.1	2.92	14720	22.31	1.33	289.2	-0.0233	6.93	1.35	305.5	0.0316	0.76	0.0019	0.0020	2.11	7.44	0.021
	296.1	2.85	14323	24.29	1.54	291.5	-0.0158	4.16	1.54	303.9	0.0261	0.85	0.0019	0.0019	2.11	7.45	0.024
	296.1	2.65	13335	24.35	0.98	292.7	-0.0117	2.14	0.97	302.7	0.0220	0.92	0.0019	0.0019	2.09	7.40	0.027
	296.1	2.58	13011	25.00	0.98	294.0	-0.0073	0.85	0.97	301.1	0.0169	0.97	0.0019	0.0019	2.09	7.38	0.029

**Table D.3 High pressure test for tube length,  $L = 20$  mm and tube orifice diameter,  $d_c = 1.1$  mm**

Inlet condition				Cold exit				Hot exit				$y_c$	Uncertainty calculations				
$P_o$	$T_o$ (°K)	Flow (kg/s) $\times 10^{-4}$	$Re$	Flow (kg/s) $\times 10^{-5}$	$P_c$ (kPa)	$T_c$ (°K)	$\frac{T_c - T_o}{T_o}$	Flow (kg/s) $\times 10^{-5}$	$P_h$ (kPa)	$T_h$ (°K)	$\frac{T_h - T_o}{T_o}$		$\frac{T_c - T_o}{T_o}$	$\frac{T_h - T_o}{T_o}$	$m_c \times 10^{-6}$	$m_o \times 10^{-6}$	$y_c$
200 (kPa)	296.4	1.58	7947	1.03	1.23	296.2	-0.0008	14.80	1.20	298.2	0.0060	0.07	0.0019	0.0019	2.02	7.29	0.013
	296.3	1.62	8141	2.55	1.09	294.2	-0.0073	13.60	1.10	298.7	0.0081	0.16	0.0019	0.0019	2.03	7.29	0.014
	296.2	1.68	8462	4.31	0.99	291.3	-0.0168	12.50	1.00	299.5	0.0111	0.26	0.0019	0.0019	2.05	7.30	0.017
	296.1	1.66	8358	6.13	0.87	289.4	-0.0226	10.50	0.90	300.3	0.0142	0.37	0.0019	0.0019	2.07	7.32	0.020
	296.1	1.68	8436	7.98	0.83	288.9	-0.0243	8.78	0.82	300.7	0.0156	0.48	0.0019	0.0019	2.07	7.34	0.024
	296.1	1.71	8614	9.87	0.77	288.8	-0.0247	7.24	0.75	301.2	0.0169	0.58	0.0019	0.0019	2.07	7.36	0.028
	296.1	1.78	8945	11.80	0.71	289.3	-0.023	5.99	0.70	301.6	0.0183	0.66	0.0019	0.0019	2.07	7.38	0.030
	296.0	1.72	8635	12.50	0.67	290.4	-0.0189	4.64	0.67	301.7	0.0190	0.73	0.0019	0.0019	2.06	7.37	0.034
	296.0	1.64	8235	13.50	0.95	291.2	-0.0165	2.81	0.92	301.4	0.0180	0.83	0.0019	0.0019	2.07	7.41	0.040
296.0	1.58	7969	15.00	0.90	293.0	-0.0104	0.85	0.90	299.7	0.0125	0.95	0.0019	0.0019	2.06	7.39	0.046	
300 (kPa)	296.0	2.21	11112	0.96	1.82	295.5	-0.0018	21.10	1.82	298.2	0.0074	0.04	0.0019	0.0019	2.04	7.34	0.009
	296.0	2.22	11167	2.58	1.68	292.4	-0.0124	19.60	1.67	298.6	0.0088	0.12	0.0019	0.0019	2.06	7.34	0.010
	296.0	2.22	11151	4.35	1.45	289.8	-0.0209	17.80	1.52	299.6	0.0122	0.20	0.0019	0.0019	2.07	7.33	0.011
	296.0	2.21	11132	6.21	1.43	287.0	-0.0305	15.90	1.37	300.6	0.0156	0.28	0.0019	0.0019	2.09	7.35	0.013
	296.0	2.26	11361	8.13	1.26	284.9	-0.0375	14.40	1.27	302.2	0.0208	0.36	0.0019	0.0019	2.11	7.36	0.015
	296.0	2.27	11425	10.00	1.15	285.4	-0.0358	12.70	1.12	302.3	0.0212	0.44	0.0019	0.0019	2.11	7.38	0.017
	296.0	2.30	11589	12.00	1.02	285.5	-0.0355	11.00	1.02	303.1	0.0239	0.52	0.0019	0.0019	2.11	7.39	0.019
	296.0	2.34	11774	13.90	0.90	286.3	-0.0327	9.45	0.91	304.1	0.0273	0.60	0.0019	0.0020	2.10	7.40	0.021
	296.0	2.38	11962	16.00	0.86	286.7	-0.0314	7.80	0.85	304.2	0.0277	0.67	0.0019	0.0020	2.10	7.42	0.023
	296.0	2.40	12061	18.00	0.98	287.9	-0.0274	5.95	0.97	304.1	0.0271	0.75	0.0019	0.0020	2.10	7.44	0.025
	296.0	2.25	11322	20.00	0.97	290.4	-0.0189	2.47	0.97	303.1	0.0237	0.89	0.0019	0.0019	2.09	7.44	0.031
296.0	2.19	11016	21.00	0.91	292.7	-0.0114	0.85	0.93	300.7	0.0159	0.96	0.0019	0.0019	2.08	7.41	0.034	
400 (kPa)	296.1	2.82	14201	0.88	2.48	295.2	-0.0032	27.30	2.64	298.4	0.0077	0.03	0.0019	0.0019	2.05	7.40	0.007
	296.1	2.93	14742	4.38	2.30	289.9	-0.0209	24.90	2.27	298.8	0.0091	0.15	0.0019	0.0019	2.09	7.40	0.008
	296.1	2.88	14512	7.78	1.90	285.4	-0.0363	21.00	1.89	301.6	0.0183	0.27	0.0019	0.0019	2.12	7.38	0.010
	296.1	2.92	14677	10.60	1.66	281.5	-0.0493	18.50	1.64	304.1	0.0268	0.36	0.0019	0.0020	2.14	7.40	0.012
	296.1	2.89	14555	12.60	1.49	280.5	-0.0527	16.30	1.47	306.0	0.0333	0.44	0.0019	0.0020	2.15	7.41	0.013
	296.1	2.91	14661	14.10	1.34	283.3	-0.0435	15.00	1.35	305.3	0.0309	0.49	0.0019	0.0020	2.13	7.41	0.014
	296.1	2.97	14940	17.40	1.20	283.9	-0.0414	12.20	1.20	306.7	0.0356	0.59	0.0019	0.0020	2.13	7.43	0.016
	296.1	2.96	14885	19.90	1.10	284.9	-0.038	9.62	1.10	307.4	0.0380	0.67	0.0019	0.0020	2.13	7.45	0.018
	296.1	3.03	15249	22.50	1.34	286.3	-0.0332	7.75	1.35	307.5	0.0384	0.74	0.0019	0.0020	2.13	7.48	0.020
	296.1	3.00	15092	24.70	1.57	288.5	-0.0257	5.32	1.56	307.0	0.0367	0.82	0.0019	0.0020	2.13	7.49	0.022
	296.1	2.81	14159	26.00	1.00	291.4	-0.0162	2.13	1.00	304.6	0.0285	0.92	0.0019	0.0020	2.11	7.44	0.026
296.1	2.75	13824	26.60	0.96	293.0	-0.0107	0.85	0.97	302.6	0.0217	0.97	0.0019	0.0019	2.10	7.41	0.027	

**Table D.4 High pressure test for tube length,  $L = 60$  mm and tube orifice diameter,  $d_c = 0.5$  mm**

Inlet condition				Cold exit				Hot exit				$y_c$	Uncertainty calculations				
$P_o$	$T_o$ (°K)	Flow (kg/s) $\times 10^{-4}$	$Re$	Flow (kg/s) $\times 10^{-5}$	$P_c$ (kPa)	$T_c$ (°K)	$\frac{T_c - T_o}{T_o}$	Flow (kg/s) $\times 10^{-5}$	$P_h$ (kPa)	$T_h$ (°K)	$\frac{T_h - T_o}{T_o}$		$\frac{T_c - T_o}{T_o}$	$\frac{T_h - T_o}{T_o}$	$m_c \times 10^6$	$m_o \times 10^6$	$y_c$
200 (kPa)	297.0	1.61	8125	0.86	1.15	296.7	-0.0011	15.30	1.22	298.9	0.0064	0.05	0.0019	0.0019	2.02	7.28	0.013
	297.0	1.60	8051	2.54	1.10	294.6	-0.0083	13.40	1.10	299.6	0.0087	0.16	0.0019	0.0019	2.03	7.27	0.015
	297.0	1.61	8104	4.31	1.00	291.6	-0.0185	11.80	1.02	300.6	0.0121	0.27	0.0019	0.0019	2.05	7.28	0.018
	297.0	1.60	8065	5.55	0.95	291.1	-0.0198	10.50	0.95	300.7	0.0125	0.35	0.0019	0.0019	2.05	7.29	0.020
	297.0	1.58	7942	7.25	0.87	291.6	-0.0185	8.53	0.87	300.6	0.0121	0.46	0.0019	0.0019	2.05	7.31	0.025
	297.0	1.68	8454	11.00	0.74	293.0	-0.0137	5.77	0.72	299.9	0.0098	0.66	0.0019	0.0019	2.04	7.33	0.031
	297.0	1.32	6641	10.70	0.96	294.5	-0.0086	2.50	0.97	299.2	0.0074	0.81	0.0019	0.0019	2.04	7.34	0.048
	297.0	1.22	6128	11.30	0.92	295.5	-0.0052	0.86	0.92	298.5	0.0050	0.93	0.0019	0.0019	2.03	7.33	0.058
300 (kPa)	297.0	2.21	11120	1.04	1.79	294.7	-0.0079	21.00	1.79	299.1	0.0070	0.05	0.0019	0.0019	2.04	7.32	0.009
	297.0	2.20	11096	2.66	1.64	292.2	-0.0164	19.40	1.64	299.8	0.0094	0.12	0.0019	0.0019	2.06	7.31	0.010
	297.0	2.20	11083	4.71	1.51	289.6	-0.0249	17.30	1.50	300.8	0.0128	0.21	0.0019	0.0019	2.08	7.31	0.012
	297.0	2.18	10954	5.90	1.38	288.5	-0.0287	15.90	1.40	301.6	0.0152	0.27	0.0019	0.0019	2.08	7.32	0.013
	297.0	2.18	10973	8.02	1.23	288.5	-0.0287	13.80	1.22	301.8	0.0159	0.37	0.0019	0.0019	2.08	7.33	0.016
	297.1	2.10	10561	9.88	1.09	289.5	-0.0256	11.10	1.05	301.6	0.0148	0.47	0.0019	0.0019	2.07	7.34	0.019
	297.1	1.99	10021	11.60	0.94	291.0	-0.0205	8.26	0.92	301.1	0.0135	0.58	0.0019	0.0019	2.06	7.35	0.024
	297.1	1.74	8775	13.60	1.17	293.4	-0.0127	3.84	1.17	299.8	0.0091	0.78	0.0019	0.0019	2.06	7.37	0.035
	297.1	1.65	8328	14.00	1.02	294.3	-0.0096	2.59	1.02	299.3	0.0074	0.84	0.0019	0.0019	2.05	7.36	0.040
	297.1	1.56	7843	14.70	0.98	295.5	-0.0055	0.86	1.00	298.9	0.0060	0.95	0.0019	0.0019	2.04	7.34	0.046
400 (kPa)	296.4	2.82	14199	0.89	2.62	292.8	-0.0124	27.30	2.59	298.4	0.0067	0.03	0.0019	0.0019	2.07	7.40	0.007
	296.4	2.83	14242	2.63	2.39	288.1	-0.0281	25.70	2.39	299.2	0.0094	0.09	0.0019	0.0019	2.10	7.39	0.008
	296.4	2.77	13963	4.44	2.18	285.9	-0.0356	23.30	2.16	299.7	0.0111	0.16	0.0019	0.0019	2.12	7.39	0.009
	296.4	2.80	14106	6.30	1.96	284.6	-0.0400	21.70	1.97	300.4	0.0135	0.22	0.0019	0.0019	2.12	7.39	0.010
	296.4	2.82	14201	7.44	1.89	284.0	-0.0421	20.80	1.87	301.2	0.0162	0.26	0.0019	0.0019	2.13	7.39	0.010
	296.4	2.76	13918	8.94	1.70	284.6	-0.0400	18.70	1.69	301.6	0.0172	0.32	0.0019	0.0019	2.12	7.39	0.012
	296.4	2.67	13443	10.80	1.46	285.3	-0.0376	16.00	1.47	301.8	0.0179	0.41	0.0019	0.0019	2.11	7.40	0.014
	296.4	2.59	13027	12.40	1.26	286.6	-0.0332	14.00	1.27	301.6	0.0172	0.48	0.0019	0.0019	2.10	7.40	0.016
	296.4	2.46	12364	14.50	1.25	288.8	-0.0257	10.00	1.25	301.2	0.0162	0.59	0.0019	0.0019	2.09	7.41	0.020
	296.4	2.39	12032	15.80	1.44	290.6	-0.0195	8.07	1.45	300.6	0.0142	0.66	0.0019	0.0019	2.09	7.42	0.022
	296.4	2.02	10177	17.70	1.30	293.4	-0.0103	2.51	1.30	299.4	0.0101	0.88	0.0019	0.0019	2.07	7.40	0.034
	296.4	1.92	9674	18.40	1.36	294.7	-0.0059	0.86	1.32	298.6	0.0074	0.96	0.0019	0.0019	2.06	7.39	0.038



**Table D.5 High pressure test for tube length,  $L = 60$  mm and tube orifice diameter,  $d_c = 0.8$  mm**

Inlet condition				Cold exit				Hot exit				Uncertainty calculations					
$P_o$	$T_o$ (°K)	Flow (kg/s) $\times 10^{-4}$	$Re$	Flow (kg/s) $\times 10^{-5}$	$P_c$ (kPa)	$T_c$ (°K)	$\frac{T_c - T_o}{T_o}$	Flow (kg/s) $\times 10^{-5}$	$P_h$ (kPa)	$T_h$ (°K)	$\frac{T_h - T_o}{T_o}$	$y_c$	$\frac{T_c - T_o}{T_o}$	$\frac{T_h - T_o}{T_o}$	$m_c \times 10^6$	$m_o \times 10^6$	$y_c$
200 (kPa)	297.4	1.58	7965	0.86	1.41	297.1	-0.0011	14.96	1.42	300.3	0.0097	0.05	0.0019	0.0019	2.02	7.26	0.013
	297.4	1.57	7885	2.37	1.33	295.2	-0.0076	13.29	1.31	300.8	0.0114	0.15	0.0019	0.0019	2.03	7.26	0.015
	297.4	1.59	8024	4.84	1.19	291.8	-0.0191	11.10	1.17	302.1	0.0155	0.30	0.0019	0.0019	2.05	7.27	0.019
	297.4	1.63	8197	6.13	1.12	290.1	-0.0246	10.16	1.12	302.8	0.0179	0.38	0.0019	0.0019	2.06	7.29	0.021
	297.4	1.65	8288	7.98	1.05	289.5	-0.0266	8.48	1.05	302.8	0.0179	0.48	0.0019	0.0019	2.07	7.33	0.025
	297.4	1.68	8474	9.87	0.95	289.4	-0.0269	6.97	0.96	302.9	0.0182	0.59	0.0019	0.0019	2.07	7.35	0.028
	297.4	1.75	8804	11.75	0.94	289.7	-0.0259	5.73	0.95	302.6	0.0172	0.67	0.0019	0.0019	2.07	7.38	0.031
	297.4	1.60	8069	13.54	1.12	291.7	-0.0195	2.49	1.12	301.6	0.0138	0.84	0.0019	0.0019	2.07	7.41	0.041
	297.4	1.57	7883	14.81	1.07	294.1	-0.0113	0.85	1.07	300.1	0.0091	0.95	0.0019	0.0019	2.05	7.38	0.046
300 (kPa)	297.5	2.19	11004	1.21	1.85	295.5	-0.0069	20.66	1.94	301.0	0.0118	0.06	0.0019	0.0019	2.04	7.29	0.010
	297.5	2.18	10987	2.66	1.78	293.2	-0.0147	19.17	1.79	301.3	0.0128	0.12	0.0019	0.0019	2.05	7.29	0.010
	297.5	2.21	11103	4.82	1.65	289.0	-0.0286	17.24	1.62	302.4	0.0162	0.22	0.0019	0.0019	2.08	7.30	0.012
	297.5	2.20	11082	6.21	1.54	287.3	-0.0344	15.80	1.54	303.1	0.0185	0.28	0.0019	0.0019	2.09	7.31	0.013
	297.5	2.25	11324	8.11	1.41	285.9	-0.0392	14.38	1.42	303.8	0.0209	0.36	0.0019	0.0019	2.10	7.34	0.015
	297.5	2.24	11263	10.06	1.31	285.0	-0.0422	12.32	1.30	304.9	0.0246	0.45	0.0019	0.0019	2.11	7.36	0.018
	297.5	2.29	11518	12.04	1.19	284.5	-0.0439	10.84	1.20	305.7	0.0273	0.53	0.0019	0.0019	2.12	7.39	0.019
	297.5	2.32	11666	14.13	1.22	284.5	-0.0439	9.04	1.22	305.9	0.0280	0.61	0.0019	0.0019	2.12	7.43	0.022
	297.5	2.34	11773	16.08	1.46	286.3	-0.0378	7.31	1.44	305.7	0.0273	0.69	0.0019	0.0019	2.12	7.46	0.024
	297.5	2.36	11883	18.12	1.78	288.4	-0.0307	5.49	1.74	304.9	0.0246	0.77	0.0019	0.0019	2.11	7.49	0.026
	297.5	2.18	10984	19.34	1.45	290.9	-0.0222	2.48	1.52	303.8	0.0209	0.89	0.0019	0.0019	2.09	7.46	0.032
	297.5	2.11	10598	20.20	1.62	294.0	-0.0120	0.85	1.62	301.7	0.0138	0.96	0.0019	0.0019	2.08	7.42	0.035
400 (kPa)	296.4	2.81	14147	1.21	2.37	294.9	-0.0052	26.89	2.38	299.1	0.0091	0.04	0.0019	0.0019	2.05	7.37	0.007
	296.4	2.82	14185	2.90	2.21	292.4	-0.0137	25.28	2.22	299.6	0.0108	0.10	0.0019	0.0019	2.07	7.36	0.008
	296.4	2.83	14221	4.75	2.08	288.9	-0.0253	23.50	2.04	300.6	0.0142	0.17	0.0019	0.0019	2.09	7.35	0.009
	296.4	2.83	14258	6.29	1.89	285.0	-0.0386	22.04	1.89	302.0	0.0186	0.22	0.0019	0.0019	2.12	7.36	0.009
	296.4	2.87	14456	8.24	1.75	282.4	-0.0475	20.48	1.74	303.1	0.0223	0.29	0.0019	0.0019	2.14	7.37	0.010
	296.4	2.88	14474	10.23	1.56	280.7	-0.0530	18.52	1.57	304.3	0.0264	0.36	0.0019	0.0019	2.15	7.39	0.012
	296.4	2.87	14460	11.66	1.47	280.0	-0.0554	17.07	1.47	304.9	0.0285	0.41	0.0019	0.0020	2.15	7.41	0.013
	296.4	2.85	14327	13.51	1.33	279.3	-0.0577	14.95	1.32	305.8	0.0315	0.47	0.0019	0.0020	2.16	7.44	0.015
	296.4	2.91	14624	14.92	1.22	278.9	-0.0591	14.13	1.22	305.7	0.0312	0.51	0.0019	0.0020	2.16	7.46	0.015
	296.4	2.92	14678	17.57	1.55	279.3	-0.0577	11.58	1.57	307.7	0.0380	0.60	0.0019	0.0020	2.17	7.52	0.017
	296.4	2.97	14952	19.51	1.82	280.5	-0.0537	10.19	1.82	307.7	0.0380	0.66	0.0019	0.0020	2.18	7.56	0.018
	296.4	2.99	15038	21.42	2.17	282.9	-0.0458	8.46	2.17	307.1	0.0359	0.72	0.0019	0.0020	2.17	7.59	0.020
	296.4	2.98	14978	22.89	2.47	285.0	-0.0386	6.86	2.42	306.3	0.0332	0.77	0.0019	0.0020	2.17	7.61	0.021
	296.4	2.78	13993	24.64	2.13	288.8	-0.0257	3.16	2.12	303.9	0.0251	0.89	0.0019	0.0019	2.14	7.56	0.025
	296.4	2.69	13538	25.87	2.42	293.4	-0.0103	1.03	2.34	300.2	0.0128	0.96	0.0019	0.0019	2.12	7.50	0.028

**Table D.6 High pressure test for tube length,  $L = 60$  mm and tube orifice diameter,  $d_c = 1.1$  mm**

Inlet condition				Cold exit				Hot exit				$y_c$	Uncertainty calculations				
$P_o$	$T_o$ (°K)	Flow (kg/s) $\times 10^{-4}$	$Re$	Flow (kg/s) $\times 10^{-5}$	$P_c$ (kPa)	$T_c$ (°K)	$\frac{T_c - T_o}{T_o}$	Flow (kg/s) $\times 10^{-5}$	$P_h$ (kPa)	$T_h$ (°K)	$\frac{T_h - T_o}{T_o}$		$\frac{T_c - T_o}{T_o}$	$\frac{T_h - T_o}{T_o}$	$m_c \times 10^{-6}$	$m_o \times 10^{-6}$	$y_c$
200 (kPa)	296.6	1.62	8155	0.87	1.26	296.0	-0.0021	15.33	1.22	297.8	0.0040	0.05	0.0019	0.0019	2.02	7.30	0.013
	296.6	1.65	8288	2.55	1.14	293.6	-0.0102	13.91	1.12	298.5	0.0064	0.16	0.0019	0.0019	2.04	7.30	0.014
	296.6	1.63	8197	4.31	1.02	291.0	-0.0190	11.97	1.05	299.6	0.0101	0.26	0.0019	0.0019	2.06	7.30	0.017
	296.6	1.65	8293	6.13	0.94	289.3	-0.0246	10.34	0.95	300.6	0.0135	0.37	0.0019	0.0019	2.07	7.32	0.021
	296.6	1.65	8317	8.01	0.88	288.0	-0.0291	8.51	0.87	301.2	0.0155	0.48	0.0019	0.0019	2.08	7.35	0.025
	296.6	1.72	8633	9.92	0.79	287.5	-0.0308	7.23	0.78	301.7	0.0169	0.58	0.0019	0.0019	2.08	7.38	0.028
	296.6	1.76	8864	11.85	0.94	288.3	-0.0280	5.76	0.95	301.3	0.0159	0.67	0.0019	0.0019	2.08	7.41	0.031
	296.6	1.61	8102	13.61	0.94	289.8	-0.0229	2.49	0.93	300.5	0.0132	0.85	0.0019	0.0019	2.08	7.44	0.041
	296.6	1.57	7921	14.88	0.98	292.4	-0.0144	0.85	0.90	299.1	0.0084	0.95	0.0019	0.0019	2.06	7.41	0.046
300 (kPa)	296.6	2.20	11076	0.87	1.93	295.1	-0.0052	21.13	1.79	298.0	0.0047	0.04	0.0019	0.0019	2.04	7.35	0.009
	296.6	2.22	11158	2.56	1.66	294.2	-0.0083	19.60	1.66	298.6	0.0067	0.12	0.0019	0.0019	2.04	7.33	0.010
	296.6	2.24	11297	4.35	1.52	289.8	-0.0229	18.09	1.51	299.5	0.0098	0.19	0.0019	0.0019	2.07	7.33	0.011
	296.6	2.21	11120	6.21	1.38	287.0	-0.0325	15.88	1.37	301.0	0.0149	0.28	0.0019	0.0019	2.09	7.34	0.013
	296.6	2.25	11340	8.13	1.27	284.9	-0.0396	14.40	1.25	303.0	0.0213	0.36	0.0019	0.0019	2.11	7.35	0.015
	296.6	2.24	11288	10.10	1.11	283.3	-0.0451	12.32	1.12	304.2	0.0254	0.45	0.0019	0.0019	2.12	7.38	0.018
	296.6	2.27	11402	12.10	1.03	282.6	-0.0473	10.55	1.02	306.1	0.0318	0.53	0.0019	0.0020	2.13	7.40	0.020
	296.6	2.32	11658	14.14	1.18	283.0	-0.0461	9.02	1.17	306.6	0.0335	0.61	0.0019	0.0020	2.13	7.45	0.022
	296.6	2.38	11956	16.21	1.43	283.9	-0.0430	7.54	1.42	306.4	0.0329	0.68	0.0019	0.0020	2.13	7.50	0.023
	296.6	2.40	12090	18.29	1.72	285.5	-0.0376	5.73	1.72	305.3	0.0291	0.76	0.0019	0.0019	2.13	7.54	0.025
	296.6	2.21	11135	19.63	1.52	289.0	-0.0257	2.49	1.62	303.0	0.0213	0.89	0.0019	0.0019	2.11	7.51	0.032
	296.6	2.16	10872	20.74	1.71	292.9	-0.0127	0.86	1.69	300.0	0.0115	0.96	0.0019	0.0019	2.09	7.46	0.035
400 (kPa)	296.7	2.84	14280	1.55	2.29	295.5	-0.0042	26.82	2.39	298.2	0.0050	0.05	0.0019	0.0019	2.05	7.39	0.007
	296.7	2.83	14263	3.29	2.35	292.7	-0.0137	25.05	2.24	298.8	0.0070	0.12	0.0019	0.0019	2.07	7.38	0.008
	296.7	2.83	14257	4.74	2.11	289.6	-0.0240	23.58	2.09	299.7	0.0101	0.17	0.0019	0.0019	2.09	7.37	0.009
	296.7	2.84	14292	6.25	1.95	286.9	-0.0332	22.15	1.94	300.6	0.0132	0.22	0.0019	0.0019	2.10	7.37	0.009
	296.7	2.83	14244	8.18	1.78	284.4	-0.0417	20.11	1.77	302.2	0.0182	0.29	0.0019	0.0019	2.12	7.38	0.011
	296.7	2.83	14254	10.21	1.60	281.5	-0.0512	18.11	1.59	304.2	0.0250	0.36	0.0019	0.0019	2.14	7.39	0.012
	296.7	2.86	14395	12.27	1.42	279.8	-0.0570	16.33	1.44	305.8	0.0305	0.43	0.0019	0.0020	2.16	7.41	0.013
	296.7	2.85	14360	14.38	1.31	278.5	-0.0614	14.14	1.30	308.6	0.0400	0.50	0.0019	0.0020	2.17	7.43	0.015
	296.7	2.93	14737	16.48	1.42	279.2	-0.0590	12.80	1.42	309.6	0.0434	0.56	0.0019	0.0020	2.17	7.46	0.016
	296.7	2.95	14852	18.66	1.73	279.9	-0.0567	10.85	1.73	310.7	0.0471	0.63	0.0019	0.0020	2.18	7.52	0.018
	296.7	2.96	14886	20.85	2.08	281.2	-0.0522	8.72	2.09	310.8	0.0474	0.70	0.0019	0.0020	2.18	7.58	0.020
	296.7	3.04	15308	23.25	2.51	283.5	-0.0447	7.16	2.49	309.9	0.0444	0.76	0.0019	0.0020	2.18	7.62	0.020
	296.7	3.08	15516	25.09	2.91	286.0	-0.0362	5.74	2.89	308.2	0.0386	0.81	0.0019	0.0020	2.18	7.64	0.021
	296.7	2.84	14293	25.91	2.39	289.3	-0.0250	2.49	2.42	305.3	0.0288	0.91	0.0019	0.0019	2.15	7.58	0.026
	296.7	2.74	13807	26.57	2.65	293.2	-0.0120	0.86	2.81	301.8	0.0169	0.97	0.0019	0.0019	2.13	7.53	0.028

**Table D.7 High pressure test for tube length,  $L = 100$  mm and tube orifice diameter,  $d_c = 0.5$  mm**

Inlet condition				Cold exit				Hot exit				$y_c$	Uncertainty calculations				
$P_o$	$T_o$ (°K)	Flow (kg/s) $\times 10^{-4}$	$Re$	Flow (kg/s) $\times 10^{-5}$	$P_c$ (kPa)	$T_c$ (°K)	$\frac{T_c - T_o}{T_o}$	Flow (kg/s) $\times 10^{-5}$	$P_h$ (kPa)	$T_h$ (°K)	$\frac{T_h - T_o}{T_o}$		$\frac{T_c - T_o}{T_o}$	$\frac{T_h - T_o}{T_o}$	$m_c \times 10^{-6}$	$m_o \times 10^{-6}$	$y_c$
200 (kPa)	296.4	1.59	7990	0.87	1.17	295.6	-0.0028	15.01	1.15	298.6	0.0074	0.05	0.0019	0.0019	2.02	7.28	0.013
	296.4	1.62	8137	2.56	1.06	292.7	-0.0127	13.61	1.05	299.0	0.0088	0.16	0.0019	0.0019	2.04	7.29	0.015
	296.4	1.63	8215	4.49	0.95	290.8	-0.0189	11.83	0.95	299.5	0.0105	0.28	0.0019	0.0019	2.06	7.30	0.018
	296.4	1.65	8290	6.11	0.85	290.1	-0.0212	10.36	0.85	299.8	0.0115	0.37	0.0019	0.0019	2.06	7.32	0.021
	296.4	1.54	7774	7.91	0.73	291.0	-0.0182	7.53	0.73	299.6	0.0108	0.51	0.0019	0.0019	2.05	7.33	0.028
	296.4	1.32	6624	10.32	0.92	293.6	-0.0097	2.84	0.90	298.7	0.0077	0.78	0.0019	0.0019	2.04	7.36	0.047
	296.4	1.19	5998	11.06	0.84	295.0	-0.0049	0.86	0.85	298.1	0.0057	0.93	0.0019	0.0019	2.03	7.34	0.060
300 (kPa)	296.4	2.21	11131	1.05	1.70	293.1	-0.0114	21.07	1.77	298.8	0.0081	0.05	0.0019	0.0019	2.05	7.33	0.009
	296.4	2.20	11067	2.43	1.69	289.7	-0.0226	19.56	1.66	299.3	0.0098	0.11	0.0019	0.0019	2.08	7.33	0.010
	296.4	2.17	10933	4.39	1.45	287.5	-0.0301	17.33	1.47	300.2	0.0128	0.20	0.0019	0.0019	2.09	7.33	0.012
	296.4	2.21	11128	6.22	1.35	286.5	-0.0335	15.89	1.35	300.8	0.0149	0.28	0.0019	0.0019	2.10	7.34	0.013
	296.4	2.19	11011	8.07	1.17	286.6	-0.0332	13.80	1.17	301.0	0.0155	0.37	0.0019	0.0019	2.09	7.36	0.016
	296.4	2.10	10595	9.93	0.96	287.7	-0.0294	11.12	0.97	300.8	0.0149	0.47	0.0019	0.0019	2.08	7.37	0.019
	296.4	1.98	9979	11.80	0.94	289.6	-0.0230	8.03	0.82	300.2	0.0128	0.60	0.0019	0.0019	2.07	7.38	0.024
	296.4	1.65	8298	13.48	0.95	292.6	-0.0131	3.00	0.95	299.1	0.0091	0.82	0.0019	0.0019	2.06	7.38	0.039
	296.4	1.56	7874	14.79	0.95	294.2	-0.0076	0.86	0.90	298.3	0.0064	0.95	0.0019	0.0019	2.05	7.37	0.046
400 (kPa)	296.4	2.90	14595	0.88	2.40	293.6	-0.0097	28.11	2.64	298.4	0.0067	0.03	0.0019	0.0019	2.06	7.41	0.007
	296.4	2.90	14594	2.53	2.47	289.9	-0.0219	26.46	2.47	299.0	0.0088	0.09	0.0019	0.0019	2.09	7.40	0.008
	296.4	2.92	14678	4.35	2.29	286.3	-0.0342	24.81	2.27	299.9	0.0118	0.15	0.0019	0.0019	2.11	7.39	0.008
	296.4	2.87	14468	6.31	2.05	284.4	-0.0407	22.43	2.02	300.9	0.0152	0.22	0.0019	0.0019	2.13	7.39	0.009
	296.4	2.84	14277	8.20	1.75	283.7	-0.0431	20.16	1.77	301.4	0.0169	0.29	0.0019	0.0019	2.13	7.39	0.011
	296.4	2.76	13913	10.10	1.46	284.3	-0.0410	17.54	1.52	301.7	0.0176	0.37	0.0019	0.0019	2.12	7.40	0.012
	296.4	2.65	13330	12.02	1.41	285.7	-0.0363	14.46	1.27	301.7	0.0176	0.45	0.0019	0.0019	2.11	7.41	0.015
	296.4	2.50	12598	13.92	1.20	287.5	-0.0301	11.11	1.02	301.3	0.0166	0.56	0.0019	0.0019	2.10	7.41	0.018
	296.4	2.43	12239	15.79	0.87	289.9	-0.0219	8.53	0.87	300.7	0.0145	0.65	0.0019	0.0019	2.08	7.39	0.022
	296.4	2.06	10368	17.68	0.96	293.0	-0.0117	2.92	0.97	299.2	0.0094	0.86	0.0019	0.0019	2.07	7.39	0.032
	296.4	1.92	9649	18.31	0.96	294.3	-0.0073	0.86	0.95	298.6	0.0074	0.96	0.0019	0.0019	2.06	7.37	0.038

**Table D.8 High pressure test for tube length,  $L = 100$  mm and tube orifice diameter,  $d_c = 0.8$  mm**

Inlet condition				Cold exit				Hot exit				$y_c$	Uncertainty calculations				
$P_o$	$T_o$ (°K)	Flow (kg/s) $\times 10^{-4}$	$Re$	Flow (kg/s) $\times 10^{-5}$	$P_c$ (kPa)	$T_c$ (°K)	$\frac{T_c - T_o}{T_o}$	Flow (kg/s) $\times 10^{-5}$	$P_h$ (kPa)	$T_h$ (°K)	$\frac{T_h - T_o}{T_o}$		$\frac{T_c - T_o}{T_o}$	$\frac{T_h - T_o}{T_o}$	$m_c \times 10^{-6}$	$m_o \times 10^{-6}$	$y_c$
200 (kPa)	296.4	1.55	7812	0.87	1.38	295.6	-0.0028	14.65	1.37	298.1	0.0057	0.06	0.0019	0.0019	2.03	7.31	0.01
	296.5	1.58	7953	2.56	1.29	293.1	-0.0117	13.24	1.27	298.8	0.0077	0.16	0.0019	0.0019	2.05	7.30	0.01
	296.5	1.63	8208	4.34	1.17	289.6	-0.0233	11.96	1.15	300.0	0.0118	0.27	0.0019	0.0019	2.07	7.31	0.02
	296.5	1.60	8054	6.17	1.07	288.0	-0.0287	9.83	1.07	300.7	0.0142	0.39	0.0019	0.0019	2.08	7.34	0.02
	296.5	1.66	8340	8.04	1.02	287.3	-0.0311	8.53	1.00	301.0	0.0152	0.49	0.0019	0.0019	2.09	7.37	0.02
	296.5	1.72	8657	9.94	0.93	287.2	-0.0315	7.26	0.92	301.0	0.0152	0.58	0.0019	0.0019	2.09	7.40	0.03
	296.5	1.74	8775	11.90	1.17	287.8	-0.0294	5.53	1.15	300.7	0.0142	0.68	0.0019	0.0019	2.09	7.45	0.03
	296.5	1.60	8042	13.48	1.07	289.9	-0.0223	2.50	1.07	300.0	0.0118	0.84	0.0019	0.0019	2.08	7.45	0.04
	296.5	1.53	7708	14.46	1.01	292.6	-0.0134	0.86	1.02	299.0	0.0084	0.94	0.0019	0.0019	2.06	7.41	0.05
300 (kPa)	297.0	2.19	11041	0.87	1.86	295.2	-0.0062	21.06	1.74	298.8	0.0060	0.04	0.0019	0.0019	2.04	7.32	0.01
	297.0	2.21	11138	2.58	1.65	292.4	-0.0158	19.55	1.64	299.4	0.0081	0.12	0.0019	0.0019	2.06	7.32	0.01
	297.0	2.24	11289	4.37	1.51	288.5	-0.0287	18.05	1.52	300.1	0.0104	0.19	0.0019	0.0019	2.08	7.33	0.01
	297.0	2.25	11330	6.25	1.39	285.4	-0.0392	16.26	1.39	301.8	0.0159	0.28	0.0019	0.0019	2.10	7.34	0.01
	297.0	2.19	11018	8.16	1.29	284.0	-0.0440	13.73	1.30	303.0	0.0199	0.37	0.0019	0.0019	2.12	7.36	0.02
	297.0	2.26	11371	10.11	1.18	283.1	-0.0471	12.48	1.17	303.9	0.0230	0.45	0.0019	0.0019	2.12	7.39	0.02
	297.0	2.31	11627	12.10	1.06	282.7	-0.0484	11.00	1.07	304.6	0.0253	0.52	0.0019	0.0019	2.13	7.42	0.02
	297.0	2.32	11689	14.15	1.18	282.8	-0.0481	9.07	1.17	304.8	0.0260	0.61	0.0019	0.0019	2.13	7.47	0.02
	297.0	2.34	11761	16.18	1.17	283.8	-0.0447	7.19	1.17	304.7	0.0257	0.69	0.0019	0.0019	2.13	7.50	0.02
	297.0	2.40	12058	18.20	1.73	287.0	-0.0338	5.76	1.72	303.7	0.0223	0.76	0.0019	0.0019	2.12	7.52	0.03
	297.0	2.19	11022	19.40	1.47	290.1	-0.0232	2.49	1.47	301.7	0.0155	0.89	0.0019	0.0019	2.10	7.49	0.03
297.0	2.11	10623	20.25	1.64	293.4	-0.0123	0.86	1.64	300.2	0.0108	0.96	0.0019	0.0019	2.08	7.44	0.04	
400 (kPa)	297.0	2.84	14318	1.22	2.52	294.6	-0.0083	27.23	2.59	299.4	0.0081	0.04	0.0019	0.0019	2.06	7.38	0.01
	297.0	2.83	14263	2.60	2.39	292.1	-0.0168	25.74	2.44	300.2	0.0108	0.09	0.0019	0.0019	2.07	7.36	0.01
	297.0	2.83	14267	4.41	2.27	288.3	-0.0294	23.94	2.27	301.4	0.0148	0.16	0.0019	0.0019	2.10	7.35	0.01
	297.0	2.86	14399	6.29	2.08	285.1	-0.0403	22.31	2.07	302.8	0.0192	0.22	0.0019	0.0019	2.12	7.35	0.01
	297.0	2.83	14221	8.23	1.88	283.2	-0.0467	20.02	1.89	303.9	0.0230	0.29	0.0019	0.0019	2.13	7.36	0.01
	297.0	2.90	14599	10.22	1.73	281.6	-0.0518	18.78	1.72	305.0	0.0267	0.35	0.0019	0.0019	2.14	7.38	0.01
	297.0	2.87	14457	12.27	1.52	280.1	-0.0569	16.45	1.57	306.4	0.0315	0.43	0.0019	0.0019	2.15	7.41	0.01
	297.0	2.91	14642	14.36	1.41	279.2	-0.0600	14.73	1.42	307.9	0.0365	0.49	0.0019	0.0020	2.16	7.43	0.01
	297.0	2.93	14743	16.49	1.42	279.0	-0.0607	12.80	1.42	309.6	0.0423	0.56	0.0019	0.0020	2.17	7.47	0.02
	297.0	2.96	14885	18.69	1.72	279.4	-0.0593	10.88	1.71	309.7	0.0426	0.63	0.0019	0.0020	2.18	7.54	0.02
	297.0	2.97	14950	20.82	2.07	281.6	-0.0518	8.88	2.07	309.6	0.0423	0.70	0.0019	0.0020	2.18	7.58	0.02
	297.0	2.95	14851	22.92	2.50	284.7	-0.0416	6.58	2.49	308.1	0.0372	0.78	0.0019	0.0020	2.17	7.61	0.02
	297.0	2.98	15006	25.03	2.91	288.0	-0.0304	4.78	2.91	306.7	0.0325	0.84	0.0019	0.0020	2.16	7.61	0.02
	297.0	2.75	13838	25.00	2.25	290.3	-0.0226	2.49	2.27	304.6	0.0253	0.91	0.0019	0.0019	2.13	7.54	0.03
	297.0	2.68	13515	25.99	2.44	293.8	-0.0110	0.86	2.47	302.8	0.0192	0.97	0.0019	0.0019	2.12	7.50	0.03

**Table D.9 High pressure test for tube length,  $L = 100$  mm and tube orifice diameter,  $d_c = 1.1$  mm**

Inlet condition				Cold exit				Hot exit				$y_c$	Uncertainty calculations				
$P_o$	$T_o$ (°K)	Flow (kg/s) $\times 10^{-4}$	$Re$	Flow (kg/s) $\times 10^{-5}$	$P_c$ (kPa)	$T_c$ (°K)	$\frac{T_c - T_o}{T_o}$	Flow (kg/s) $\times 10^{-5}$	$P_h$ (kPa)	$T_h$ (°K)	$\frac{T_h - T_o}{T_o}$		$\frac{T_c - T_o}{T_o}$	$\frac{T_h - T_o}{T_o}$	$m_c \times 10^{-6}$	$m_o \times 10^{-6}$	$y_c$
200 (kPa)	296.7	1.62	8180	0.87	1.23	295.9	-0.0028	15.38	1.35	297.2	0.0016	0.05	0.0019	0.0019	2.02	7.33	0.01
	296.7	1.65	8296	2.55	1.21	294.5	-0.0076	13.93	1.25	298.4	0.0057	0.15	0.0019	0.0019	2.03	7.30	0.01
	296.7	1.61	8122	4.31	1.17	291.5	-0.0178	11.82	1.12	300.2	0.0118	0.27	0.0019	0.0019	2.06	7.29	0.02
	296.7	1.66	8359	6.13	1.01	289.6	-0.0240	10.48	1.02	300.7	0.0135	0.37	0.0019	0.0019	2.07	7.32	0.02
	296.7	1.67	8388	8.03	0.97	287.7	-0.0304	8.64	0.95	301.6	0.0162	0.48	0.0019	0.0019	2.08	7.36	0.02
	296.7	1.72	8645	9.94	0.89	287.3	-0.0318	7.24	0.87	301.7	0.0166	0.58	0.0019	0.0019	2.09	7.39	0.03
	296.7	1.73	8688	11.87	0.96	287.9	-0.0297	5.39	0.92	301.2	0.0152	0.69	0.0019	0.0019	2.09	7.43	0.03
	296.7	1.63	8183	13.76	1.02	289.6	-0.0240	2.49	1.02	300.5	0.0128	0.85	0.0019	0.0019	2.08	7.45	0.04
	296.7	1.57	7919	14.88	0.98	292.5	-0.0144	0.85	0.97	299.1	0.0081	0.95	0.0019	0.0019	2.06	7.41	0.05
300 (kPa)	296.1	2.21	11101	0.87	1.66	295.2	-0.0032	21.18	1.77	297.2	0.0037	0.04	0.0019	0.0019	2.04	7.36	0.01
	296.1	2.22	11173	2.57	1.58	293.4	-0.0093	19.63	1.62	298.1	0.0067	0.12	0.0019	0.0019	2.05	7.34	0.01
	296.1	2.25	11310	4.36	1.49	289.1	-0.0237	18.11	1.47	299.1	0.0101	0.19	0.0019	0.0019	2.08	7.34	0.01
	296.1	2.21	11149	6.23	1.39	286.3	-0.0332	15.92	1.37	300.2	0.0139	0.28	0.0019	0.0019	2.10	7.36	0.01
	296.1	2.26	11379	8.14	1.24	284.3	-0.0401	14.46	1.25	301.7	0.0186	0.36	0.0019	0.0019	2.11	7.37	0.02
	296.1	2.26	11400	10.13	1.13	282.4	-0.0465	12.51	1.12	302.8	0.0224	0.45	0.0019	0.0019	2.13	7.41	0.02
	296.1	2.32	11657	12.14	1.01	281.5	-0.0493	11.01	1.00	303.9	0.0261	0.52	0.0019	0.0019	2.13	7.43	0.02
	296.1	2.33	11733	14.20	1.18	281.7	-0.0486	9.11	1.17	303.6	0.0251	0.61	0.0019	0.0019	2.14	7.50	0.02
	296.1	2.39	12013	16.29	1.42	282.5	-0.0462	7.57	1.27	304.6	0.0285	0.68	0.0019	0.0020	2.14	7.53	0.02
	296.1	2.44	12267	18.37	1.73	284.4	-0.0397	6.00	1.74	303.8	0.0258	0.75	0.0019	0.0019	2.14	7.57	0.02
	296.1	2.25	11321	20.00	1.54	288.1	-0.0271	2.49	1.54	302.1	0.0200	0.89	0.0019	0.0019	2.12	7.54	0.03
	296.1	2.17	10917	20.83	1.73	291.7	-0.0151	0.86	1.72	300.2	0.0139	0.96	0.0019	0.0019	2.10	7.49	0.03
400 (kPa)	296.3	2.83	14235	0.88	2.58	295.2	-0.0039	27.40	2.54	297.4	0.0037	0.03	0.0019	0.0019	2.06	7.42	0.01
	296.3	2.82	14220	2.58	2.37	294.1	-0.0076	25.67	2.37	299.0	0.0091	0.09	0.0019	0.0019	2.06	7.38	0.01
	296.3	2.84	14290	4.39	2.21	289.5	-0.0230	24.00	2.17	300.3	0.0135	0.15	0.0019	0.0019	2.09	7.36	0.01
	296.3	2.84	14289	6.27	1.98	286.0	-0.0349	22.12	1.99	301.1	0.0162	0.22	0.0019	0.0019	2.11	7.37	0.01
	296.3	2.88	14477	8.21	1.80	283.5	-0.0434	20.55	1.82	302.3	0.0200	0.29	0.0019	0.0019	2.13	7.38	0.01
	296.4	2.88	14497	10.24	1.66	280.9	-0.0523	18.56	1.64	303.8	0.0247	0.36	0.0019	0.0019	2.15	7.40	0.01
	296.4	2.87	14424	12.31	1.49	279.0	-0.0588	16.34	1.49	305.7	0.0312	0.43	0.0019	0.0020	2.16	7.43	0.01
	296.4	2.90	14609	14.41	1.33	278.1	-0.0618	14.61	1.33	307.2	0.0363	0.50	0.0019	0.0020	2.17	7.45	0.01
	296.4	2.93	14742	16.56	1.43	277.9	-0.0625	12.73	1.44	308.2	0.0397	0.57	0.0019	0.0020	2.18	7.50	0.02
	296.4	2.97	14941	18.77	1.73	278.2	-0.0615	10.91	1.72	308.9	0.0420	0.63	0.0019	0.0020	2.19	7.56	0.02
	296.4	3.03	15233	20.99	2.09	279.4	-0.0574	9.28	2.09	309.2	0.0431	0.69	0.0019	0.0020	2.19	7.62	0.02
	296.4	3.04	15293	23.20	2.49	281.3	-0.0509	7.19	2.47	308.6	0.0410	0.76	0.0019	0.0020	2.19	7.67	0.02
	296.4	3.11	15659	25.35	2.93	284.4	-0.0407	5.76	2.81	306.9	0.0353	0.81	0.0019	0.0020	2.19	7.68	0.02
	296.4	2.83	14265	25.84	2.44	288.4	-0.0270	2.50	2.39	304.1	0.0257	0.91	0.0019	0.0019	2.15	7.61	0.03
	296.4	2.83	14245	27.44	2.69	292.4	-0.0137	0.86	2.69	301.7	0.0176	0.97	0.0019	0.0019	2.14	7.55	0.03

## VITA AUCTORIS

- 1961 Born in Baghdad, Iraq, in December.
- 1983 Received Bachelor of Science from the University of Baghdad, Baghdad, Iraq in June.
- 1987 Mechanical and Electrical Contractors – Self Employed, Baghdad-Iraq.
- 1996 Senior Design Engineer, PACE Consulting, Kuala Lumpur, Malaysia.
- 2005 Candidate for the Master of Applied Science Degree in Mechanical Engineering at the University of Windsor, Windsor, Ontario, Canada.

### **Professional Affiliation**

1. Member of Professional Engineers Ontario (P.Eng.), Ontario, Canada.
2. Member of the American Society of Heating Refrigerating and Air Conditioning Engineering. Vice President of the Student Chapter at the University of Windsor, Windsor, Ontario, Canada.